2010-06

Dynamics of particle clouds in ambient currents with application to open-water sediment disposal

Gensheimer, Robert James.

Cambridge Massachusetts Institute of Technology

Dynamics of Particle Clouds in Ambient Currents with Application to Open-Water Sediment Disposal

by

Robert James Gensheimer III

B.S. Ocean Engineering
United States Naval Academy, 2008

Submitted to the Department of Civil and Environmental Engineering
in partial fulfillment of the requirement for the degree of

Master of Science in Civil and Environmental Engineering

at the

MASSACHUSETTS INSTITUTE OF TECHNOLOGY

June 2010

Signature of Author . . . .
Department of Civil and Environmental Engineering
May 7, 2010

Certified by . . . .
E. Eric Adams
Senior Research Engineer & Lecturer of Civil and Environmental Engineering
Thesis Supervisor

Accepted by . . . .
Daniele Veneziano
Chairman, Departmental Committee for Graduate Students

Dynamics of Particle Clouds in Ambient Currents with Application to Open-Water Sediment Disposal

by

Robert James Gensheimer III

Submitted to the Department of Civil and Environmental Engineering
on May 7, 2010, in partial fulfillment of the
requirements for the degree of
Master of Science in Civil and Environmental Engineering

Abstract

Open-water sediment disposal is used in many applications around the world, including land reclamation, dredging, and contaminated sediment isolation. Timely examples include the land reclamation campaign currently underway in Singapore and the Boston Harbor Navigation Improvement Project. Both of these projects required the precise dumping of millions of cubic meters of purchased sediment, in the former example, and dredged material (both clean and contaminated), in the latter example. This shows the significant economic and environmental interests in the accurate placement of sediment, which requires knowledge of how particle clouds behave in ambient currents.

Flow visualization experiments were performed in a glass-walled recirculating water channel to model open-water sediment disposal by releasing particles quasi-instantaneously into the channel with ambient currents. For releases at the surface, criteria were developed to characterize ambient currents as "weak," "transitional," or "strong" as a function of particle size. In "weak" ambient currents, particle clouds advected downstream with a velocity equal to the ambient current, but otherwise the behavior and structure was similar to that in quiescent conditions. The parent cloud's entrainment coefficient (α) increased with decreasing particle size and elevation above the water surface, between values of 0.10 and 0.72, but for most experiments, the range was less significant (0.11 to 0.24). A substantial portion of the mass initially released, up to 30 %, was not incorporated into the parent cloud and formed the trailing stem. This was also heavily dependent on the initial release variables, with the greatest sensitivity on particle size. The "loss" of sediment during descent, defined as the fraction of mass missing a designated target with a radius equal to the water depth, was quantified and found to increase sharply with current speed. The cloud number (N_c), which relates the particle settling velocity to a characteristic thermal descent velocity, provides a basis for scaling laboratory results to the real world and formulating guidelines to reduce the losses that could result from open-water sediment disposal.

Thesis Supervisor: E. Eric Adams
Title: Senior Research Engineer and Lecturer of Civil and Environmental Engineering

Acknowledgements

First and foremost, I would like to thank my thesis advisor, Dr. E. Eric Adams for his countless hours of discussion, guidance, and assistance while enrolled in classes, performing research, and writing this thesis. My degree at MIT would not have been possible without him, and he was always understanding of my unique time constraints as a Naval Officer.

I would also like to recognize everyone working on particle clouds with me at MIT and in Singapore: Professors Adrian Wing-Keung Law and Zhenhua Huang at NTU, CENSAM researchers Drs. Daichin and Shao Dongdong, and graduate students Ruo-Qian Wang at MIT and Zhao Bing at NTU.

My work would have also not been possible without the assistance of many students in Parsons Laboratory. I would like to particularly thank Mitul Luhar, Jeff Rominger, Gaj Sivandran, and Kevin Zhang for their assistance with everything from mopping up leaks to coding MATLAB. I also want to thank Mike Barry for his stories and outbursts; they were simply priceless.

The entire Environmental Fluid Mechanics group was always helpful, particularly Professor Heidi Nepf for any issue related to experiments or her laboratory, and I would also like to thank Professor Ole Madsen for permitting me to borrow his flume.

I must also acknowledge Aaron Chow, one of Eric's former students, who helped me immensely with my initial experimental setup, as well as UROP Joe Poole, who assisted with the daunting task of cleaning and repairing my flume before experiments could begin.

I would like to recognize Sheila Frankel for making Parsons Laboratory a better community to work each and every day.

I am also grateful to Dr. Tom Fredette with the U.S. Army Corps of Engineers. He was always willing to answer my questions and was very helpful.

Finally, my family and friends outside of the MIT community were always supportive of my endeavors. I would like to particularly thank my mother and father, as well as my three siblings, Katie, Bill, and Maryl.

Contents

List of Figures

14

List of Tables

1 Introduction

This chapter introduces the applications of open-water sediment disposal in the field, provides a brief description of a particle cloud and its descent in a less dense ambient, and outlines the contents included within this thesis.

1.1 Motivation

Open-water sediment disposal is used in many applications associated with both the littoral zones and offshore locations around the world, including land reclamation, coastline extension, dredging, and contaminated sediment isolation (with or without capping). The final example listed is an application of open-water sediment disposal that stems from the significant volume of sediment, particularly contaminated sediment, that is dredged from harbors and navigation channels; in the United States alone, it is estimated that approximately 10 % of the 190 to 230 million m^3 of sediment dredged annually contains heavy metals and/or organic chemicals (McDowell, 1999; Suedel et al., 2008). However, its use for all of these functions raises questions concerning the ability to accurately place sediments in a targeted area, as well as the loss of sediments (and potentially contaminants as well) to the ambient environment during disposal operations. Sediment that remains in suspension during disposal introduces additional environmental concerns such as increased turbidity, which adversely affects aquatic vegetation, fisheries, and overall water quality.

Timely and continuing examples of open-water sediment disposal include the land reclamation campaign currently underway in Singapore, as well as the Boston Harbor Navigation Improvement Project of the late 1990s and early 2000s. In the former example, the island nation will soon increase the land area of the country by more than 25 % when compared to its size in the 1960s (Wong, 2005). This equates to more than 100 km^2 of land, and creates a requirement for more than 1 billion m^3 of sediment to accomplish the task. The latter example is a single illustration of the ongoing trend of ports and harbors around the world increasing navigation depths and maintaining these depths for their approaches, turning basins, and anchorages. The specific example cited in Boston Harbor utilized Confined Aquatic Disposal (CAD) Cells to isolate the approximately 750,000 m^3 of contaminated sediment dredged while deepening the harbor's navigation channels (ENSR, 2002).

These examples, and the volumes of sediment identified, clearly demonstrate the importance of understanding the mechanisms of sediment descent both to dispose sediment accurately, and to minimize sediment losses to the ambient environment. Historical cases in the field have claimed the losses have been minimal, on the order of 1 to 5 % (Truitt, 1988), or have neglected accounting for them at all. Ruggaber (2000) was the first to analyze the physical mechanisms for these losses based on the characteristic cloud behavior as it descended in the water column. In his experiments, he explained the effects of practical release parameters such as release location and moisture content. However, his work was done entirely in quiescent conditions, and in order to extend the applicability and understanding of particle clouds related to open-water sediment disposal, realistic open-water conditions must also be included in the analysis. Most

water bodies are not quiescent, but instead, they are continually under the influence of surface waves and time varying (e.g., tidal) currents; documenting cloud behavior and sediment losses in ambient currents is the focus of this research.

1.2 Description of a Particle Cloud

Sediment that has been released in a sufficiently instantaneous manner in open-water forms a particle cloud, which can be viewed as a sudden release of buoyancy into the surrounding fluid. This assumption makes a particle cloud no different than a heavy fluid with the same density (e.g., a cloud composed of very fine particles would be analogous to a heavy brine). This reduces the particle cloud from a multiphase to a single phase density field, and in the literature this type of sudden release of buoyancy (either lighter or heavier than the surrounding ambient fluid) is called a "thermal" (Scorer, 1957; Woodward, 1959). Depending on the density of the ambient fluid, there can be "light thermals" and "dense thermals." Hereafter, because open-water sediment disposal involves the release of heavier particles into an ambient fluid with a lower density (i.e., rivers, estuaries, and oceans), the word "thermal" will be used since only "dense thermals" are applicable and therefore discussed.

There are three distinct phases of a descending particle cloud, which are generally also the descriptors given to the behavior of instantaneously released sediment in open-water: 1) convective decent, 2) dynamic collapse, and 3) passive diffusion (Clark et al., 1971; Koh and Chang, 1973; Brandsma and Divoky, 1976; Johnson and Holliday, 1978). A schematic of these three phases of open-water sediment disposal is shown in Figure 1-1, and each phase is summarized below:

19

1. Convective Descent:

   In the first phase, the released sediment forms a particle cloud that resembles a high-density plume. Its downward descent is governed by its negative buoyancy, and ideally, most of the mass is included within the cloud. As the cloud is transported downward, it entrains ambient fluid, decreasing the difference in density between the ambient environment and the particle cloud.

2. Dynamic Collapse:

   The second phase is characterized by the collapse of the particle cloud when either it has entrained enough ambient fluid that it reaches a level of neutral buoyancy or the cloud impacts the bottom. As the cloud collapses, the vertical momentum is converted to horizontal momentum, leading to the horizontal spread of the particle cloud.

3. Long-term or Passive Diffusion:

   In the final phase, when the dynamic motion and spreading of the particle cloud has ceased, individual particles that formerly made up the cloud advect and diffuse due to ambient currents; their suspended motion depends on the individual settling velocities of the particles (this is independent and unrelated to the third regime of convective descent, which is discussed shortly).

Each phase of open-water sediment disposal is important for understanding the long-term fate of dredged material, but the dynamics of particle clouds and short-term fate of dredged material is encompassed within convective descent. Therefore, the research presented hereafter will focus entirely on the first phase of the descent of particle clouds.

The convective descent phase can be divided into three sub-phases, according to the descent velocity of the particle cloud: 1) initial acceleration phase, 2) thermal phase, and 3) dispersive phase (Rahimipour and Wilkinson, 1992; Noh and Fernando, 1993). These regimes are shown in Figure 1-2 and are described in greater detail below:

1. Initial Acceleration Phase:

Prior to a particle cloud release, the particles are closely packed and at rest. Upon release, the sediment (or sediment/fluid mixture if it contains water) accelerates and expands rapidly. Ambient water is entrained, in part due to the shearing effect at the edge of the cloud which produces turbulent instabilities and disperses the particles. The entrainment reduces the difference in density between the cloud and the ambient environment, and after reaching its maximum velocity, the cloud begins to decelerate and enters the second phase.

Theoretical (Escudier and Maxworthy, 1973) and experimental (Baines and Hopfinger, 1984) investigations have demonstrated that the initial acceleration phase is a function of the initial buoyancy, and that its length for a thermal is approximately equivalent to 1 to 3 initial cloud diameters. Later studies on dense thermals (Neves and Almeida, 1991) have generally confirmed these results, and similar development scales have been recorded by numerical studies for particle clouds, and confirmed by experimental findings (Li, 1997).

2. Self-Preserving or Thermal Phase:

As the density of the particle cloud continues to decrease (as the less dense ambient fluid is entrained into it), thermals and particle clouds asymptotically decelerate. It is assumed that this self-preserving phase has been reached when i) the

21

transverse profiles of vertical velocity and buoyancy are similar at all depths, and ii) the rate of entrainment of fluid as a function of depth is proportional to the characteristic velocity for the same observed depth (Batchelor, 1954; Morton, Taylor, and Turner, 1956). As eddies on the boundary grow, and correspondingly more ambient fluid is entrained into the aft (top) of the cloud, the cloud evolves into an axisymmetric vortex ring, or spherical vortex described by Hill (1894). During this evolution, the distribution of buoyancy shifts from its original profile of a Gaussian-type, to one that is bimodal (due to the shift of the maximum from the center of the cloud to the centers of the vortex rings when looking at a two-dimensional cross section of the spherical vortex). The spherical vortex continues to entrain fluid and re-entrain particles from the stem (particles that were not originally incorporated into the cloud; this will be developed in more detail later) down through the center of the cloud, and an upflow exists on the outside of the cloud. This leads to greater horizontal spreading, or flattening, of a particle cloud, and causes the cloud to resemble an upside-down mushroom-shaped thermal.

Ruggaber (2000) demonstrated that the thermal phase of particle clouds can also be subdivided into what he called "turbulent thermals" and "circulating thermals." These two regimes correspond to the absence and presence of the spherical vortex, respectively, in the transition discussed above. For non-cohesive sediment, this evolution is marked by the change from large growth rates ($\alpha = 0.2$ to 0.3), where α is the entrainment coefficient, to linear growth rates ($\alpha \sim B/K^2$) consistent with buoyant vortex ring theory (where B is the buoyancy of the particle cloud; and K is the cloud circulation). The transition was observed when the radius of the particle

cloud had reached a value four times greater than its initial pre-release radius (Ruggaber and Adams, 2000). Thermal and buoyant vortex ring theory (including the entrainment coefficient) is explained in more detail in Chapter 2.

3. Dispersive or Particle-Settling Phase:

In the final phase of convective descent, the deceleration of the particle cloud eventually reduces the descent velocity of the thermal to a value comparable to the settling velocity of individual particles within the particle cloud. As this occurs, the internal motion of the thermal is suppressed and insufficient to hold the particles in suspension, and the individual particles all move downward and "rain out" of the neutrally buoyant cloud at a nearly constant velocity. These settling particles are collectively called a "swarm" (Bühler and Papantoniou, 1991; 2001; Bush, Thurber, and Blanchette, 2003) or "cluster" (Slack, 1963; Bühler and Papantoniou, 1999) that is bowl-shaped and continues to expand due to the weak dispersive forces between adjacent particles (Rahimipour and Wilkinson, 1992) or to the shear induced outward diffusion of turbulence and lateral displacement flow caused by the wake of each particle (Bühler and Papantoniou, 2001).

This study focuses on the second phase, the thermal phase, of descent because of its applicability to a wide range of depths for open-water sediment disposal. The initial acceleration phase lasts for a short period of time, and the dispersive phase is reached for greater depths than those being investigated. In the self-preserving or thermal phase, most of the sediment is incorporated in the axisymmetric upside-down mushroom cloud, or self-similar "cap," or "parent cloud." However, some sediment is also contained in an irregular "trailing stem." Figure 1-3 shows the distinction between the parent cloud and

trailing stem using photographs taken during two different experimental trials. Although most sediment is incorporated into the parent cloud, the trailing stem is also of interest because this material is more easily dispersed by currents and waves; further, the concentration of pollutants may be higher than in the parent cloud due to the generally finer particle composition. The terms "parent cloud" and "trailing stem" will be used throughout the rest of this thesis to refer to the two distinct structures that make up a particle cloud.
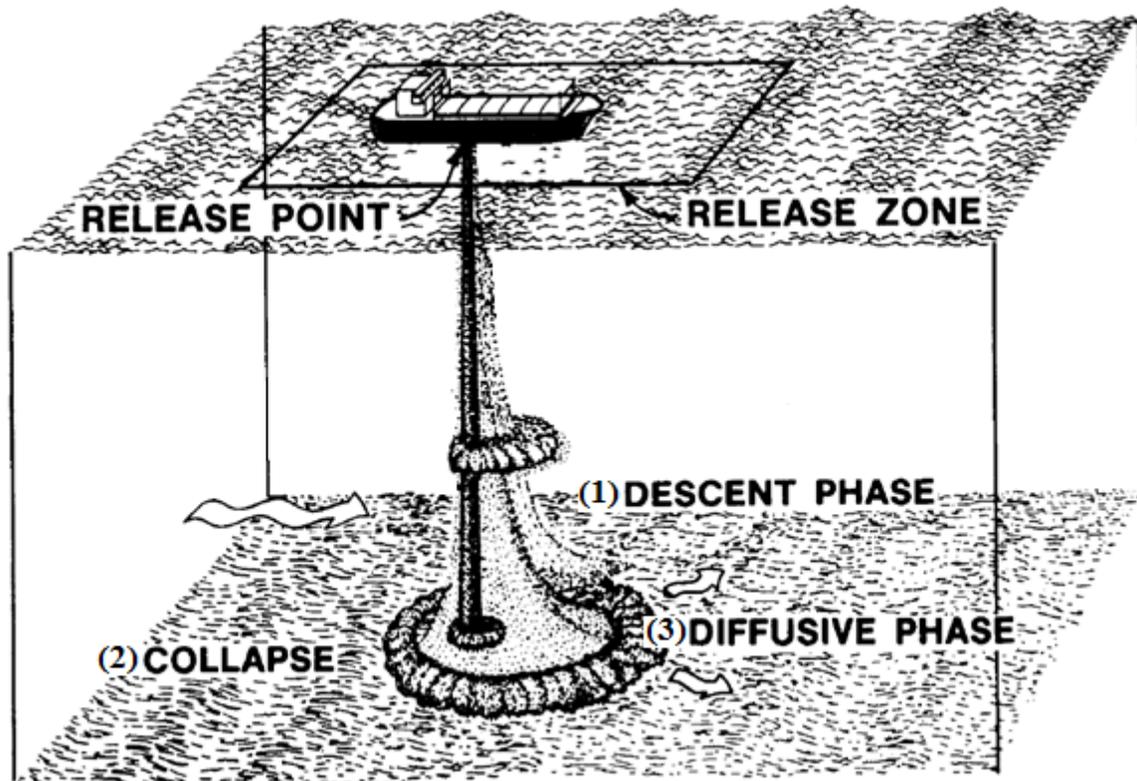
Figure 1-1: The three descent phases of particle clouds during open-water sediment disposal: convective descent, dynamic collapse, and passive diffusion (after Montgomery and Engler, 1986).
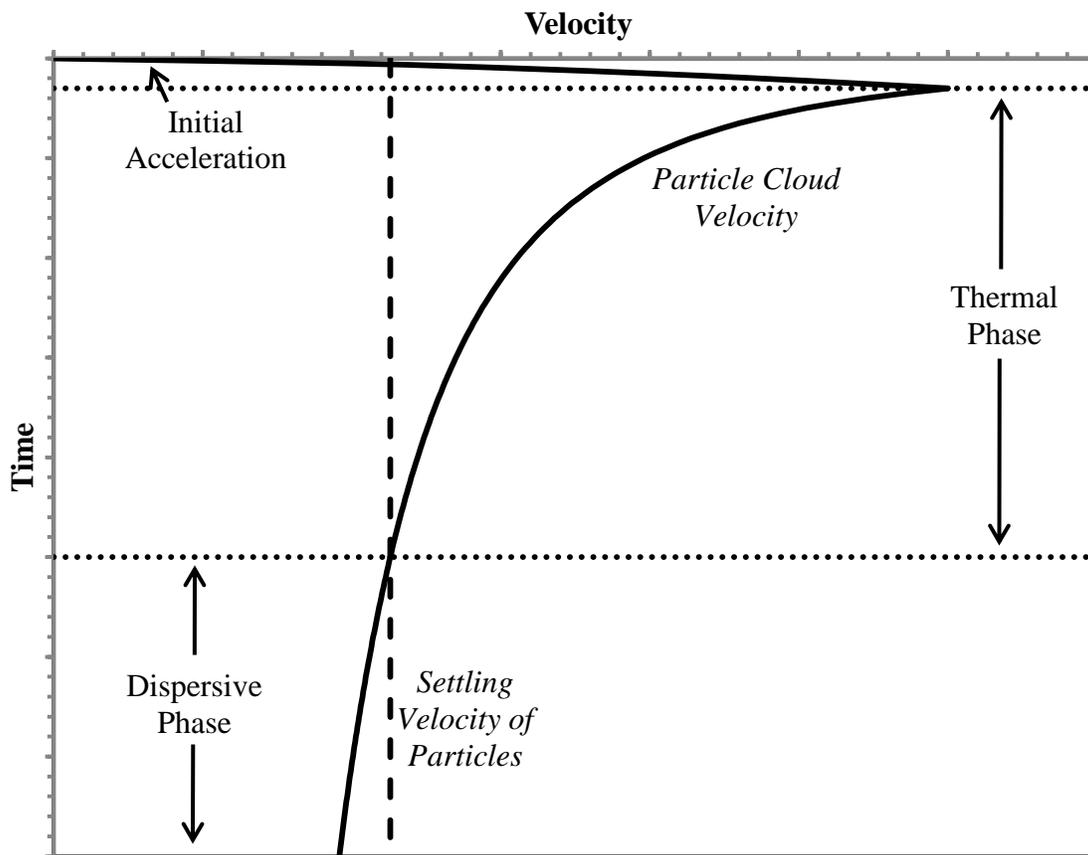
Figure 1-2: The descent velocity of an idealized particle cloud in the regimes of convective descent (after Rahimipour and Wilkinson, 1992; Ruggaber, 2000).
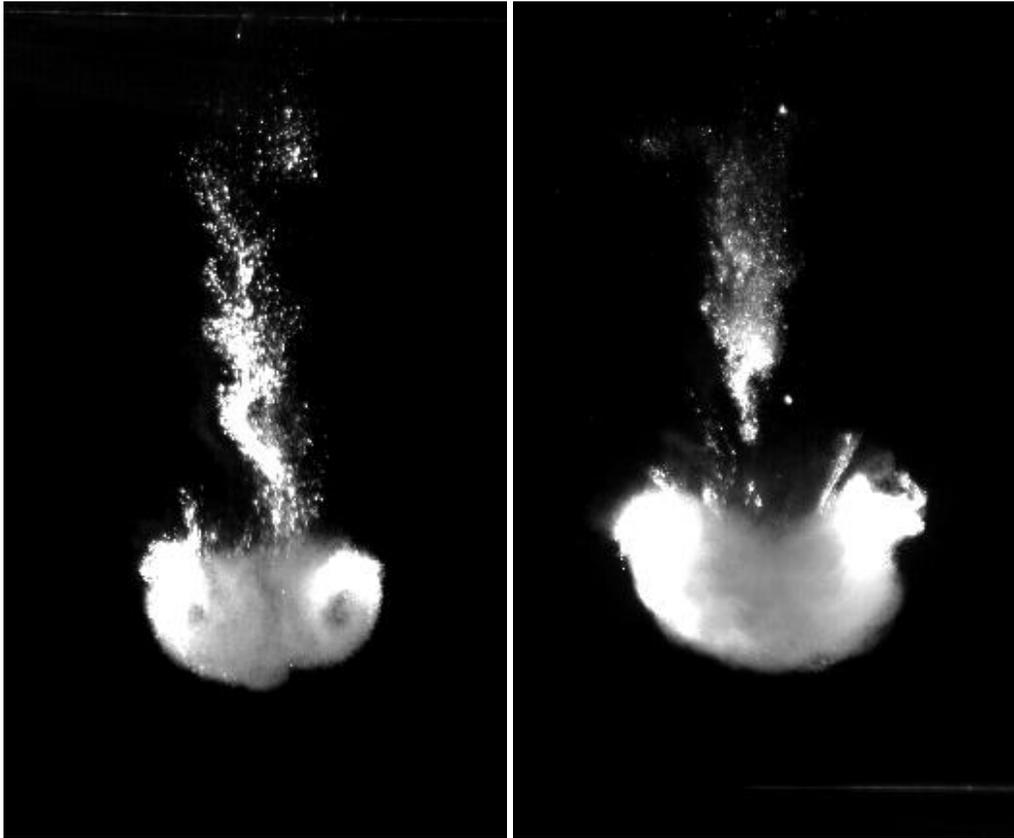
Figure 1-3: The different structures of a particle cloud in the self-preserving or thermal phase: the "parent cloud" (upside-down "cap" on the bottom of each image) and "trailing stem" (top). The particle cloud on the left is composed of larger particles than that on the right. Most of the sediment is usually incorporated into the parent cloud, but the trailing stem is of greater interest in this study because of its susceptibility to being dispersed by ambient currents.

1.3 Overview of Thesis Contents

This thesis will review thermals and buoyant vortex rings as they apply to particle clouds, and the methods used to relate the particle clouds created in the laboratory to the real world will be explained. Further, the following questions will be investigated:

- How do the release variables that are seen in the field (i.e., release height – initial momentum, water content – sediment moisture, and particle size and compaction) influence the creation of the self-similar thermal?

- How do self-similar particle clouds created in quiescent conditions compare to those in ambient currents? Is there a threshold above which the ambient current is too strong for the thermal to develop?

- Do the basic characteristics of particle clouds such as growth rate and descent depend on the release variables, and are these patterns consistent with and without the presence of ambient currents?

- Does an ambient current amplify the potential for more sediment to be left out of the parent cloud (therefore increasing the fraction of mass found in the trailing stem)?

- Can ambient currents increase the total sediment losses to the ambient environment? Do these losses originate from material that in the thermal phase of descent were originally within the parent cloud, the trailing stem, or both?

- Are losses to the water column consistent as a function of the magnitude of the ambient current? Are reasonably low percentages of particle cloud losses measured in similar time windows that are currently designated by regulatory agencies?

2 Theory and Background

This chapter provides additional information on previous studies of thermals, buoyant vortex rings, and particle clouds. Ruggaber (2000) performed a rigorous review of thermals, buoyant vortex rings, and particle clouds, and the historical (more than a decade since) literature review portions of the first three sections of this chapter largely summarize his work. Other sections and subsections provide additional details on laboratory particle cloud studies as they relate to open-water sediment disposal, as well as field cases that highlight the short-term fate of dredged material following open-water sediment disposal; the primary focus of the field cases that have been selected is on the aspect of their investigations which concentrated on quantifying sediment losses.

2.1 Thermals

Because the second phase of convective descent for particle clouds resembles the classical thermal, it is pertinent to review the theory of classical thermals and studies of them which have been performed in the recent past.

2.1.1 Theoretical Analysis of Thermals

A number of researchers have analyzed thermals using numerical models that are formulated on the basis of the conservation equations (i.e., mass, momentum, and buoyancy), including Koh and Chang (1973), Li (1997), and many others. Koh and

Chang (1973) implemented an integral analysis by treating the thermal as a descending, expanding control volume, and in doing so, arrived at the following conservation equations:

Conservation of Mass:

$$\frac{d}{dt}\left(\rho r^3\right) = 3\alpha\rho_a r^2 w \tag{2-1}$$

Conservation of Momentum:

$$\frac{d}{dt}\left(V\left[\rho + k\rho_a\right]w\right) = B - 0.5\rho_a C_D \pi r^2 w^2 \tag{2-2}$$

Conservation of Buoyancy:

$$\frac{d}{dt}B = \frac{d}{dt}\left(V\left[\rho - \rho_a\right]g\right) = 0 \tag{2-3}$$

where ρ is the density of the thermal; ρ_a is the density of the ambient fluid; r is the thermal radius; w is the mean descent velocity of the thermal centroid; α, k, and C_D are the entrainment, added mass, and drag coefficients, respectively; V is the thermal volume; B is the thermal buoyancy; and g is the gravitational constant. Equation 2.1 makes Sir Geoffrey Taylor's basic entrainment assumption that the mean inflow velocity is proportional to w, and Equation 2.3 assumes that no buoyancy is lost to the environment outside the control volume (e.g., the thermal wake). If the densities of the thermal and the ambient fluid are assumed to be approximately equal (i.e., a Boussinesq approximation), and if $w = \frac{dz}{dt}$, then:

$$r = \alpha z \tag{2-4}$$

where z is the vertical position of the particle cloud's center of mass. The continuity equations and entrainment assumption result in a linear relationship between the thermal radius and its vertical position.

By building upon the dimensional analysis solutions by Batchelor (1954), the following similarity solutions were derived by Turner (1973) by neglecting viscosity and pressure for an axisymmetric turbulent thermal suddenly released into an environment of a uniform density:

$$
\left.
\begin{array}{c}
r = \alpha z \\[2mm]
w = \left(\dfrac{B}{\rho_a}\right)^{\frac{1}{2}} z^{-1} f_1\left(\dfrac{\boldsymbol{r}}{r}\right) \\[4mm]
g' = \left(\dfrac{B}{\rho_a}\right) z^{-3} f_2\left(\dfrac{\boldsymbol{r}}{r}\right)
\end{array}
\right\}
\qquad (2\text{-}5)
$$

where $\boldsymbol{r}$ is the vector position from a vertical line below the source (axis of symmetry); g' is the modified gravitational constant, $\left(\dfrac{\rho-\rho_a}{\rho_a}\right) g$; and f_1 and f_2 are profile functions. By once again setting $w = \dfrac{dz}{dt}$ and also neglecting the distribution of velocity and buoyancy within the thermal, the following time dependencies are realized:

$$
r \sim \alpha \left(\frac{B}{\rho_a}\right)^{\frac{1}{4}} t^{\frac{1}{2}}; \quad w \sim \left(\frac{B}{\rho_a}\right)^{\frac{1}{4}} t^{-\frac{1}{2}}
\qquad (2\text{-}6)
$$

Using a simplified model, both Wang (1971) and Escudier and Maxworthy (1973) derived solutions to the three conservation equations for the initial accelerating motion and final decelerating motion of a buoyant thermal. In both investigations, the asymptotic solutions were conceived by first non-dimensionalizing the length ($\tilde{r}$), time ($\tilde{t}$), and velocity ($\tilde{w}$) scales:

$$\tilde{r} = \frac{r}{r_o}$$

$$\tilde{t} = t \left(\frac{g\Delta_o \alpha}{r_o}\right)^{\frac{1}{2}} \qquad\qquad (2\text{-}7)$$

$$\widetilde{w} = w \left(\frac{\alpha}{r_o g\Delta_o}\right)^{\frac{1}{2}}$$

where Δ_o is the initial buoyancy, $\frac{\rho_o - \rho_a}{\rho_a}$; and r_o is the initial length scale. By neglecting

the drag forces and invoking the same assumption as made in Equation 2.3 for a spherical

thermal, Escudier and Maxworthy (1973) reported the asymptotic solutions shown below:

Short times: $(\tilde{r} - 1) \ll 1$

$$(\tilde{r} - 1) \approx \frac{\tilde{t}^2}{2(1+k)-\Delta_o} \; ; \quad \widetilde{w} \approx \frac{\tilde{t}}{1+k-\Delta_o} \qquad (2\text{-}8)$$

Long times: $(\tilde{r} - 1) \gg 1$

$$(\tilde{r} - 1) \approx \frac{\tilde{t}^{\frac{1}{2}}}{2(1+k)^{\frac{1}{4}}} \; ; \quad \widetilde{w} \approx \frac{\tilde{t}^{-\frac{1}{2}}}{2^{\frac{3}{4}}(1+k)^{\frac{1}{4}}} \qquad (2\text{-}9)$$

When Equation 2.9 is returned to dimensional form, it is similar to Equation 2.6, except

for the presence of constants and the inclusion of the added mass coefficient. The result

is below:

$$r = \left(\frac{3\alpha B}{4\pi\rho_a}\right)^{\frac{1}{4}} \frac{t^{\frac{1}{2}}}{2(1+k)^{\frac{1}{4}}} \; ; \quad w = \left(\frac{3B}{4\pi\rho_a}\right)^{\frac{1}{4}} \frac{t^{-\frac{1}{2}}}{(2\alpha)^{\frac{3}{4}}(1+k)^{\frac{1}{4}}} \qquad (2\text{-}10)$$

Baines and Hopfinger (1984) performed a study on thermals with large density

differences (i.e., the density of the thermal and the ambient fluid are not equal), thus

removing the linear correlation between the thermal radius and vertical position. The

relationship they developed specifically includes a ratio of densities:

$$r = \alpha z \left(\frac{\rho_a}{\rho}\right)^{\frac{1}{3}} \tag{2-11}$$

The inclusion of and dependence of the thermal radius on the ratio of the ambient density to the thermal density is due to the high rate of entrainment of ambient fluid. As a result, the Boussinesq approximation is reached nearly immediately after the release of a thermal; Baines and Hopfinger concluded from theoretical and experimental analyses that for a dense thermal, the Boussinesq approximation was reached after the descent of approximately four initial radii (and even sooner for a rising, light thermal).

2.1.2 Laboratory Studies of Thermals

The principal experiments on buoyant thermals concentrated on light thermals in the 1950s and 1960s as researchers were motivated to understand the fluids of meteorological phenomena such as heat convection; later, dense thermals were also investigated for the purpose of understanding the descent of dredged material. For these studies that specifically analyze particle clouds, details of the investigations are included in Section 2.3. However, dense thermals can also be created with dense solutions such as brine. This was done by Richards (1961) when he released a thermal of brine from a hemispherical cup into a step-stratified mix of freshwater and salt water. Using dimensional analysis, Richards associated its descent and entrainment as follows (for while the thermal remained in the upper, freshwater layer):

$$z^2 = c_1 \alpha^{-\frac{3}{2}} \left(\frac{B}{\rho_a}\right) t \tag{2-12}$$

The experiments recorded a wide range of entrainment values, from 0.13 to 0.50. Further, Richards concluded that there was not any evidence of a relationship between the

configuration of the release and the resulting value of α, but that the speed of the inversion of the release cup did affect the resulting α. Particularly, at times if it was slow enough to induce more of a pour-like condition, then a plume resulted instead of a thermal. However, for this wide range of entrainment values, he found that $c_1 = 0.73$ for nearly all of the thermals he produced in the given set of experiments. Turner (1964) confirmed that the dependence of c_1 on α is small, finding a value of 0.69, but reported a slight dependence on the shape and angle of spread of the thermal and added mass coefficient.

2.2 Buoyant Vortex Rings

The evolution of a particle cloud from, using terms that Ruggaber (2000) coined, the "turbulent thermal" to the "circulating thermal" includes the formation of a buoyant vortex ring. These have been studied for more than a century; hence, the pertinent details of them are included in this section. A photograph of the two-dimensional cross-section of a vortex ring is shown in Figure 2-1 as a reference.

2.2.1 Theoretical Analysis of Buoyant Vortex Rings

The discussion of thermals above focused on the sudden release of buoyancy into a less dense ambient. Buoyant vortex rings also progress under the influence of buoyancy, but in addition to buoyancy, they also require momentum, or impulse (I), and circulation (K) to be initiated. Lamb (1932) performed a rigorous mathematical review of the hydrodynamic impulse and circulation of many varieties of vortices, including the vortex ring. These mathematical expressions can be used to deduce characteristics of the
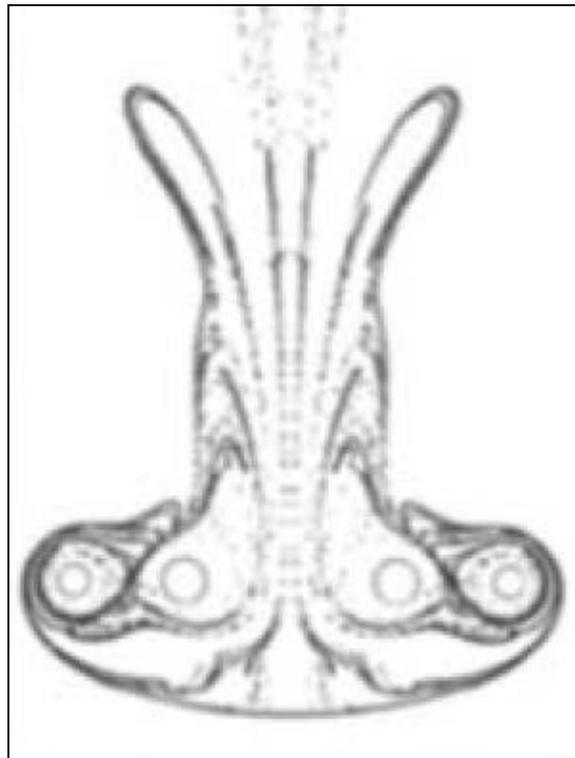
Figure 2-1: Two-dimensional cross-sections of vortex rings; the top figure is a photograph (Yamada and Matsui, 1978) and the bottom image is a computational figure (Shariff, Leonard, and Ferziger, 1989).

buoyant vortex ring, and one of note is the vertical velocity of the vortex ring, w_{vr}, which

Turner (1957) wrote by assuming similarity and is shown below:

$$w_{vr} = c\frac{K}{r} \tag{2-13}$$

where c is a constant that varies based on the shape of the vortex ring; and r is the mean

radius of the torus (equivalent to the previously defined radius of the thermal).

Saffman (1995) published an overview of vortex dynamics, which he hoped

would serve as an updated reference on vortex motion presented in Chapter VII of

Lamb's *Hydrodynamics* (1932). Saffman's review of vorticity and vortex rings, lines,

sheets, and patches is thorough, and he also included Hill's (1894) spherical vortex and

the axisymmetric vortex ring, which is of the most interest in this research. This is an

example of a vortex jump, where the vorticity is confined within a uniform sphere

translating through an ambient fluid; outside the sphere, flow is irrotational. When

determining the distribution of vorticity, one can assume that at a particular instant, the

origin of a cylindrical polar coordinate system, (b, θ, y), is at the center of the sphere,

and the distribution of vorticity, $\boldsymbol{\omega}$, is equal to $(0, \omega_\theta, 0)$. For a constant A:

$$\omega_\theta = Ab, \quad b^2 + y^2 < a^2; \qquad \omega_\theta = 0, \quad b^2 + y^2 > a^2 \tag{2-14}$$

where a is the radius of the sphere. From this, the velocity field can be determined,

which due to the axisymmetric characteristic of the spherical vortex, can be described

using a Stokes stream function. The pressure can be found using Bernoulli, and when an

additional pressure term, $2A\mu y$, is added inside the sphere to account for viscosity, the

velocity field also satisfies the Navier-Stokes equations both inside and outside the

spherical vortex.

2.2.2 Laboratory Studies of Buoyant Vortex Rings

Turner (1957) assumed a constant circulation and that the buoyancy increases the impulse of a ring in a uniform ambient fluid. In addition to theoretically analyzing the velocity of a vortex ring, he formulated a new linear relationship between the radius and vertical location based on a new entrainment coefficient:

$$r = \alpha' z \tag{2-15}$$

or

$$\alpha' = \frac{F}{2\pi c K^2} \tag{2-16}$$

where F is the ratio of buoyancy to the density of the ambient fluid and remains constant. This complicates the entrainment, since the circulation is actually produced by the buoyancy, thus making assumptions such as a uniform environment and constant circulation convenient. Realistically, this only applies well after the initial acceleration phase when a thermal has reached the circulating thermal phase. Turner produced vortex rings in experiments in a glass tank with a depth of approximately 1.52 m by forcing dyed fluid into the tank. He found values of c that ranged between 0.13 and 0.27, and observed that the motion became stable at a density difference of 4 %. These experimental results were visited again by Turner (1960) for further analysis with vortex pairs, particularly experiments which he had also previously performed in stratified environments. These experiments had an increased density difference as high as 18 % (Turner, 1957).

Maxworthy (1974) used a piston to eject a finite mass of fluid through a sharp-edged orifice. This created a turbulent vortex ring, which Maxworthy determined had an entrainment coefficient with a value of 0.011 ± 0.001. He also found that the effective

drag coefficient for an equivalent spherical volume was 0.09 ± 0.01. Maxworthy believed that both of these experimental results were independent of Reynolds number.

In a second set of experiments designed to analyze vortex rings at high Reynolds number ($Re = 10^3$ to 10^5), Maxworthy (1977) used both flow visualization and laser-Doppler techniques in a larger tank with a length of 2 m. He found that the formation process was actually highly Reynolds number dependent, and additionally, made qualitative observations of the "organization" of the vortex core which heavily influenced the growth of the vortex ring. The "well-organized" rings, with the clear core and outer-flow interfaces, experienced lower growth rates ($\alpha = 0.001$). The "disorganized" rings had entrainment values more than an order of magnitude larger ($\alpha = 0.015$), and Maxworthy hypothesized that this was due to the relative level of turbulence between the vortex ring and the ambient fluid.

Sau and Mahesh (2008) numerically simulated the dynamics of vortex rings when injected into a cross-flow, with an interest in fuel injectors, turbojets, and other high velocity injectors. When compared to the quiescent ambient condition, in a cross-flow a coherent vortex ring lost its symmetry or did not form at all, depending on the velocity ratio and the stroke ratio. The velocity ratio is defined as the ratio of the average nozzle exit velocity to the free stream cross-flow velocity; the stroke ratio is defined as the ratio of the stroke length to the nozzle exit diameter (i.e., an aspect ratio). Below velocity ratios of approximately two, a vortex ring was not formed, but instead, a hairpin vortex formed. Above velocity ratios of two with a low stroke ratio, a coherent asymmetric vortex ring was formed; however, for larger stroke ratios the vortex ring was trailed by a column of vorticity. In both cases, the vortex ring adopted a "tilt." In the former case,

the vortex ring tilted downstream, whereas in the latter case with the trailing vorticity, the vortex ring tilted upstream. In general, Sau and Mahesh also confirmed that a larger stroke ratio enhanced mixing and entrainment, which was partially due to the trailing vorticity.

2.3 Particle Clouds

Particle clouds have been studied both experimentally in the laboratory and with numerical modeling. In the past two decades, the focus has remained finding a greater understanding of the behavior of particle clouds (e.g., growth and circulation) and the transition depths between their different phases. Summaries of many of these investigations are included in this section.

Tamai, Muraoka, and Murota (1991) studied two-dimensional (i.e., line) releases of particle clouds which result from split-hull barges in the field. They used a mixed sand that was composed of two uniform grain sizes, a fine sand (d_{50} = 0.15 mm) and a coarse sand (d_{50} = 3.38 mm). The sand was dumped from an acrylic box with a width of 5 *cm* and an opening time of 0.3 *s* into a flume. When the mixture was released together, the coarser sand settled on the bottom while the finer sand remained in suspension and formed what the authors called a "turbidity cloud." Additional experiments studied releases with only the coarse sand and found that qualitative characteristics such as the linear growth rate and descent velocity as a function of time were similar to turbulent thermals formed by an instantaneous discharge of buoyancy.

Rahimipour and Wilkinson (1992) analyzed particle clouds using sheet illumination in order to expose the internal structure of particle clouds composed of

graded sand ranging in diameter from 0.150 *mm* to 0.350 *mm*. Various experiments were performed to capture the descent velocity of particle clouds composed of different particle sizes and initial volumes, and the authors found that these velocities were comparable to those found for a miscible thermal of the same size and buoyancy. These comparisons were based on the use of the cloud number, which Rahimipour and Wilkinson defined as the ratio of the individual particle settling velocity to the characteristic thermal descent velocity; the cloud number is shown in its "local" form below:

$$N_c = \frac{w_s R}{\left(B/\rho_a\right)^{1/2}} \tag{2-17}$$

where w_s is the settling velocity of the individual particles; R is the local radius of the particle cloud (i.e., at a particular time or depth); B is the buoyancy of the particle cloud; and ρ_a is the density of the ambient fluid. The descent velocities were most similar for a particle cloud and a miscible thermal for small values of the cloud number, N_c. However, as the cloud continued to descend (and the local cloud number increased with the size of the cloud), and particularly following the raining out of individual particles, there was a greater discrepancy between the velocity of the "swarm" and that of a miscible thermal.

Using this information, Rahimipour and Wilkinson developed the following relationship between the entrainment coefficient and the cloud number:

$$\alpha = 0.31\left(1 - 0.44N_c^{1.25}\right) \quad for\ N_C < 1 \tag{2-18}$$

The relationship above fulfilled the authors' observation that for small values of the cloud number ($N_c < 0.3$), the growth and entrainment rates of particle clouds was the same as for miscible thermals (nearly constant), but entrainment decreased with increasing cloud

number; this was specifically observed when $N_c > 1$. Once the cloud number was greater than 1.5, the growth slowed enormously. Thus, in the final phase a cloud's radius can be described by the following relationship:

$$R = 1.5 \left(\frac{B}{\rho_a}\right)^{1/2} \frac{1}{w_s} \quad for\ N_c > 1.5 \tag{2-19}$$

Noh and Fernando (1993) investigated the two-dimensional characteristics of particle clouds released into water to determine the transition between which particle clouds form a descending thermal and individual particles settle as a swarm. Particles were released using a two-dimensional funnel that was triangular in cross section but was 15.3 *cm* in length, therefore creating a two-dimensional particle cloud (i.e., a line release). Glass beads and 50 *ml* of water with fluorescein were added to the funnel and released into a rectangular tank with a depth of 111.9 *cm*. The particles had mean diameters of 0.080 *mm*, 0.240 *mm*, 0.510 *mm*, and 0.720 *mm*. The authors found that, initially, the particle/fluid mixture created a particle cloud resembling a thermal, but eventually, the particles settled out of the dyed water, creating a bowl-shaped swarm. Meanwhile, the fluid cloud showed signs of decaying turbulence and vortices.

The authors found that for experiments with the various particle sizes, the transition between the self-similar thermal and dispersive phases of descent occurred at a critical fallout depth, z_f, which is defined by:

$$\frac{z_f w_s}{\nu} \sim \left(\frac{Q}{\nu w_s}\right)^{\alpha} \quad with\ \alpha \cong 0.3 \tag{2-20}$$

where Q is the total buoyancy of the particle cloud; ν is the kinematic viscosity of the ambient fluid; and z_f is the depth measured from the surface to the frontal position of the particle cloud (leading edge of descent, i.e., the deepest portion of the cloud). Noh and

Fernando speculated that previous assumptions about the transition being wholly dependent on particle size, or of a related quantity, that determines the particle settling velocity, were incomplete. The authors hypothesized that the accepted transition between the second and third phases of convective descent, when $w_c \sim w_s$, where w_c is the descent velocity of the particle cloud, can fluctuate around this approximation in the presence of ambient turbulence or fluid motion. This would theoretically allow a particle cloud to remain in the thermal phase when $w_c < w_s$, but this could not be observed in this study.

Johnson and Fong (1995) carried out experiments using sand, silt, clay, and fine crushed coal at the U.S. Army Corps of Engineers' Waterways Experiment Station by modeling a split-hull barge and hopper dredge on a 1:50 scale. By performing tests in water depths ranging from 0.61 m to 1.83 m and focusing on the phase following convective descent, dynamic collapse, the authors developed a numerical model called STFATE (Short-Term FATE). This model made widespread revisions to a previous mathematical model originally developed by Koh and Chang (1973). STFATE can be used for calculating the water column concentrations and bottom deposition that result from the disposal operations of dredged material. The authors concluded that STFATE reproduced the fate of dredge material disposed in open water with an acceptable error. They found that the average simulated and measured descent speeds had percentage differences less than 25 %, and the average bottom surge speeds varied by approximately 10 %. The model also calculated that 2 to 3 % of the original material for silt and clay disposals was stripped from the parent cloud during descent.

Li (1997) performed a numerical study that investigated the motion induced by a finite release of particles that are heavier than the stagnant fluid into which they are

released by using a three-dimensional numerical model that was based on the conservation of mass, momentum, and density excess. The model was valid as long as the particles could be characterized by a single, continuous field of density difference with a specific settling velocity, and also assuming that the Boussinesq approximation was valid. Using the cloud width as the length scale for the mixing length, Li's model reproduced the bimodal distribution of buoyancy, but only for particle sizes ranging from 0.15 *mm* to 0.30 *mm*. For larger particle sizes (0.6 mm to 1.18 mm), coherent vortex rings were not simulated by the model.

Ruggaber (2000) performed flow visualization experiments using silt and non-cohesive glass beads of various sizes that were released quasi-instantaneously into a glass tank nearly 2.5 *m* deep. His focus was to study how realistic modes and variables of sediment disposal operations (e.g., particle size, water content, and initial momentum) affected cloud behavior (i.e., particle cloud descent velocity, growth rate, and loss of particles) and the entrainment (α), drag (C_D), and added mass (k) coefficients as a function of time. By holding the dry release mass constant (40 g), he was able to use the laboratory release volume and realistic volumes in field operations to scale the particles to field size by employing the cloud number (more on the specifics of this scaling is explained in Section 0). Ruggaber found that the releases of cohesive sediment produced a wide range of growth rates, but the non-cohesive releases closely following the theoretical phases of convective descent. Initially, thermals were promptly developed, which was followed by an asymptotic deceleration and large growth rates ($\alpha =$ 0.2 to 0.3). Then, the growth slowed greatly once the circulation increased,

48

corresponding to the presence of a buoyant vortex ring. For large particles ($N_c > 10^{-4}$), the growth was reduced to $\alpha = 0.1$ to 0.2.

Ruggaber also used his experimental results to calibrate an "inverse" integral model which employed the conservation equations in order to find α and k using measured data from the particle cloud experiments (i.e., descent velocity and radius). He found that in the thermal phase, C_D and k are nearly zero. Conversely, once particle clouds transitioned to a "circulating thermal," the significant reduction in growth, α, caused by larger particles (when the cloud number is greater than 10^{-4}), increased k to a value similar to a solid sphere. These results demonstrated that constant values are appropriate for smaller particle sizes, but when $N_c > 10^{-4}$, time varying coefficients are required to properly document the cloud behavior. Ruggaber was also the first to quantify the difference between the parent cloud and trailing stem using a sediment capture mechanism that he suspended within the tank, and this will be discussed more in the next section.

Bühler and Papantoniou (2001) presented methods that predicted the growth and velocity of particle clouds for both the thermal and swarm regimes of decent. In addition to using theoretical relationships, experiments were performed to determine the constants in these relationships. These experiments were carried out in a tank with a depth of 1.1 *m* by releasing particles through a funnel positioned near the water surface. These particles ranged in size for one series of tests from 1.5 *mm* to 2 *mm*, and for a second series of tests they ranged from 2 *mm* to 3 *mm*. The particle clouds were illuminated from below using a light sheet, and tests were performed with different thermal buoyancies (i.e., different

initial mass of particles). The front velocity and width of the particle clouds were determined by using video frames that were captured at intervals of 4/25 *s*.

For their theoretical analysis, Bühler and Papantoniou retained earlier expressions that the transition between the thermal and swarm stages occurred when the velocity of the particle cloud front is comparable to the settling velocity of individual particles:

$$w_f = c_s w_s \tag{2-21}$$

where w_f is the velocity of the front of the particle cloud; and c_s is a constant found with experiments; the experiments described above determined this value to be 1.4. When Equation 2-21 is used, the authors expressed the transitional depth between descent regimes as:

$$z_f = \frac{c_T}{c_s w_s} \left(\frac{B}{\rho_a}\right)^{1/2} \tag{2-22}$$

where c_T is a constant (equal to 2.6 for a spherical shape and 2.94 for a spheroid shape).

Bush, Thurber, and Blanchette (2003) conducted experiments by releasing heavy particles (i.e., glass spheres ranging in size from 0.002 cm to 0.1095 cm) into both homogeneous and stratified ambient environments (i.e., a cylindrical tank with a depth of 90 cm that was filled with either water or salt water with a linear stratification). Particle releases had various dry weights from 0.2 *g* to 50 *g* and also contained small amounts of water (5 ml to 10 ml). Flow visualization was enhanced using food coloring dyes and fluorescein. For the releases performed in the homogeneous ambient, the investigators found that the particle clouds evolved into the three clear phases of a classical fluid thermal discussed in Chapter 1. Although the transition between the initial acceleration phase and self-similar thermal phases was not initially clear, the transition between the

second phase and the dispersive phase was obvious. The second transition was quantified

using the particle Reynolds number, Re_p, which the authors defined as:

$$Re_p = \frac{w_s r_s}{\nu} \tag{2-23}$$

where r_s is the radius of the individual particles. For values in the range of 0.1 to 300, the

fallout height of individual particles in the dispersive phase into the bowl-shaped swarm

(measured depth since release), z_f, was found to be:

$$\frac{z_f}{r_s} = (11 \pm 2) \left(\frac{Q^{1/2}}{w_s r_s} \right)^{5/6} \tag{2-24}$$

For higher particle Reynolds numbers ($Re_p > 4$), the relationship could be simplified and

depended exclusively on the number and size of particles released, and it assumed the

form:

$$z_f = (9 \pm 2) r_s N_P^{1/2} \tag{2-25}$$

where N_P is the number of particles released.

Bush et al. also found a correlation between initial buoyancy (in the form of total

initial payload, or mass of particles released), and the length of the initial acceleration

phase. Although the rate of growth or expansion of the cloud is ultimately independent

of the initial payload mass ($\alpha \sim 0.25$), when comparing trials with initial masses ranging

from 1.0 g to 20.0 g, the latter cases traveled a greater distance z from the point of release

for the thermal-like flows to be established. The authors concluded that the entrainment

coefficient α had no dependence on the Rayleigh number and potentially had a weak

dependence on the particle Reynolds number (they also suggested that it could be

approximated by a mean constant value, even with its dependence on N_c). Bush et al.

also measured the descent of the cloud and were able to normalize the descent velocity with respect to the settling velocity of individual particles as a function of initial buoyancy, as seen below:

$$\frac{W}{w_s} = C_2 \; \frac{Q^{1/2}}{zw_s} \tag{2-26}$$

where W is the measured cloud descent at two depths, $z = 30$ *cm* and $z = 50$ *cm*. In the thermal phase, $C_2 = (3.0 \pm 0.4)$, but in the swarm phase the descent is independent of buoyancy and wholly a function of the independent particle settling velocity.

Dong et al. (2007) used the STFATE model discussed earlier to simulate the deposition, dispersion, and accumulation of a muddy dredged material removed from Kaohsiung Harbor, Taiwan. The authors included four primary input parameters to accomplish this: 1) water quality and bottom information; 2) dredged mud characteristics; 3) equipment used on the disposal vessel; and 4) physical and chemical properties of the ambient water. Aerial photographs were also taken of the site to calibrate the mathematical model. The dredged mud was disposed at a site where the water depth was 500 *m*, and disposal operations used two disposal durations: 20 *s* for a fixed disposal site and 1200 *s* for a mobile site. When compared to the longer disposal duration, the authors found that the shorter disposal time resulted in a reduced dispersion influence distance from the disposal site, but a second consequence of the shorter disposal time was a longer recovery time for the water body to return to its original state. Thus the impact of the 20 *s* disposal on the seawater quality in the immediate areas was less severe but for a longer duration than the 1200 *s* disposal duration with the faster dispersion but larger geographical impact. When these trends from the field data were compared with the

simulations from STFATE, an average error of 27.8 % was recorded. The errors for the dispersion length and area were less than this average, with values of 23 % and 22 % respectively, but the dispersion width had errors ranging from 10 to 67 %. The authors attributed the extreme errors to the lack of the photographs' ability to capture the diluted mud clouds from the air.

Gu, Huang, and Li (2008) performed an experimental study on unsorted particle clouds being discharged into a cross-flow. Experiments simulated the discharge of sand from a bottom-dump barge by instantaneously releasing particles ranging in size from 0.15 *mm* to 1.18 *mm* into an open channel with a water depth of 0.3 *m*. The velocity of the cross-flow ranged from 8.96 *cm/s* to 26.88 *cm/s*. The investigators found that particle clouds in cross-flows can exhibit significant differences when compared to the stagnant ambient case, which was done by analyzing the descent of the leading edge of the cloud, Z_{le}, and the longitudinal width of the cloud between the left-most and right-most longitudinal edges, L_{le}, in their non-dimensional forms, $Z_{le,n}$ and $L_{le,n}$, which are shown below:

$$Z_{le,n} = \frac{Z_{le}}{l_s} \; ; \quad L_{le,n} = \frac{L_{le}}{l_s} \qquad (2\text{-}27)$$

where $l_s = V^{1/3}$; and V is the initial volume of sand that is released. Gu et al. found that the size (i.e., longitudinal width) of the particle cloud increased under the influence of a cross-flow (and increased with increasing magnitude of the cross-flow). They concluded that two reasons for this were: 1) the cross-flow damaged or destroyed the double vortices, and 2) it enhanced the mixing of the particle cloud with the ambient fluid. As a consequence of the increased mixing, the descent of the particle cloud was reduced because of the decrease in the density difference between the particle cloud and the

53

ambient. The authors hoped that their experimental results could be used to calibrate a numerical model, but this was not discussed in any further detail.

2.4 Short-Term Fate of Dredged Material

This section presents a number of investigations that have taken place in both the field and laboratory in an attempt to quantify the amount of dredged material (represented as a percentage of the initial release mass or volume) that is lost during disposal to the water column. This aspect of the study of particle clouds is the most applicable to open-water sediment disposal because of the economic concerns of losing clean sediment that is being purposely dropped for applications such as land reclamation; obvious environmental concerns also exist due to the increase in turbidity and the possible spread of contaminants during contaminated sediment isolation.

2.4.1 Field Studies of Sediment Losses

An interest in the fate of dredged material, both short and long-term, has existed for several decades, and several of the historical cases are presented below:

- Long Island Sound

One of the earliest field studies on open-water sediment disposal was completed by Gordon (1974). The study included seven separate operations that all utilized the New Haven disposal site in Long Island Sound. The depth of the disposal site ranged from approximately 18 m to 20 m, and maximum near-bottom currents (2 m above the bottom) had measured velocities of 0.16 m/s (neap tides) to 0.30 m/s (spring tides). Although the volumes of the dumps ranged from 900 m^3 to 2300 m^3, the sediment was predominantly

(60 to 90 %) in the silt to clay-size range. Gordon used a transmissometer to measure suspended solids and estimated that 1 % of the total dredged material that was dumped by the scows remained in the water column as residual turbidity and was eventually dispersed over a significant distance. He found that 80 % of the original material settled within a radius of 30 *m* around the drop site, and 90 % was deposited within a radius of 120 *m*.

- San Francisco Bay

Another report was released by Sustar and Wakeman (1977) on the monitoring activities of disposal sites by Alcatraz, the Farallon Islands, and Carquinez. The Farallon Islands is a deepwater disposal site (depths greater than 180 *m*), and although no quantifiable data were taken from releases, photographs of the bottom indicate that most of the parent material impacted the bottom within a relatively small area (150 m by 300 m). At the Carquinez site, the water depth was approximately 14 *m* during disposal operations, with currents up to 0.25 *m/s*. Using transmissometers and other instruments, the total suspended solids that were unaccounted for during the dumping operations ranged from 1 to 5 % of the material released.

- Dredged Material Research Program Sites

Six sites were studied under the auspices of the U.S. Army Corps of Engineers' (USACE) Dredged Material Research Program (DMRP) by Bokuniewicz et al. (1978), including two sites in Long Island Sound and one deeper site off Seattle (approximately 60 m). By looking at a number of different release mechanisms, types of sediment, and site conditions, the authors concluded that the fraction of the original sediment that remained in suspension in the water column was generally very small. They observed

that the reason for this is that the sediment releases are most accurately described by a semi-continuous jet, which entrains such a large volume of ambient fluid that it is difficult for dredged material to escape into the ambient water column. Most of the lost sediment was material that never made it into the jet.

- New York Bight

The three previous case studies that have been highlighted used water-column sampling techniques to determine losses, but Tavolaro (1982; 1984) used a mass balance approach to determine the losses associated with dredging, transporting, and disposing of material in New York Harbor, where the disposal site resided at depths between 15 m and 25 m. The dredged material was composed of both maintenance and new material, for a total of 229 barge loads (over 600,000 m^3 of material). In order to calculate losses during disposal, volumes were converted to dry masses, and bathymetric data were taken before and after disposal operations. Tavolaro determined that 3.7 % of the original material was unaccounted for and never made it to the bottom of the disposal site.

- Duwamish Waterway

During a disposal demonstration in a depression in the Duwamish Waterway, Truitt (1986) used a mass balance to determine the fraction of the material that was transported out of the disposal area. The capping demonstration consisted of a single barge with approximately 840 m^3 of silty material being disposed in water with depths around 20 m to 21 m. Bottom currents had values up to 0.06 m/s, whereas the surface could reach 0.30 m/s. Truitt found that 7 to 14 % of the original material in the barge was transported out of the immediate vicinity of the drop zone or was unaccounted for, but that when only suspended solids are considered, 2 to 4 % of the original material was

transported well outside of the disposal area due to the "confining effects" of a depression on the bottom where the material was being dumped.

- Disposal Area Monitoring System, New England

In 1977, the New England District of the U.S. Army Corps of Engineers established the Disposal Area Monitoring System (DAMOS). The directive of this program is to continuously monitor all disposal operations that occur in the waterways under its jurisdiction, from Western Long Island Sound to Rockland, Maine. By using tools such as bathymetric data, sediment-profile imaging, and plan-view imaging surveys, the topography of the seafloor is analyzed before and after disposal operations (in both the short- and long-term). Examples of recent monitoring activities include checking marine life and benthic activity near a mound of disposed material on the seafloor at the New London Disposal Site in 2007 (AECOM, 2009a), as well as historical and new mounds on the bottom of the Portland Sound Disposal Site, also in 2007, which found a mix of organic activity depending on the age of the mound (AECOM, 2009b). Several historical cases directly investigated the fate of dredged material in Massachusetts Bay, Rockland, Maine, and again in Boston Harbor. These examples are listed next:

- Massachusetts Bay Deep Water Disposal Site

From 1982 to 1983, significant portions of Boston Harbor were dredged (both the Inner Harbor and President Roads), and this material was disposed of at the Boston Foul Ground – currently known as the Massachusetts Bay Deep Water Disposal Site. The material was discharged using both a hopper dredge and a clamshell/scow dredge in order to allow the New England District of the U.S. Army Corps of Engineers to investigate the feasibility of using hopper dredges in the New England region (SAIC, 1984). The

Massachusetts Bay Deep Water Disposal Site has a gently sloping bottom with a depth of 90 *m* at the northerly boundary, and this increases to a maximum of 93.5 *m* in a depression near the southern edge. Acoustic backscatter measurements were used to determine the amount of the original material that remained in suspension following disposal operations, and it was found that 40 minutes following disposal, the distribution of suspended material varied between concentrations of 5 *mg/l* and 12 *mg/l*. This was the equivalent of 3 % of the total material discharged by the hopper dredge.

- Rockland Disposal Site

The Rockland Disposal Site is located in the western portion of Penobscot Bay, and was first used between 1973 and 1974 for disposal of dredged material from Rockland Harbor. In 1985, the New England District of the U.S. Army Corps of Engineers commissioned a study to monitor the transport of dredged material during disposal operations; additional tasks included performing bathymetric and side scan surveys of the area in the immediate vicinity after 275,400 m^3 of material was disposed of from dredging in Searsport (SAIC, 1988). The water depths ranged from 65 *m* to 80 *m*, and the specific sediment transport study was performed throughout an entire tidal period and during a flood tide. Weather restricted the study from including monitoring during ebb tide as well. Three separate barges with volumes of 1205 m^3, 1450 m^3, and 2780 m^3 of a silty clay material were towed into the disposal site and discharged. Acoustic measurements were used again, and it was determined that the worst case scenario (performing disposal operations during maximum flood tide) resulted in 6 % of the original material being transported out of the disposal area. If disposal was distributed

evenly over the entire tidal cycle, then only 1 % of the original mass was estimated to be transported out of the disposal site.

- Historical Massachusetts Bay Disposal Sites

In 2008, the New England District of the U.S. Army Corps of Engineers investigated the potential for capping the historical Massachusetts Bay Disposal Sites, called the Boston Lighthouse Disposal Site and the Interim Massachusetts Bay Disposal Site (AECOM, 2009c). From the 1940s to the 1970s, industrial, radioactive, and construction waste and material were disposed of at these sites within metal drums. Their corrosion and potential leaks have caused concern and prompted the capping demonstration which sought to find a method to prevent an environmental clean-up operation. Because the condition of many of the drums is unknown, the USACE wanted to avoid a direct impact on the drums (the power of sediment disposals was proven with photographs of craters on the bottom) with the material being used for capping (clean sediment which was dredged from Boston Harbor). This required GPS coordinated dumps which aimed to land the capping material adjacent to the drums, and allowing the flank and apron of the material to eventually cover the drums. This process would be repeated until all the drums were submerged. This method called for highly accurate placement of the dredged material, and an interest still existed to maintain minimal losses to the environment; its feasibility remains under consideration.

2.4.2 Field Studies of Density Currents

The short-term fate of dredged material is not limited to material remaining in suspension in the water column or being swept away by ambient currents (events that

occur during the convective descent of a particle cloud), and in fact when particle clouds impact the bottom they may have the right characteristics for generating a density current. Density currents are bottom flows driven by the kinetic energy of the dynamic collapse of a particle cloud (i.e., when the particle cloud impacts the bottom it causes some particles to remain in suspension and be transported along the sea floor), and although this is the second phase of the descent of a particle cloud, it is important to differentiate this from immediate losses during its descent.

Several of the previous investigations that have been summarized acknowledged the presence of resuspension, but this was not always distinguished in the final tally of the percentage of the original material lost. One of the most thorough investigations of density currents was done by Drapeau, Gauthier, and Lavallée (1999). They focused on sediment and the point of impact at the bottom by considering four governing parameters: 1) the sediment grain size; 2) the water depth; 3) the volume of sediment disposed; and 4) the proportion of sediment that settles at the point of impact versus the sediment that remains in suspension. The last parameter is what is capable of forming a density current. Field studies were conducted at Rivière-du-Loup and Rimouski in the St. Lawrence Estuary and at Anse-á-Beaufils in the Gulf of St. Lawrence using sediment traps, current meters, and side scan sonar. Results varied, but in areas where the tidal currents approached 70 *cm/s* (Rivière-du-Loup) to 80 *cm/s* (Rimouski), at times near slack water (tidal currents of ± 2 cm/s), density currents with magnitudes of 50 *cm/s* were reached at Rimouski. Density currents were created only when a particle cloud impacted the bottom sufficiently early relative to when the descent velocity of the cloud would

approach the settling velocity of individual particles had the depth been infinite. Drapeau et al. quantified this with a kinetic energy index, K_{ei}, given below:

$$K_{ei} = 0.5(w_c - w_s)^2 \qquad (2\text{-}28)$$

For the various field sites, the authors were able to match this index with the proportion of sediment that formed into a density current. Because the descent velocity of a cloud decelerates as it descends, this value naturally decreased as water depth increased.

One aspect of the research being presented in this thesis in the following chapters is the distribution of mass between the parent cloud and trailing stem, which was carried out by analyzing the deposition traces of the particle clouds on the bottom. Potential losses to the ambient environment due to the ambient currents were also predicted using data collected in the same manner. This was done without any sediment on the bottom prior to sediment releases, thereby reducing the effect and potential for resuspension of bottom sediment due to the impact of the particle cloud, but theoretically density currents could still occur. However, as stated previously, the all encompassing focus of this study, the dynamics of particle clouds, remains completely within the realm of convective descent, and more information is provided in Chapter 4 on the analysis process and its results.

2.4.3 Laboratory Studies of Sediment Losses

In addition to the laboratory studies which have sought to understand the dynamics of particle clouds under conditions which closely resemble the environment during open-water sediment disposal, very few laboratory studies have attempted to quantify the losses during a release. In Section 2.3, the investigation that Ruggaber

(2000) performed concerning the dynamics of particle clouds was highlighted, but he also studied the distribution of mass between the parent cloud and the trailing stem. He did this by constructing a sediment trap, which was designed to allow the parent cloud to descend below it before closing a window-shade like device that captured the trailing stem for collection. Ruggaber focused his sediment trap experiments on particular sediment release conditions and placed the sediment trap at two different depths within the rectangular tank where he performed his experiments.

The first group of experiments focused on sediment releases above and below the water surface using four different particle sizes: 0.010 *mm* silt, 0.024 *mm* glass beads, 0.129 *mm* glass beads, and 0.264 *mm* glass beads. For each release, 40 *g* of a single particle size was mixed with 40 *cm³* of water and agitated so that the particles were put into suspension. The sediment trap was placed at depths of 13.3 *cm* and 36.8 *cm* below the release apparatus. For the above surface releases experiments, Ruggaber found that the percentage of the original mass which failed to be incorporated into the parent cloud and formed the trailing stem ranged from 1.6 ± 0.4 % for the largest glass beads to 7.9 ± 2.7 % for the silt; these measurements were made from the shallow sediment trap depth. For the below surface releases and the shallow sediment trap depth, the trailing stem was 21 ± 5 to 31 ± 7 % of the original mass, with no appreciable correlation between the mass of material in the trailing stem and the particle size. At the deep sediment trap depth for the below surface releases, the trailing stem was 8.4 ± 1.2 to 18 ± 4 % of the original mass, again without an appreciable correlation. Together, with additional experiments that mixed different particle sizes, Ruggaber concluded that there were no size-dependent "stripping" mechanisms of the parent cloud or trailing stem, but rather both were well

mixed and the trailing stem is a function of material that fails to be incorporated into the parent cloud immediately after the release. Further, the reason for the discrepancy in values between the shallow and deep sediment trap depths was that as the parent cloud decelerated and approached the settling velocity of individual particles, some of the particles in the trailing stem would actually be re-entrained as the trailing stem spread out vertically due to the parent cloud's descent.

In Ruggaber's second group of experiments, he focused on the release of dry and wet 0.264 *mm* glass beads from above the water surface. Similar to his first group, 40 *g* of particles was used but kept dry for the one set of experiments and mixed with 17 *cm³* of water for the wet experiments. The wet experiments allowed the particles to settle out of suspension prior to release. For this group of experiments, the shallow and deep sediment trap depths were 12.7 *cm* and 63.5 *cm* below the release apparatus, respectively. For the dry sediment releases, the trailing stem was 5.0 ± 0.7 % of the original mass when captured at the shallow depth and 5.8 ± 1.5 % of the original mass when captured at the deep sediment trap depth. For the wet sediment releases, the trailing stem was 1.6 ± 0.2 % of the original mass when captured at the shallow depth and 1.9 ± 0.4 % of the original mass when captured at the deep sediment trap depth. Ruggaber concluded that the presence of water in the sediment prior to release helped maintain the cohesion of the initial volume, therefore increasing the percentage of mass that initially makes it into the parent cloud. Given the standard deviations of the data, he concluded again that the mass present in the trailing stem was material that failed to be incorporated into the parent cloud, not particles that were stripped from the parent cloud.

In the final group of sediment trap experiments, Ruggaber focused on settled 0.264 *mm* glass beads released both above and below the water surface while mixing them with 42 *cm³* of excess water prior to release. By doing this, a "supernatant" layer of water was added above the particles, and he wanted to explore how much of this extra fluid was incorporated into the parent cloud. This is important because in the field, and particularly when using environmental dredges, a large amount of excess fluid is present with dredged material when disposed. To accomplish this, Ruggaber added 10 *g* of 0.010 *mm* silt to the 40 *g* of glass beads and the entire particle/fluid mixture was homogenized and allowed to settle for several seconds prior to release. During these experiments, only one sediment trap depth was used (63.5 cm), and he found that for the above water releases, 5.1 ± 1.7 % of the total mass of silt, or 7.0 ± 2.4 % of the silt in the supernatant, was captured and had failed to be incorporated into the parent cloud. For the below surface releases, 15 ± 2.3 % of the total mass of silt, or 20 ± 3.2 % of the silt in the supernatant, was captured and had failed to be incorporated into the parent cloud.

Ruggaber concluded that most of the excess water included with dredged material is incorporated into the parent cloud, and if contaminants are present, that they will also be transported to the bottom. One notable element of the data from this group of experiments and the first group of experiments was the dramatic increase in trailing stem material for below surface releases. Ruggaber attributed this to a "stalling effect" due to ambient fluid attempting to enter the release mechanism to maintain hydrodynamic equilibrium within the release cylinder while the release was still underway. He felt that in the field this problem would not be as pronounced because a barge would float higher

in the water as material was released, whereas in the laboratory the release apparatus was at a fixed depth below the surface.

2.5 Focus of Current Research

Ruggaber performed a thorough investigation on the distribution of material between the parent cloud and trailing stem, but as with his study on the dynamics of particle cloud, it was done in quiescent conditions. In Chapters 3 and 4, the methodology and results of the following three focal points of this investigation will be detailed:

- The thresholds between "weak," "transitional," and "strong" ambient currents, and the correlation between these thresholds and the creation of a self-similar thermal; this is a unique problem that presents itself only in the presence of ambient currents.

- The dynamics of particle clouds (i.e., cloud growth, descent, and translation) in ambient currents and notable differences of these characteristics in a flowing environment compared to the quiescent condition.

- Quantifying the mass of particles in the trialing stem versus the parent cloud when released in an ambient current of various magnitudes, and these results will be compared to the values Ruggaber tabulated.

3 Experimental Methods

This chapter discusses the experimental facilities, apparatus, and methods that were used to conduct the research on particle clouds in ambient currents.

3.1 Particle/Sediment Types

Particles of various sizes were used to represent non-cohesive sediment ranging from fine to coarse grain sizes, as well as clumps of cohesive sediment. The particles that were primarily used are glass beads manufactured under the trade name Ballotini Impact Beads by Potters Industries, Inc. (Malvern, Pennsylvania). These have an approximate density of 2.5 g/cm^3 and range in size from 0.045 mm to 0.850 mm. These glass beads were chosen for their uniformity and high reflectivity, therefore enhancing the visualization of the particle clouds (which will be discussed later in this chapter). The individual sizes of the glass beads were chosen for their similarity to sizes selected by Ruggaber (2000) to make comparisons more effective. Additional experiments were done with ground silica silt (SIL-CO-SIL from U.S. Silica Co., Berkeley Springs, West Virginia) with a density of approximately 2.65 g/cm^3 and diameter of 0.040 mm. The largest particles used, with nominal diameters that exceeded 2.0 mm, were non-spherical aquarium pebbles made of recycled glass by American Specialty Glass, Inc. (North Salt Lake, Utah), and these represented clumps of fine clays found in the real world. In all releases that were performed, 40.0 g of particles were used. Table 3-1 shows the basic

properties of the different particles used, and provides a designation for each that will be used throughout the rest of the this thesis.

Table 3-1: Particle types and sizes used to represent both particles and clumps of sediment in experiments modeling open-water sediment disposal.

Particle Name	Designation	Range of Diameters [mm]	Median Diameter, d_s [mm]	Density, ρ_s [g/cm^3]
Specialty Glass Clear Plate 0	SG 0	1.59 - 3.18	2.38	2.5
Specialty Glass Clear Plate 00	SG 00	0.794 - 1.59	1.19	2.5
Ballotini Impact Glass Bead A	A	0.600 - 0.850	0.725	2.5
Ballotini Impact Glass Bead B	B	0.425 - 0.600	0.5125	2.5
Ballotini Impact Glass Bead D	D	0.212 - 0.300	0.256	2.5
Ballotini Impact Glass Bead AE	AE	0.090 - 0.150	0.120	2.5
Ballotini Impact Glass Bead AH	AH	0.045 - 0.090	0.0675	2.5
SIL-CO-SIL 40 Silica	SIL	0.040	0.040	2.65

3.2 Sediment Release Conditions

In order to ground the research in the laboratory as much as possible with open-water sediment disposal in the field, realistic modes of sediment release were imitated. The following variables can be varied when releasing sediment in the laboratory, which relate to various states of release in open-water sediment disposal:

- Sediment type and size. As shown in Table 3-1, the current investigation used experiments with both silt and glass beads ranging in size from 0.040 *mm* to 3.18 *mm*. The large range is needed because in the field, not only does sediment change in size, but at times particles will "clump" together because of their cohesiveness or other release variables.

68

- Release elevation. Sediment can be released above, below, or at the surface of the water. This contributes to the initial momentum of the sediment entering the water, and affects the regimes of convective descent, and this will be discussed in the next chapter. In the field, a mechanical dredge can operate an any elevation, but sediment being disposed of from a barge will operate at or below the surface.

- Moisture and water content. Sediment can possess varying degrees of water content depending on release location and other factors. Sediment can range from dry to saturated or supersaturated sediment with excess fluid that forms a supernatant layer on top of the particles. Dredged sediment often includes some water that is removed from the bottom. When contaminated sediments are dredged, the quantity of water may be much greater because of the use of environmental dredges, which seal fluid in the bucket in order to reduce the local spread of contaminants. Sediment that is being transported to a disposal site can also have moisture added from the spray of waves and rain water, or by hosing operations designed to allow the sediment to be released more smoothly (from split-hull barges).

- Settled or suspended sediment. When the sediment is dry or moist, it can only be settled within the release mechanism, but if excess fluid is present, then the sediment can either be suspended in the supernatant or allowed to settle. It is often not a homogeneous mixture, as the coarse grains settle while the fines remain in suspension. However, homogeneity was assumed in this study.

Finally, there are different types of releases. Two of the most common are the back hoe type dredge (Figure 3-1) and the split-hull barge (Figure 3-2). The first is an example of a "point" release, whereas the latter is an example of a "line" release.

Figure 3-1: Photograph of a back hoe type dredge, which is an example of a point release (*photo: Z. Huang, 2009*).

Figure 3-2: Photograph of a split-hull barge, which is an example of a line release (*photo: T. Fredette, 2009*).

3.3 Experimental Set-Up and Mechanisms

The experiments were performed at MIT's Parsons Laboratory using a unique sediment release mechanism that was mounted over a recirculating water channel. The channel was equipped with an image visualization and acquisition system.

3.3.1 Sediment Release Mechanism

A release mechanism was fabricated after the design of Ruggaber (2000), which allows for all of the release conditions aforementioned to be performed in a "point" style release. A rendering of the release mechanism is shown in Figure 3-3. It was constructed with an aluminum base and structure that secures a trap door made of Lexan™, and this covers a round opening on the base. PVC pipes of various sizes fitted with rubber gaskets were attached to the structure over the opening (allowed for different aspect ratios of releases of the same total volume). Cylinders of the following inside diameters, $D_{c,i}$, could be fitted to the release mechanism:

- 2.54 *cm*

- 3.175 *cm*

- 3.81 *cm*

The use of a cylinder enables the best comparisons between experimental results and numerical simulations that utilize forced piston-like releases, even though hemispherical cups used by some previous investigators may actually resemble a back how dredge more accurately. However, these add an additional element of asymmetry, which was desirable to avoid.

A cylinder with an inside diameter of $D_{c,i} = 3.81$ *cm* was used for all trials discussed in the remainder of this thesis. The reason for this is that the height of sediment in the cylinder, *H*, was lowest, allowing for the fastest release – thus making the experiments closer to meeting the assumption of a nearly instantaneous release. Information can be learned by using the smaller cylinders, most notably in the calibration of numerical models, and this will be discussed in the final chapter of this thesis. With the application of open-water sediment disposal, the aspect ratio has a greater effect on the initial momentum of the release due to the dilution of the particles (and water if added) in the air prior to contacting the water surface. This is under investigation at Nanyang Technological University in Singapore. By exclusively using the 3.81 *cm* cylinder in this study, the following sediment conditions have these approximate aspect ratios ($H/D_{c,i}$):

- Dry Glass Beads: 0.66

- Dry Silt: 0.62

- Saturated Glass Beads: 0.82

- Saturated Silt: 0.78

- Supersaturated Glass Beads: 1.35

- Supersaturated Silt: 1.31

Note: Saturated releases have slightly more water added than required to ensure that all voids are filled. This is covered in more detail in the next chapter.

The aluminum base also had a spring attached to it at, and the spring was also connected to the trap door on its other end. Thus, when the trap door was triggered by pulling a plug (its anchor), the release of the sediment was nearly instantaneous
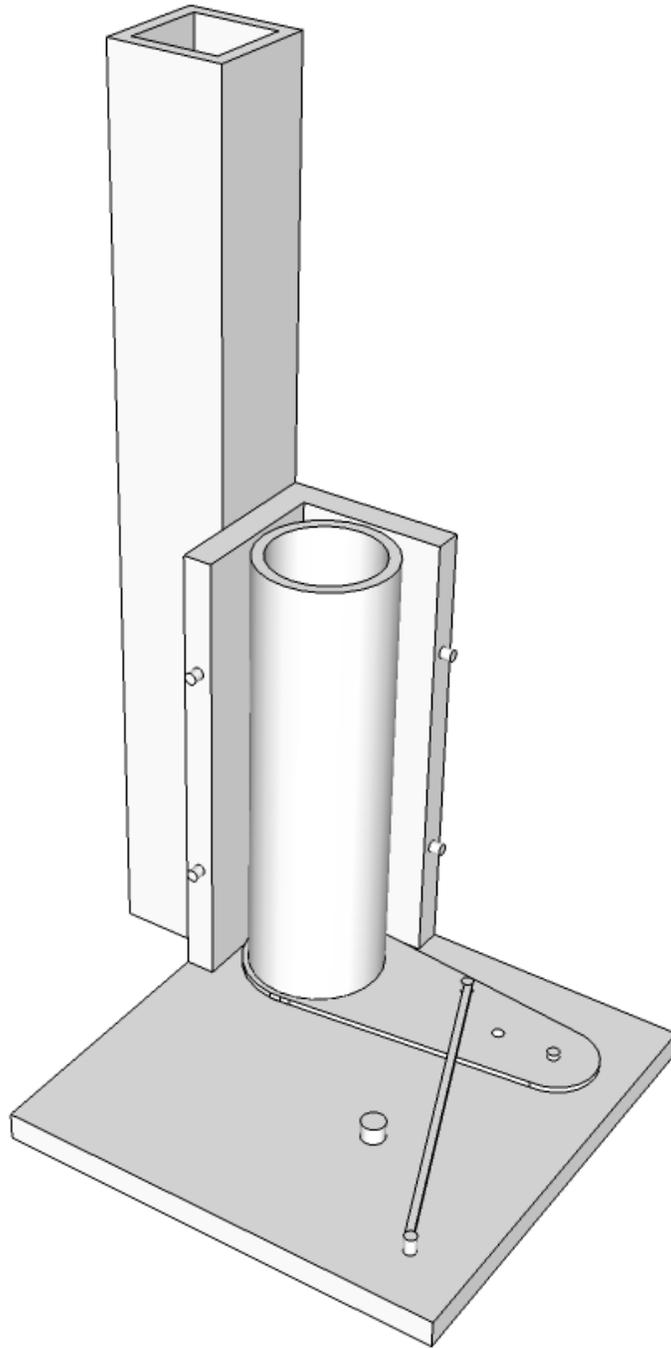
Figure 3-3: The release mechanism used for studying the dynamics of particle clouds released in ambient currents (base is 15.2 cm x 15.2 cm).

(measured opening time of the trap door was 0.0625 s), and the material was smoothly allowed to enter the recirculating channel. The release mechanism successfully performed dry and wet releases at different (fixed for each trial) elevations with different size particles.

3.3.2 Recirculating Water Channel

The experiments were performed in a recirculating water channel at MIT's Parsons Laboratory with dimensions of length, width, and depth of 35 *m*, 0.8 *m*, and 0.9 *m*, respectively. Channel sidewalls and bottom panels were constructed with glass, making visualization possible. A 7.5 *kW* electric motor with a variable frequency drive was able to produce currents with a range of 0 *cm/s* to 18 *cm/s* for the water depth of 60 *cm*. The required frequency input, between 0.0 *Hz* and 60.0 *Hz*, for a desired current velocity was calibrated by using measurements at standard current speeds and deriving the function below:

$$N = 3.3189u \quad for\ 0 \le N \le 60\ Hz \tag{3-1}$$

where *u* is the ambient current speed in units of *cm/s*; and *N* is the required frequency in *Hz*. The velocities varied over the width and depth of the recirculating water channel by less than 10 %, which was often within the range of uncertainty provided by the standard deviations of the velocity measurements that were carried out with an Acoustic Doppler Velocimeter (ADV) manufactured by Nortek USA (Annapolis, Maryland).

The release mechanism was positioned in the middle of the lateral dimension of the channel approximately one third of the length from the upstream end. Particle clouds were illuminated by positioning the head of a 6-*Watt* Argon-ion laser (Coherent Inc.,

Santa Clara, California) downstream of the release in order to illuminate a vertical light sheet in the stream-wise direction. Because of the limitations of the fiber optic cable that connected the body of the laser to the laser head within the channel, 4.5 *Watts* was the laser power setting used for all trials. A photograph of this experimental setup is shown in Figure 3-4. The configuration of the laser head allowed the centerline of a particle cloud to be captured, even as it advected downstream when released in the presence of ambient currents. Images were taken by positioning a Prosilica CCD camera, sold from Allied Vision Technologies, Inc. (Newburyport, Massachusetts), perpendicular to the laser sheet and outside of the channel looking through the glass of the sidewall. The flow went from right (upstream) to left (downstream) when viewed through the window of the camera. The Prosilica camera operated at a rate of 80 *Hz*, and the details of the data acquisition and processing are discussed in the next section.

Figure 3-4: The recirculating channel (shown in the drained condition) with the laser head, camera, and release mechanism positioned for experimental trials.

3.3.3 Image Acquisition and Processing

The black and white images from the Prosilica camera (operating at 80 Hz) were acquired using the Data Acquisition and Image Acquisition Toolboxes in MATLAB®. These images were taken in the "landscape" orientation, providing images that were 648 pixels wide by 485 pixels tall. Before each new set of experimental trials, an image of a ruler was taken with the CCD camera in the event any camera settings were inadvertently altered in the interim between trials. These images were used to create a scale between pixels and units of length, which varied among different trials between 0.126 *cm/pixel* and 0.128 *cm/pixel*. These scales were later used in the image processing code to deliver the cloud characteristics such as growth and descent velocity.

The image processing code itself was a customized code that was developed to analyze the images and plotted characteristics such as cloud growth, descent, and translation using functions from the Image Processing Toolbox. The code could analyze a given set of images from an experimental trial and run specific operations, including finding the parent cloud (called "cloud" in the code) and distinguishing it from the trailing stem (all other material, including the parent cloud, was called "bulk" in the code). The full MATLAB® m-file for this code is included in Appendix A. Once this was completed, the parent cloud was used to define elements such as the cloud radius, cloud descent, longitudinal translation, and descent velocity. The first of these outputs is the equivalent radius, which is defined by assuming the parent cloud is a spherical body; this output was checked by directly looking at the images, and as expected, when analyzing a two-dimensional cross section of the parent cloud, this method often underestimates the true horizontal radius and overestimates the vertical radius. The

83

second and third outputs just mentioned used the centroid of the parent cloud, not the leading edge, in order to prevent any asymmetrical behavior from heavily influencing the results; asymmetrical qualities of the particle cloud can result from the particle cloud interacting with an ambient current. The final output, the descent velocity, takes the derivative of the descent over time. Since this is a second order output, a running average was employed to smooth the local variations of the curves when plotted in the next chapter.

All of the tasks mentioned above were initially accomplished with commands such as "edge detection," but eventually functions such as "threshold" and "regionprops" were incorporated into the algorithm, decreasing the run time of the image processing from over 20 minutes to less than 2 minutes. While many characteristics of the particle clouds were deciphered by analyzing the images, the bottom of the recirculating channel was also divided into a grid system in order to collect particles after experiments.

3.3.4 Bottom Grid, Deposition Traces, and Collection Methods

In order to quantify the mass of particles in the parent cloud and trailing stem, as well as determine the movement and loss of particles when sediment is released in ambient currents, the particles were collected from the bottom of the recirculating channel. This was done methodically by superimposing a two-dimensional grid onto the bottom from beneath the glass so that particles could be collected and their location documented following experimental trials. Analytical techniques were developed that allowed the final resting place of particles on the bottom to yield a mass balance of particles between the parent cloud and trailing stem, as well as practical

recommendations on the advection of sediment beyond a drop zone as a function of current magnitude; it is important to note that a dynamic collapse of the particle cloud was not observed for any of the glass beads (it was for the silica). The method for collecting particles from the bottom would not have been feasible if a significant surge or resuspension of particles existed. The specifics of the collection methods with their interpretations are discussed in more detail prior to presenting their results in Chapter 4.

The grid (shown in Figure 3-5) recorded the location of particles for experiments in quiescent conditions (right side of Figure 3-5) in order to characterize the deposition area. For experiments with currents (left side of Figure 3-5), the deposition area was stretched significantly. Dimensions that are labeled on the figure are referenced in more detail in the next chapter. After each set of experiments, the channel was drained and the particles were allowed to dry prior to collection. The spacing between grid intervals was 7.62 *cm*, and the intervals (areas between the lines) were numbered 1 (downstream end) through 20 (upstream end). The release mechanism was fixed over grid interval 14. In general, ~ 99 % of the particles were collected from the bottom; although in ambient currents with higher magnitudes, a combination of release variables sometimes contributed to a greater percentage of particles advecting beyond the grid.
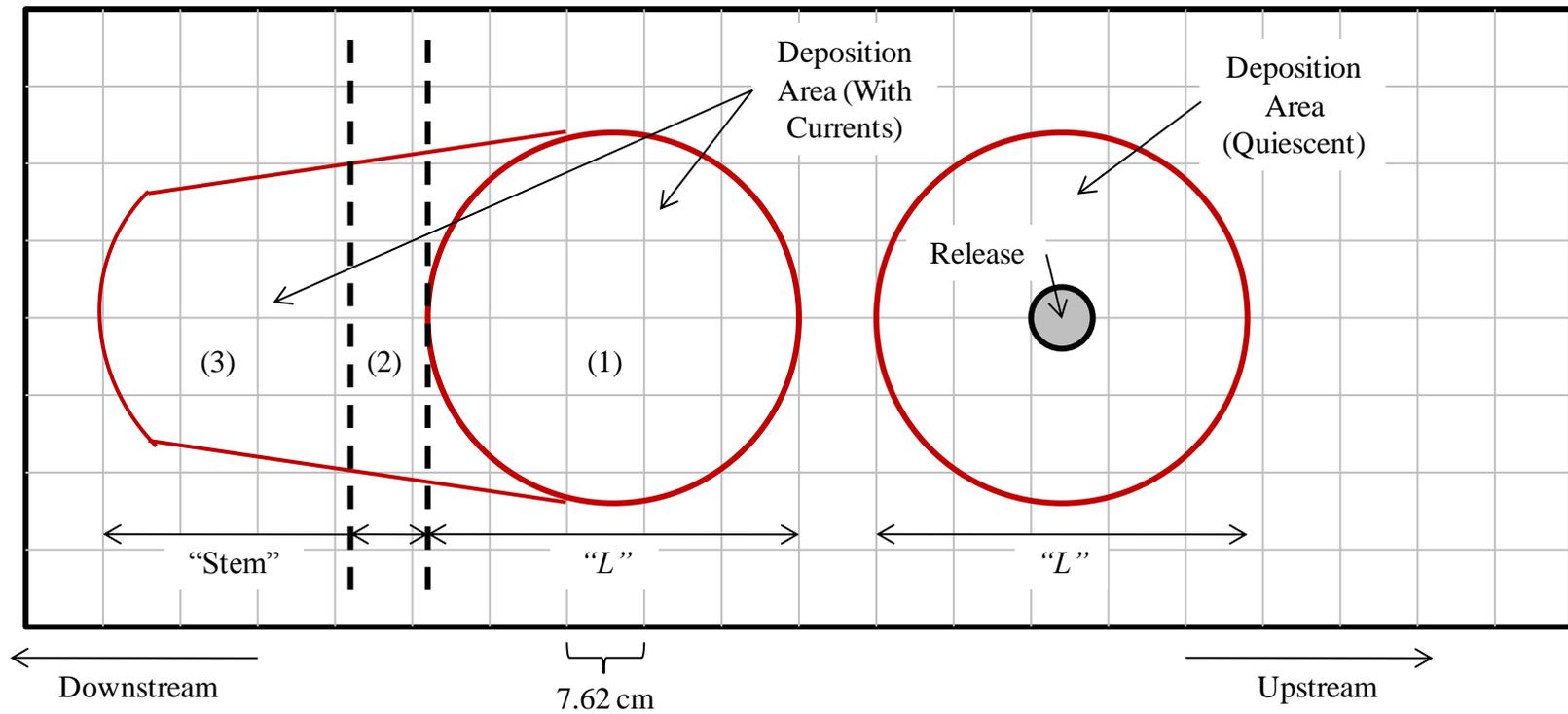
Figure 3-5: Plan view of the longitudinal grid system used to collect and document particles on the bottom of the recirculating water channel.

3.4 Scaling Analysis

Experiments required the scaling of three significant elements: 1) laboratory particle diameters and release volumes to their relevant field scale grain sizes and release volumes; 2) the release heights of operations in the field with the release apparatus in the laboratory; and 3) the water depths and current speeds between the laboratory and field.

3.4.1 Particle Scaling

In order to scale the particle sizes and release volumes, two characteristic velocity scales were analyzed: 1) the individual particle settling velocity, w_s; and 2) the characteristic thermal decent velocity, w_t. Using the same method which Ruggaber (2000) utilized, the laboratory and field particle sizes were related by using individual settling velocities and release volumes. The settling velocities of individual particles were found using an empirical relationship developed by Dietrich (1982) for spherical particles:

$$log(W_*) = -3.76715 + 1.92944[log(D_*)] - 0.09815[log(D_*)]^{2.0} \qquad (3\text{-}2)$$

$$-0.00575[log(D_*)]^{3.0} + 0.00056[log(D_*)]^{4.0}$$

where

$$W_* = \frac{\rho_a w_s^3}{(\rho_s - \rho_a)g\nu} \qquad (3\text{-}3)$$

and

$$D_* = \frac{(\rho_s - \rho_a)g d_s^3}{\rho_a \nu^2} \qquad (3\text{-}4)$$

where d_s is the median diameter of the particles; ρ_s is the density of the particles; and ρ_a is the density of the ambient fluid. These relationships are used together with the

characteristic thermal descent velocity, which Rahimipour and Wilkinson (1992) defined as:

$$w_t = \left(\frac{B_o}{\rho_a r_o{}^2}\right)^{1/2} \tag{3-5}$$

where B_o is the initial buoyancy of the particle cloud; and r_o is the initial radius of the release volume. The initial buoyancy can be calculated using:

$$B_o = m\left(1 - \frac{\rho_a}{\rho_s}\right)g \tag{3-6}$$

where m is the mass of particles released.

In order to relate the individual settling velocities and release volumes, and therefore scale the particle diameters used in the laboratory with relevant field-size particles, the cloud number, N_c, was used. As covered in the last chapter, Rahimipour and Wilkinson (1992) defined it as the ratio of the individual particle settling velocity to the characteristic thermal descent velocity, based on the initial cloud size, r_o:

$$N_c = \frac{w_s}{w_t} = \frac{w_s r_o}{\left(B_o/\rho_a\right)^{1/2}} \tag{3-7}$$

Cloud number scaling is made possible by utilizing the known laboratory properties of particle diameter and release volume (assuming a void ratio for the random close packing of spheres), and then specifying various field release volumes according to realistic modes of open-water sediment disposal. For example, a back hoe type dredge has a volume of approximately 1 m^3, whereas a split-hull barge can vary greatly in size, but a volume of 1000 m^3 is a good average approximation. The individual grain settling velocities of both laboratory and field sized particles are found using Dietrich's empirical

relationships. It is important to note that Equation 3-2 was developed with data for particles ranging in size from 0.01 *mm* to 100 *mm*, so predictions outside this range may have a greater uncertainty. Using a constant release of 40.0 *g* of particles ($V = 27.0$ cm^3, $B = 24,400$ g cm/s^2 for the silt; $V = 28.7$ cm^3, $B = 23500$ g cm/s^2 for the glass beads), Table 3-2 shows the field sized particles that were determined for the designated field volumes. This is also shown in Figure 3-6 with the field size particles grouped into realistic sets of individual particles versus clumps for the back hoe dredge and split-hull barge, respectively.

Table 3-2: Cloud number scaling of the laboratory particles to their relevant field sizes using a constant release volume in the laboratory and realistic release volumes found in the field.

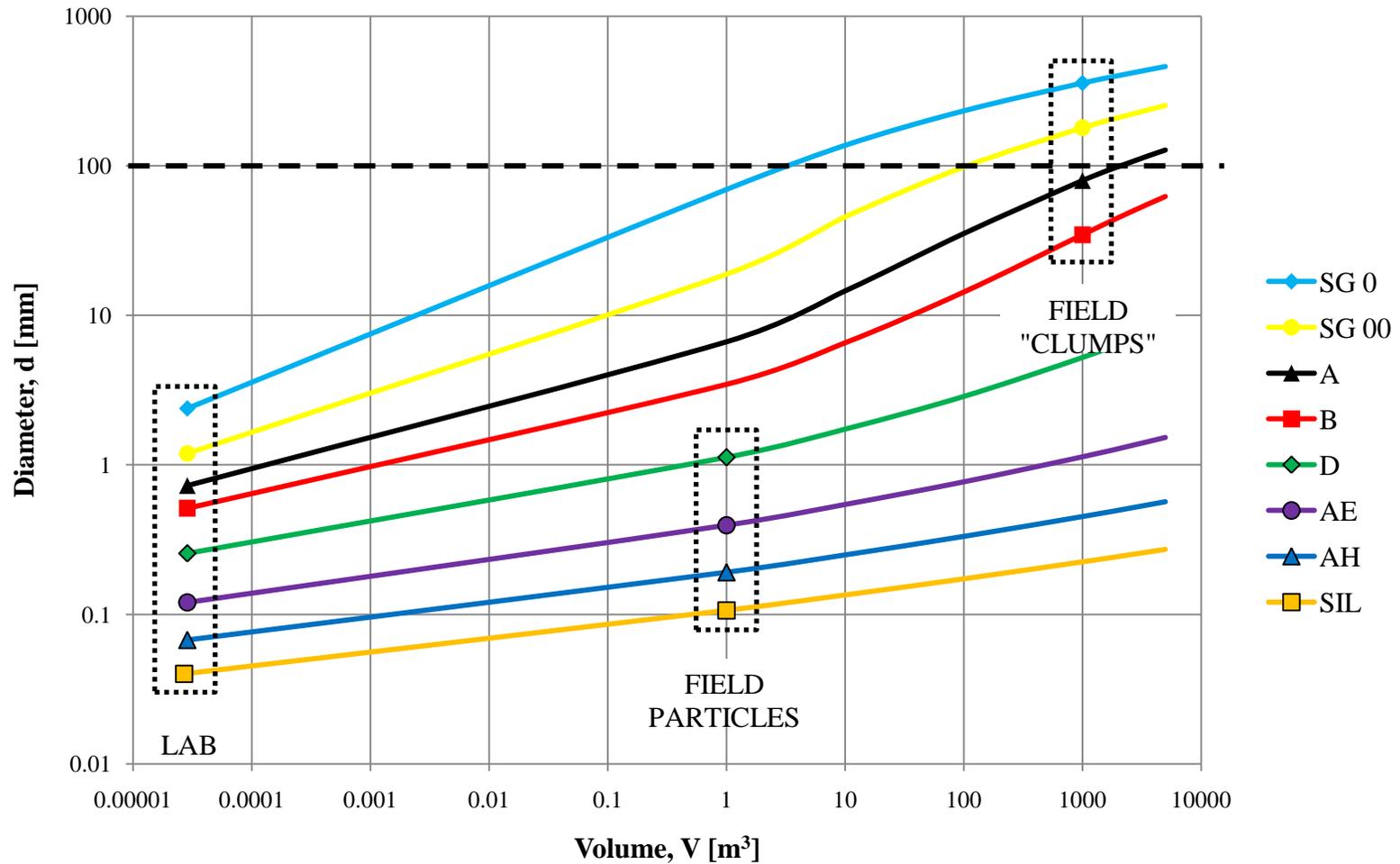| Designation	Lab Median Diameter [mm]	Field Diameter [mm] vs. Field Volume				
		1 m^3	10 m^3	100 m^3	1000 m^3	2500 m^3
SG 0	2.38	69.4	137	233	357	415
SG 00	1.19	18.8	45.5	98.2	179	220
A	0.725	6.64	14.5	35.2	79.5	105
B	0.5125	3.45	6.55	14.3	34.5	48.6
D	0.256	1.12	1.73	2.87	5.22	6.87
AE	0.120	0.39	0.54	0.77	1.13	1.33
AH	0.0675	0.19	0.25	0.33	0.45	0.51
SIL	0.040	0.11	0.13	0.17	0.22	0.25

Figure 3-6: Cloud number scaling of the laboratory particles to their relevant field sizes and volumes using a constant release volume in the laboratory (for all particle sizes). Typical field size particles (for a back hoe dredge) and "clumps" (for a split-hull barge) are designated with dashed boxes.

3.4.2 Release Height Scaling

The scaling of the release heights of the sediment releases between the laboratory and the field was accomplished by using a ratio of volumes; this was subsequently used to create a length scale. This is applicable to the back hoe style dredge which releases material above the surface; a split-hull barge removes the initial momentum variable, so for the laboratory releases an arbitrary location below the surface can be chosen without significantly influencing the results. Using the volume of glass beads released in a single discharge (28.7 cm^3) and the typical volume of a back hoe (1 m^3), a ratio of the field volume to laboratory volume is 35,000. To make this a length ratio, the cube root is utilized and results in a length ratio of 32.7. In a field visit to one of the areas of Singapore being reclaimed in July 2009, a back hoe was dropping sediment at approximately 4 *m* above the water surface – this estimate accounted for the freeboard of the barge and any elevation the back hoe had above the deck of the barge (E. E. Adams, personal communication, 2009). Using the new length scale, a release of height of 12.2 *cm* above the water surface would be appropriate in the laboratory to model this release height. To be consistent, the length scale found from the volumetric ratio was also applied in the scaling of the depths and currents, which also incorporated Froude scaling to compare the laboratory to the field.

3.4.3 Depth and Current Scaling

Finally, scaling of the water depths and currents speeds in the laboratory and in the field was accomplished by looking at the length scale found in the previous section and two characteristic velocity scales: 1) the ambient current velocity, u_a; and 2) the

shallow water wave speed, u_s. Together, the two velocities form Froude scaling, which is the ratio of the ambient current to the shallow water wave speed, u_a/u_s, where

$$u_S = \sqrt{gh} \qquad (3\text{-}8)$$

where h is the water depth. Using the length scale from the release height scaling, the experimental depth that was kept at a constant 60 *cm* in the recirculating channel scales to a field depth of 19.6 *m*. Therefore, the work in the laboratory can analyze a number of field locations with various depths, such as the Federal Navigation Channel of Boston Harbor, where the depth is 12.2 *m* at Mean Lower Low Water (MLLW). This is done by looking at the behavior of the particle clouds for only the first 37.3 *cm* of descent, at which point when they pass this "imaginary plane" they have effectively impacted the bottom (if focusing primarily on low tide; at high tide the sediment must travel further). By employing Froude scaling, the length ratio of 32.7 yields a corresponding velocity ratio of 5.7. This velocity ratio can be used to tie the laboratory current velocities to certain "time windows" surrounding low and high slack water using a sinusoidal semidiurnal tidal cycle.

As an illustration, during the Boston Harbor Navigation Improvement Project, contaminated sediment was initially permitted to be released into the CAD Cells one hour before high tide until two hours after high tide, and later disposal was allowed for two hours around low tide to increase the total time available for disposal operations (ENSR, 2002). During a post-disposal monitoring period of the CAD Cells, the maximum recorded currents in the navigation channels of Boston Harbor were 1.10 *m/s* during flood flow and 1.17 *m/s* during ebb flow (Tubman, 2007). This equates to approximately a 9 *cm/s* to 10 *cm/s* current in the laboratory for the time of one hour before or after low and

high slack water and approximately a 17.4 *cm/s* current in the laboratory for two hours after low or high tide. Later Boston Harbor maintenance dredging projects eventually extended the allowable periods of disposal into CAD Cells further between one hour prior to and two hours following low or high slack water (Thalken, 2006). The recirculating water channel was capable of generating currents of magnitudes up to 18 *cm/s* with the prescribed depth of 60 *cm*.

3.5 Experimental Procedure

For a given set of experiments, independent variables were chosen in combinations that most resembled realistic modes of sediment releases in the field; in the interest of time, every possible combination was not performed, but rather two control groups were chosen as representatives for "particle" releases and "clump" releases. The reason for this is that the release variables contribute to the sediment falling as independent particles or as clumps. Ruggaber (2000) found that the behavior of cohesive sediments depends on the percentage of solids by weight, and one result he recorded was that when the particle cloud was more than 50% solids by weight, the sediment descended as clumps. This has also been observed in the field, and it is one of the reasons for choosing two different particle sizes to represent field-scale particles and field-scale clumps. Although these are discussed more in the next chapter, the particle sizes which represented these releases were D Glass Beads ("particles") and B Glass Beads ("clumps"). The recirculating water channel was filled to the prescribed depth of 60 *cm*, and for quiescent releases, it was allowed to sit for thirty minutes in order to allow any internal motion to dissipate. For releases with ambient currents, the motor was tuned

to the appropriate frequency between 0.0 *Hz* and 60.0 *Hz* using Equation 3.1. At the depth used for all experiments, the maximum possible ambient current magnitude was slightly greater than 18 *cm/s*, but most trials used speeds of 6 cm/s and 12 cm/s because of their correlation to times before and after the one hour time window surrounding slack water in Boston Harbor. The motor was allowed to run five to ten minutes after turning it on before experiments began in order to allow the ambient current to reach a steady state.

Once the conditions in the recirculating water channel were ready, the laser's alignment in the center of the water channel was checked, and an image of a ruler was taken with the CCD camera (as mentioned earlier, in the event any camera settings were inadvertently altered between trials). Eight trials were performed for a given set of experimental release conditions, in order to verify repeatability and allow ensemble averaging when analyzing the deposition patterns of the particle clouds on the bottom of the water channel. The particles were collected using the grid previously discussed, and more details on interpretations of the results are provided in the next chapter. Between different sets of experiments, the water channel was drained, and after collecting the particles, was also cleaned before repeating the entire process for a new set of release variables.

4 Experiments

Particle cloud experiments were performed using the procedure outlined in Section 3.5 with the focus of exploring how different release variables affected the dynamics of the descending particle clouds, as well as quantifying the mass in the parent cloud versus the trailing stem. These methods were also used to deliver practical recommendations on the potential for losing a significant portion of the original material to the ambient environment in the real world when sediment is disposed in ambient currents.

4.1 Groups of Experiments

As previously mentioned, one of the release variables, the cylinder size, was kept at a constant diameter of $D_{c,i} = 3.81$ *cm* for all trials. Otherwise, sets of experiments fully tested the effect of particle size, release height, and water content for particle clouds in both quiescent and flowing conditions. To explore the influence of particle type and size, all other release variables were kept constant (surface releases with saturated particles) while the different particles were tested. These ranged in size from 0.040 *mm* to 3.18 *mm*. These experiments are collectively called Group 1 (Table 4-1). Experiments in Group 2 (Table 4-2) and Group 3 (Table 4-3) employed the following techniques to fully test the other variables of open-water sediment disposal for particles and clumps, respectively, by exclusively using representative particle sizes. As mentioned before, D

Glass Beads were chosen to represent field particles (for a back hoe dredge volume), and B Glass Beads were chosen to represent field clumps (for a split-hull barge volume).

- Release elevation.
  - Above surface. Sediment released above the water surface was released from an elevation of 5 *cm*, which when using the length scale derived from the volumetric ratio discussed in Chapter 3, scales to the release height of approximately 1.6 *m* in the field. The laboratory release elevation scales to less than the release height of the back hoe dredge that was observed in Singapore Harbor (12.2 cm would be the appropriate height), but this was done purposely to reduce variability among releases. At the larger elevation, an asymmetry was observed when the particles entered the water, which was due to the vertical spread of the particles within the air prior to entering the water; this was only visible when the release mechanism was oriented such that the trap door opened across the field of view. Thus, to reduce the asymmetry but still add additional momentum to particles entering the water, the above surface experiments discussed hereafter used an elevation of 5 *cm* above the water surface. The asymmetry is currently under investigation by researchers at Nanyang Technological University in order to quantify its effects at higher release heights (D. Shao and B. Zhao, Personal Communication, 2010).
  - At surface. Sediment released at the water surface was actually released from an elevation of 1 *cm* above the water surface. Particles were not released flush with the water surface due to the construction of the release

mechanism. Releases had to retain uniform release variables when comparing releases in quiescent conditions and ambient currents, so the base of the release mechanism was raised slightly above the water surface to prevent the formation of eddies and wake when currents were present.

- o Below surface. Sediment released below the surface was released from an elevation of 5 *cm* below the water surface (in the tables documenting the different groups of experiments, the water surface is defined as $z = 0$ cm, thus making this a negative elevation). This was chosen not to mirror the above surface release, but rather to have all supersaturated releases (both above and below the water surface) possess the same aspect ratio, $H/D_{c,i}$ (i.e., the same amount of supernatant fluid above the particles within the cylinder prior to release).

In Tables 4-1, 4-2, and 4-3, the release elevation follows the particle type with a positive or negative sign (indicating the release was above or below the water surface) followed by a number, which is the elevation with units of *cm*.

- Moisture and water content.

  - o Dry. Sediment that is dry has no water added to the release.

  - o Saturated. Based on the constant volume of sediment released ($V = 27.0$ cm^3 for the silt; $V = 28.7$ cm^3 for the glass beads), and assuming a void ratio for random close packing of spheres, approximately 10 *ml* of water is required to saturate the particles. Ruggaber (2000) increased this amount to 17 *ml* to ensure that all voids were filled, without adding too large a layer of excess supernatant above the particles (less than 0.6 cm), and the

same was done in this investigation. This increase also removes the potential that minor leaks in the cylinder could alter the saturation of the sediment.

- o Supersaturated. For supersaturated sediment releases, 40 *ml* of water was added to the cylinder with the particles. When the particles were settled, this created a layer of supernatant fluid above the particles that was approximately 2.6 *cm* thick, which is slightly more than the height of the particles in the cylinder (i.e., the total height of the particle/fluid mixture was slightly more than double that of the dry release).

In Tables 4-1, 4-2, and 4-3, the particle moisture is indicated using the following abbreviations: "R" is dry; "A" is saturated; and "P" is supersaturated. These letters follow the numeric release elevation for that particular set of experiments.

- Settled or suspended sediment.
  - o Settled. Particles that are dry, saturated, or supersaturated can be allowed to settle before the release is performed. For all experiment groups in this research, this condition is implied for all dry and saturated releases. To fulfill this condition for both saturated and supersaturated releases, after the particle/fluid mixtures were homogenized, the particles were allowed to settle for several seconds prior to release, ensuring that they were not in suspension. When particles are settled and supersaturated, an excess "supernatant" layer of water forms above the particles in the release cylinder.

o   Suspended.   This condition was only used if the particles were supersaturated.   In this scenario, after homogenizing the particle/fluid mixture, the contents of the cylinder were agitated using a stirring rod and immediately released once all particles were in suspension.

In Tables 4-1, 4-2, and 4-3, settled particles are designated with the letter "T," and suspended particles are designated with the letter "S."   These letters follow the abbreviations for particle moisture.

Experiments in Group 1, Group 2, and Group 3 are shown in Tables 4-1, 4-2, and 4-3. These experiment designations also include the strength of the ambient current, which is the final number in the name of the experiment.   Thus, an experiment's designation flows in the following order: particle type, release elevation, moisture content, settled or suspended particle condition, and magnitude of the ambient current.

Table 4-1: Group 1 experiments explored the effect of particle size by using surface releases of saturated sediment.

Experiment Designation	Particle Type	Release Location [z = 0 at surface]	Water Content	Particle Condition	Current Magnitude
SG 0+1AT 0	SG 0	+ 1 cm	Saturated	Settled	0 cm/s
SG 00+1AT 0	SG 00	+ 1 cm	Saturated	Settled	0 cm/s
A+1AT 0	A	+ 1 cm	Saturated	Settled	0 cm/s
B+1AT 0	B	+ 1 cm	Saturated	Settled	0 cm/s
D+1AT 0	D	+ 1 cm	Saturated	Settled	0 cm/s
AE+1AT 0	AE	+ 1 cm	Saturated	Settled	0 cm/s
AH+1AT 0	AH	+ 1 cm	Saturated	Settled	0 cm/s
SIL+1AT 0	SIL	+ 1 cm	Saturated	Settled	0 cm/s

Table 4-2: Group 2 experiments explored the effects of release height, moisture content, and particle condition on glass beads representing field particles (for a back hoe dredge volume).

Experiment Designation	Particle Type	Release Location [z = 0 at surface]	Water Content	Particle Condition	Current Magnitude
D+5RT 0	D	+ 5 cm	Dry	Settled	0 cm/s
D+5RT 12	D	+ 5 cm	Dry	Settled	12 cm/s
D+1RT 0	D	+ 1 cm	Dry	Settled	0 cm/s
D+1RT 6	D	+ 1 cm	Dry	Settled	6 cm/s
D+1RT 12	D	+ 1 cm	Dry	Settled	12 cm/s
D+1AT 0	D	+ 1 cm	Saturated	Settled	0 cm/s
D+1AT 6	D	+ 1 cm	Saturated	Settled	6 cm/s
D+1AT 12	D	+ 1 cm	Saturated	Settled	12 cm/s
D+1PT 0	D	+ 1 cm	Supersaturated	Settled	0 cm/s
D+1PT 6	D	+ 1 cm	Supersaturated	Settled	6 cm/s
D+1PT 12	D	+ 1 cm	Supersaturated	Settled	12 cm/s
D-5PS 0	D	- 5 cm	Supersaturated	Suspended	0 cm/s
D-5PS 6	D	- 5 cm	Supersaturated	Suspended	6 cm/s
D-5PS 12	D	- 5 cm	Supersaturated	Suspended	12 cm/s

Table 4-3: Group 3 experiment explored the effects of release height, moisture content, and particle condition on glass beads representing field clumps (for a split-hull barge volume).

Experiment Designation	Particle Type	Release Location [z = 0 at surface]	Water Content	Particle Condition	Current Magnitude
B+5RT 0	B	+ 5 cm	Dry	Settled	0 cm/s
B+5RT 12	B	+ 5 cm	Dry	Settled	12 cm/s
B+1RT 0	B	+ 1 cm	Dry	Settled	0 cm/s
B+1RT 6	B	+ 1 cm	Dry	Settled	6 cm/s
B+1RT 12	B	+ 1 cm	Dry	Settled	12 cm/s
B+1AT 0	B	+ 1 cm	Saturated	Settled	0 cm/s
B+1AT 6	B	+ 1 cm	Saturated	Settled	6 cm/s
B+1AT 12	B	+ 1 cm	Saturated	Settled	12 cm/s
B+1PT 0	B	+ 1 cm	Supersaturated	Settled	0 cm/s
B+1PT 6	B	+ 1 cm	Supersaturated	Settled	6 cm/s
B+1PT 12	B	+ 1 cm	Supersaturated	Settled	12 cm/s
B-5PS 0	B	- 5 cm	Supersaturated	Suspended	0 cm/s
B-5PS 6	B	- 5 cm	Supersaturated	Suspended	6 cm/s
B-5PS 12	B	- 5 cm	Supersaturated	Suspended	12 cm/s

4.2 "Weak," "Transitional," and "Strong" Ambient Currents

After ambient currents were introduced to the particle cloud experiments, it was immediately discovered that the strength of the ambient current had a significant influence on the formation of the self-similar thermal when particles were released into the water channel. Increasing ambient current speeds appeared to prolong the initial acceleration phase and distort the spherical vortex (therefore delaying creation of a self-similar thermal), and with strong enough ambient currents, a thermal with a spherical

vortex never formed. These observations were translated into three velocity ranges for the currents that are designated as "weak," "transitional," and "strong." "Weak" currents are characterized by the presence of a spherical vortex that forms at a similar depth and grows to a similar size when compared to particle clouds in quiescent conditions. "Transitional" currents are distinguished by a delay in formation and distortion of the spherical vortex, which can be manifested quantitatively by increased growth and a corresponding slowed descent. Finally, when a spherical vortex never forms and the coherency of the particle cloud is destroyed, these are termed "strong" currents. The thresholds between "weak" and "transitional" ambient currents and "transitional" and "strong" ambient currents are designated as the "weak threshold" and the "strong threshold," respectively.

4.2.1 Threshold Dependence on Particle Size

Not only do two separate thresholds exist, but the magnitude of the ambient current at these thresholds is dependent upon particle size. The weak threshold was identified for each particle size from experiments executed with increasing current speeds (i.e., 3 cm/s, 6 cm/s, etc.), and the results of these trials are shown for all glass bead sizes in Table 4-4. These releases were all completed at the surface with saturated conditions. The current magnitudes identified in the second column of Table 4-4 demark "transitional" ambient currents, or the weak threshold, above which the particle clouds no longer behaved as though they were descending in quiescent conditions (or "weak" currents). This was documented based on qualitative observations of the distortion of the spherical vortex, or the apparent increase in growth of the cloud; these ranges were

106

confirmed by quantitative data on select cases that showed an increased spread of the parent cloud. The third column of Table 4-4 identifies the strong threshold using the entirely qualitative observations on the smaller particle sizes. It was not possible to quantify the strong threshold for the entire range of particles because of limitations on the maximum current speed which could be established with the experimental setup.

Table 4-4: The weak threshold (between "weak" and "transitional" ambient currents) and strong threshold (between "transitional" and "strong" ambient currents) as a function of particle size contained within the particle cloud.

Particle Name	Ambient Current Weak Threshold [cm/s]	Ambient Current Strong Threshold [cm/s]
Glass Bead A	18 +	N/A
Glass Bead B	16	N/A
Glass Bead D	12	18
Glass Bead AE	6	10.5
Glass Bead AH	3	6

Observations revealed that increasing the particle size produced an increase in the weak threshold and an increase in the range of "transitional" currents (i.e., an even greater increase in the strong threshold). This is shown pictorially in Figure 4-1, by using two different colored lines to represent two sizes of particles – black is "small" particles, and red is "large" particles – to mark the evolution of the ambient currents from "weak" to "strong" as a function of particle size. The dashed lines represent the weak thresholds, and the dotted lines represent the strong thresholds. The three types of ambient currents and the corresponding thresholds are distinguished by using the coherency of the spherical vortex as an indicator.

Using the magnitude of the ambient currents and data recorded from the image analysis, the weak threshold was analyzed using three different ratios that involved the
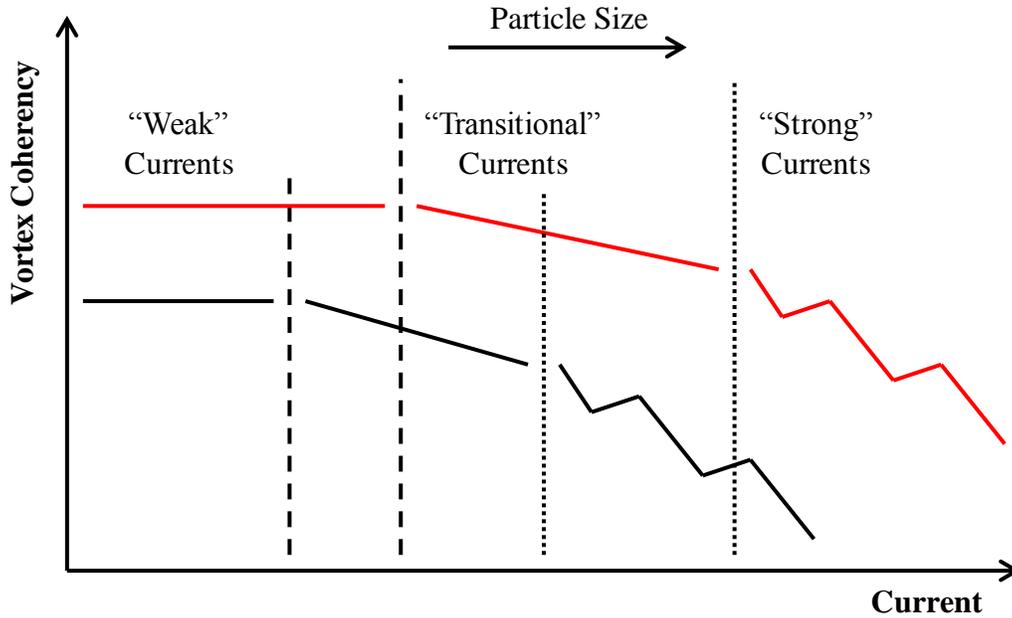
Figure 4-1: Qualitative depiction of the evolution of the strength of ambient currents from "weak" to "transitional" to "strong" as a function of particle size using the coherency of the spherical vortex. The dashed lines show the weak thresholds, and the dotted lines show the strong thresholds for "small" particles (black) and "large" particles (red).

weak critical ambient current velocity, $u_{a,crit,1}$, divided by: 1) the characteristic thermal descent velocity, w_c (i.e., a predictive analysis); 2) the measured maximum descent velocity, $w_{c,max}$; and 3) the measured average descent velocity, $\overline{w_c}$. The strong threshold was also analyzed using a similar form of the first ratio, substituting the strong critical ambient current velocity, $u_{a,crit,2}$, in the numerator for $u_{a,crit,1}$.

4.2.1.1 *The Weak and Strong Thresholds: Analysis 1*

Analyses of both the weak threshold between "weak" and "transitional" currents and strong threshold between "transitional" and "strong" currents were completed in order to make the critical ambient current velocities, $u_{a,crit,1}$ and $u_{a,crit,2}$, predictable quantities that are determined by the size, density, and volume (buoyancy) of the material being disposed. Using the non-dimensional form of the individual particle settling

velocity, W_* (Equation 3-3), and the characteristic thermal descent velocity, w_t (Equation 3-5), the following relationship was developed that describes the threshold between "weak" and "transitional" currents:

$$\frac{u_{a,crit,1}}{w_t} = 0.0194ln(W_*) + 0.1419 \tag{4-1}$$

Using the same non-dimensional parameters, a similar relationship was derived for the threshold between "transitional" and "strong" currents:

$$\frac{u_{a,crit,2}}{w_t} = 0.0234ln(W_*) + 0.2075 \tag{4-2}$$

Equations 4-1 and 4-2 are plotted together in Figure 4-2 with the weak and strong thresholds that were observed and recorded in Table 4-4.
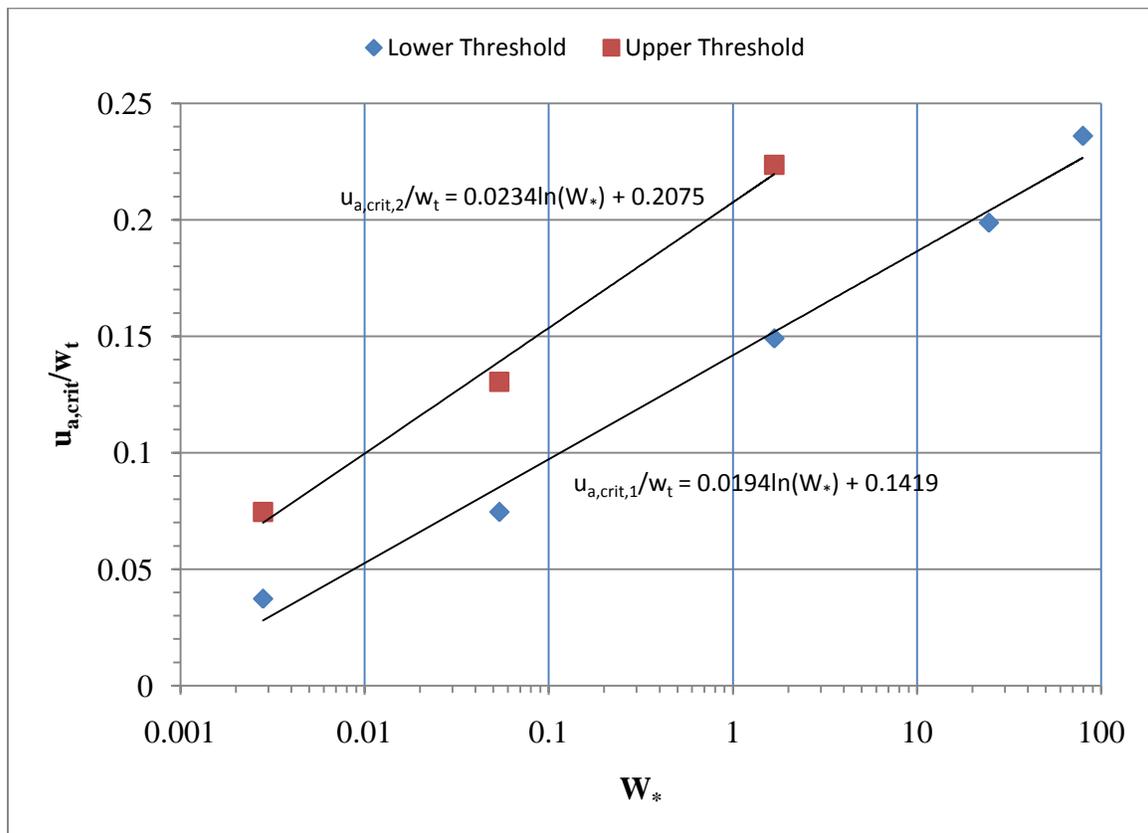
Figure 4-2: The weak threshold and strong threshold observations plotted with the relationships for the critical ambient current velocities, Equations 4-1 and 4-2.

4.2.1.2   The Weak Threshold: Analysis 2

A second analysis was completed on the weak threshold data using the measured maximum descent velocity, $w_{c,max}$, extracted from the image analysis as a basis for normalization (the velocity profiles for particles of different sizes are shown in Figure 4-3). This was done because the characteristic thermal descent velocity is actually larger than the descent velocities recorded, and it was desirable to know how the weak threshold compares with the actual descent velocity. The maximum descent velocity was chosen because it is virtually independent of facility; it is reached very quickly after release. Thus, in both the field and the laboratory, it will nearly always be encountered.
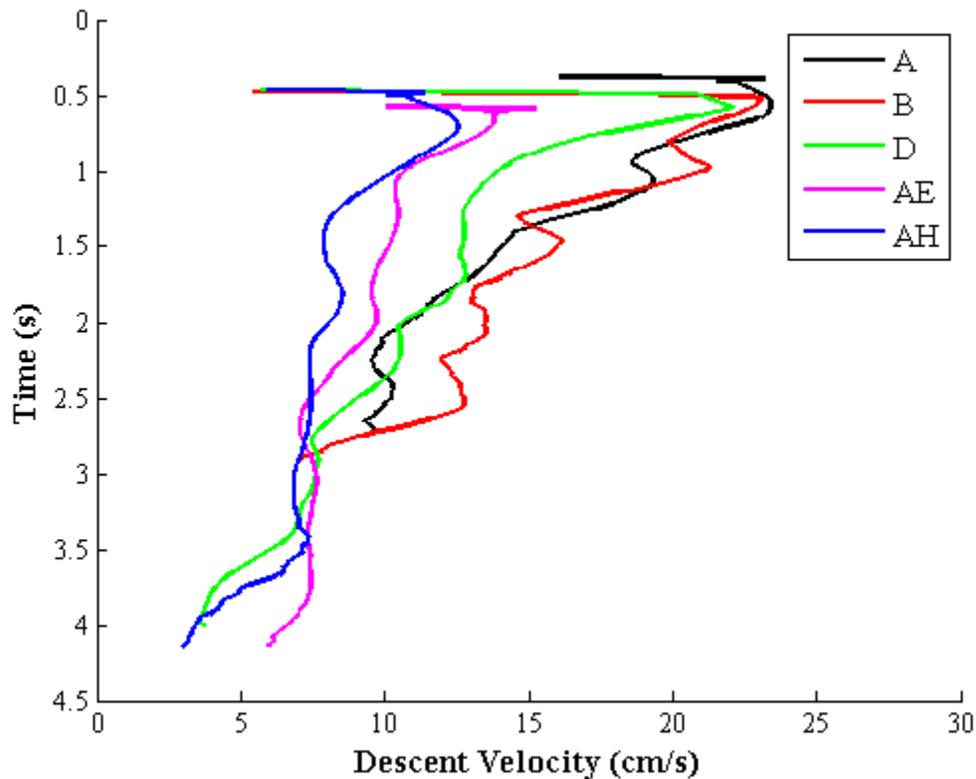
Figure 4-3: The descent velocity for five different sizes of particles when released at the surface in a saturated condition (Note: the descent velocity is found by taking the derivative of the descent of the cloud over time, so a 25-point moving average has been applied to reduce roughness at the local scale; this averages data points every 0.3125 s).

For this analysis, data were used from experiments that were performed at the surface with saturated particles in quiescent conditions. This created the ratio $u_{a,crit,1}/w_{c,max}$, which is shown in Table 4-5. The results show that the ratio is on the order of one for the largest particle sizes and decreases for smaller particles. This is significant because, as will be discussed in more detail later in this thesis, it is related to the sediment disposal time windows allowed by regulations.

Table 4-5: Ratio of the critical ambient current velocity at the weak threshold between "weak" and "transitional" currents to the maximum descent velocity of particle clouds.

Particle Name	Ambient Current Weak Threshold [cm/s]	Maximum Cloud Descent Velocity [cm/s]	$u_{a,crit,1}/w_{c,max}$
Glass Bead A	18 + (*)	23.5	0.8
Glass Bead B	16	22.8	0.7
Glass Bead D	12	21.6	0.6
Glass Bead AE	6	13.8	0.4
Glass Bead AH	3	12.5	0.2

(*) Glass Bead A's weak threshold was observed to be greater than 18 cm/s when tested using the standard experimental setup; in the ratio calculation 19 cm/s was used because this was observed for a reduced water depth.

4.2.1.3   The Weak Threshold: Analysis 3

A third analysis was completed on the weak threshold data that used the measured average descent velocity, $\overline{w_c}$, which was found by calculating $\frac{z_2 - z_1}{t_2 - t_1}$ from the image analysis. Calculating the average descent velocity in this manner is highly facility dependent (i.e., upon the water depth), but it was explored because the results suggest that the weak threshold between "weak" and "transitional" ambient currents is reached when $u_{a,crit,1}/\overline{w_c} \sim 1$; these values are shown in Table 4-6. Figure 4-4 shows the

descent of these five particle clouds as a function of time for a surface release with saturated particles. These values are in very good agreement for the glass bead sizes A, B, and D, but varies more for sizes AE and AH.

Table 4-6: Ratio of the critical ambient current velocity at the weak threshold between "weak' and "transitional" currents to the average descent velocity of particle clouds. The fallout depth is calculated using Equation 2-24.

Particle Name	Fallout Depth [cm]	Average Cloud Descent Velocity [cm/s]	$u_{a,crit,1} / \overline{w_c}$
Glass Bead A	66.1	19.9	1.0
Glass Bead B	86.5	15.3	1.0
Glass Bead D	162	12.9	0.9
Glass Bead AE	372	10.4	0.6
Glass Bead AH	768	8.8	0.3

The reason for the discrepancy for the smaller sized glass beads can be attributed to the method used to calculate the average parent cloud descent velocity. This was accomplished by using two sets of data points, (t, z), from the data output of the image analysis, and then taking a ratio of total descent (change in distance) over change in time. The "initial" data point was always set at the beginning of the thermal regime of convective descent. However, a second effect of particle size (more of which will be discussed later in this chapter) is that the particle clouds with smaller particles entrain more fluid, causing greater growth (shown in Figure 4-5 for illustration purposes). Thus, the "final" data points for the larger particle sizes were temporally located after the reduction in entrainment, but for the smaller particle sizes, high rates of entrainment were still occurring. Therefore, the average parent cloud descent velocities recorded for the larger particle sizes (A, B, and D) include a greater portion of the thermal stage of descent than the smaller particle sizes (AE and AH). To determine more accurate

experimental values for the descent of the smaller particle sizes, a deeper water channel would be required. To quantify the depth required to compute an appropriate average descent velocity, the relationship derived by Bush et al. (2003) to determine the fallout depths where the particle cloud enters the dispersive phase of convective descent was used (Equation 2-24). These depths, which are all shown in Table 4-6, vary between 66 *cm* and 770 *cm* for the glass bead particle sizes. Therefore, this shows that the ratio $u_{a,crit,1}/\overline{w_c} \sim 1$ is an excellent indicator of the weak threshold when the average descent velocity is measured over more than a third of the depth over which the thermal can theoretically remain intact.
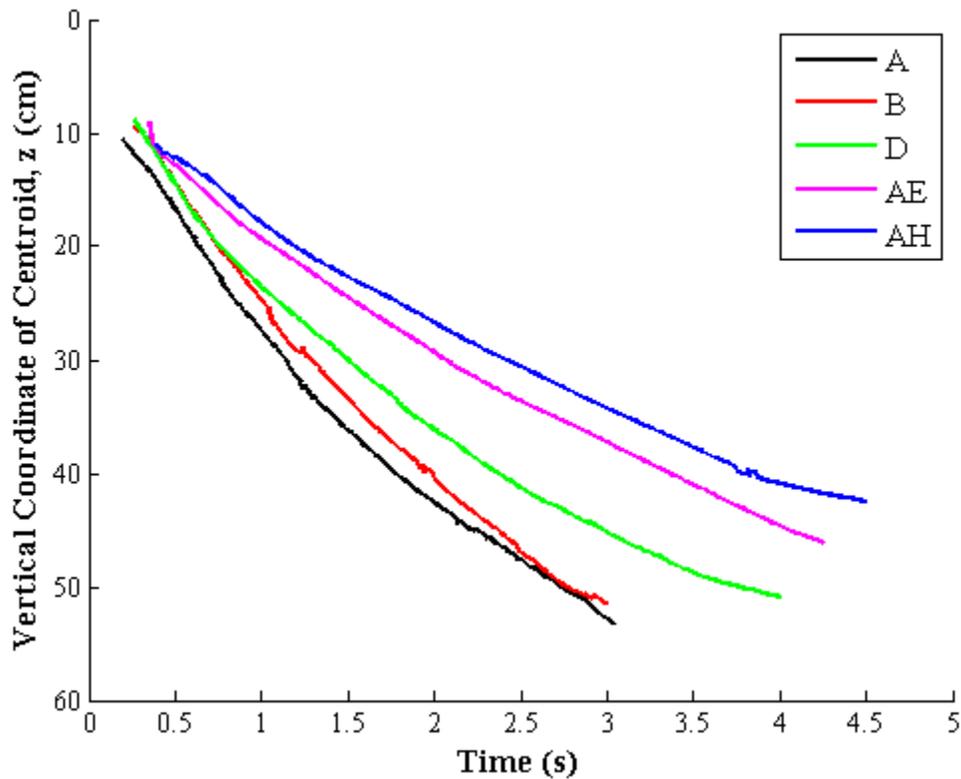
Figure 4-4: Vertical coordinate of the centroid of a descending particle cloud versus time for five different sizes of particles when released at the surface in a saturated condition.
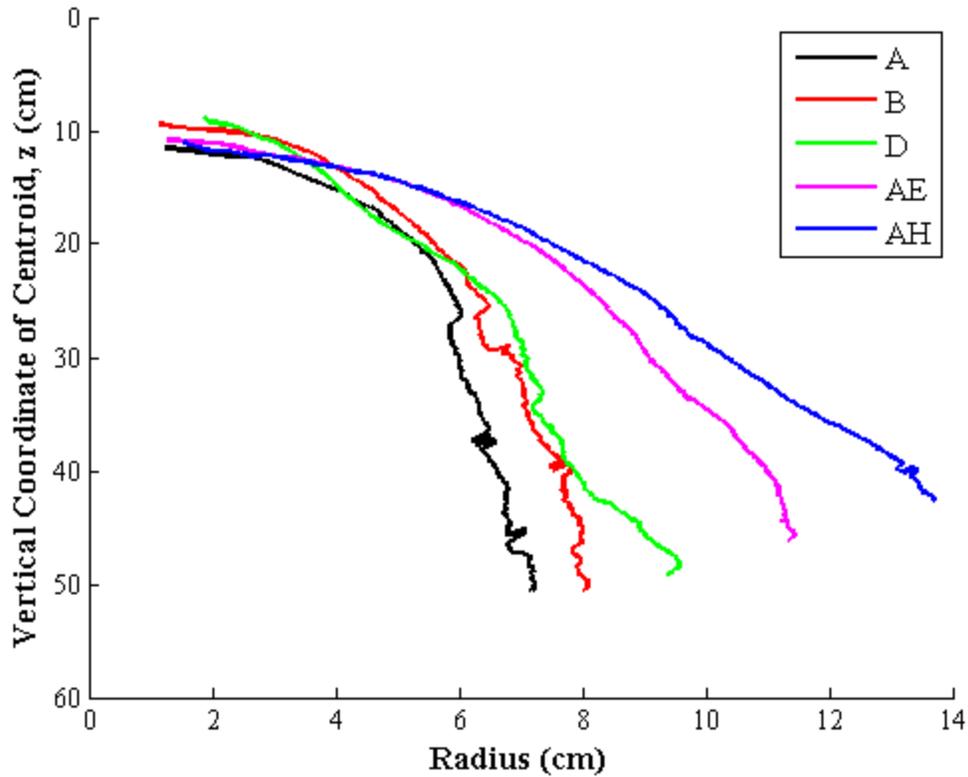
Figure 4-5: Vertical coordinate of the centroid of a descending particle cloud versus parent cloud radius for five different sizes of particles when released at the surface in a saturated condition.

Vortex rings and their reaction to cross-flows were studied in more detail by Sau and Mahesh (2008) and were summarized in Chapter 2, although not with particle clouds as the intended application. They defined their non-dimensional ratio, $\overline{W_{exit}}/u_a$, as something similar to the inverse of the weak threshold ratio described in this section, $u_{a,crit,1}/\overline{w_c}$ (except that instead of the average parent cloud descent velocity, $\overline{w_c}$, the average nozzle exit velocity was used, $\overline{w_{exit}}$). Sau and Mahesh concluded that a critical point existed when this ratio was two, instead of unity. However, this includes no dependency on particle size, but the two ratios can be compared by using the smallest

size glass bead. For Glass Bead AH, the weak threshold was 3 *cm/s*. Then, using the diameter of the release cylinder, $D_{c,i}$ = 3.81 *cm*, as the "nozzle" diameter and the Reynolds number that Sau and Mahesh kept constant for most cases (600), the resultant equivalent average nozzle exit velocity is approximately 1.6 *cm/s*. This makes $u_{a,crit,1}/\overline{w_c} \sim 2$. Thus, the numerical results and the ratios that define the weak threshold between "weak" and "transitional" currents are in agreement. Sau and Mahesh also quantified the formation of a vortex ring using a stroke ratio, and in this study different aspect ratios, $H/D_{c,i}$, were employed by releasing particles with different amounts of water content into the ambient currents (instead of changing the cylinder size). The results of the particle/fluid mixture will be discussed in more detail later in this chapter.

4.2.2 Cloud Characteristics in Various Ambient Currents

In "weak" ambient currents, $u_{a,crit,1}/\overline{w_c} < 1$ or $u_{a,crit,1}/w_{c,max} < 0.1$, cloud descent (Figure 4-6) and growth (Figure 4-7) are similar to the quiescent case. Particle clouds are advected in the longitudinal direction (downstream, denoted in Figure 4-8 with negative distances from the point of release) with a speed approximately equal to the ambient velocity, independent of particle size. Although Figure 4-8 shows a slight discrepancy for the advection velocities of the B and D sized particles, this variability also exists when particle clouds are released in quiescent conditions. Therefore, the deviations in advection speed from the ambient current velocity are inconclusive. In Figure 4-8, both the B and D Glass Beads appear to cross the reference 6 *cm/s* and 12 *cm/s* lines in a random manner.
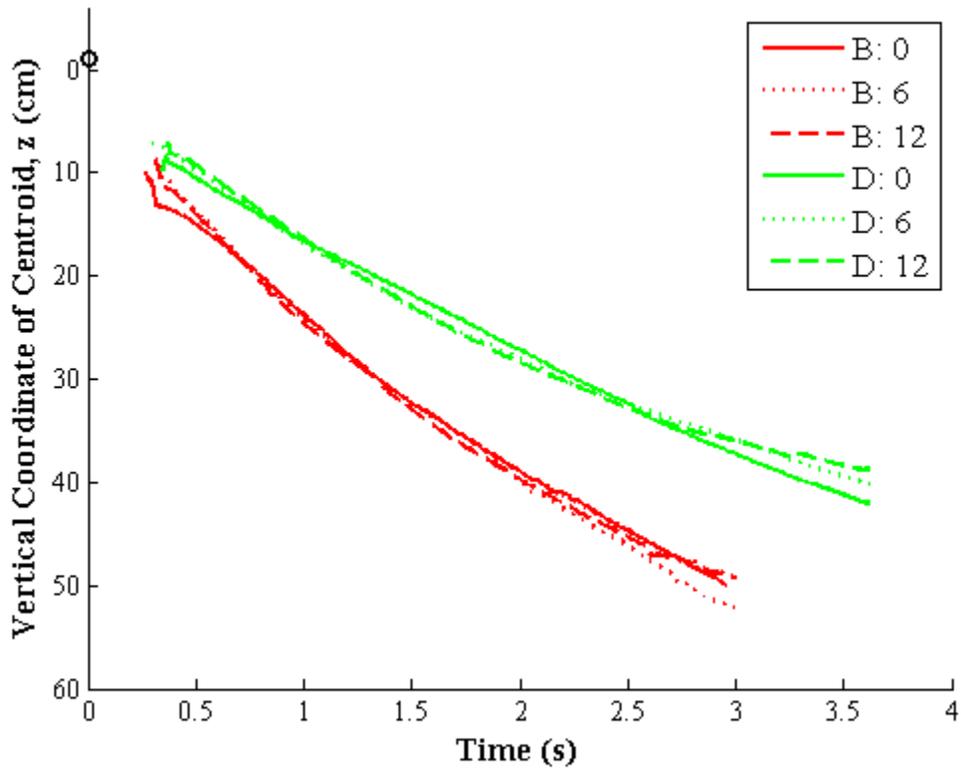
Figure 4-6: Vertical coordinate of the centroid of a descending particle cloud versus time for two different sized particles under two different ambient current velocities when released at the surface in a supersaturated (settled) condition. The open circle shows the pre-release height of the sediment.
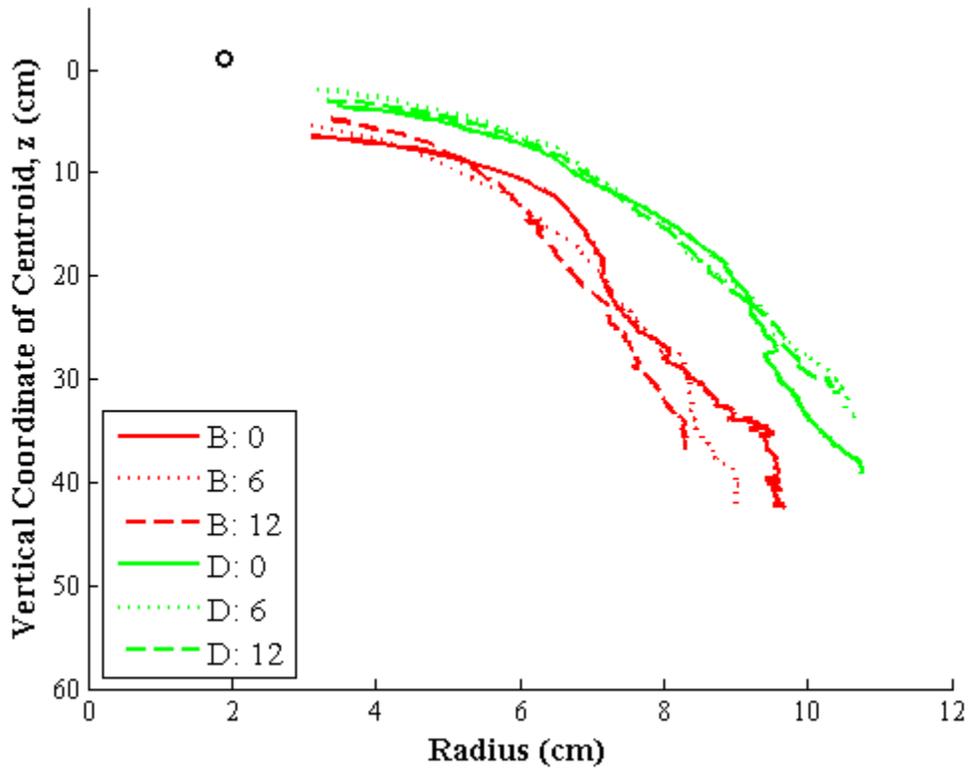
Figure 4-7: Vertical coordinate of the centroid of a descending particle cloud versus cloud radius for two different sized particles under two different ambient current velocities when released at the surface in a supersaturated (settled) condition. The open circle shows the pre-release height and radius of the sediment.
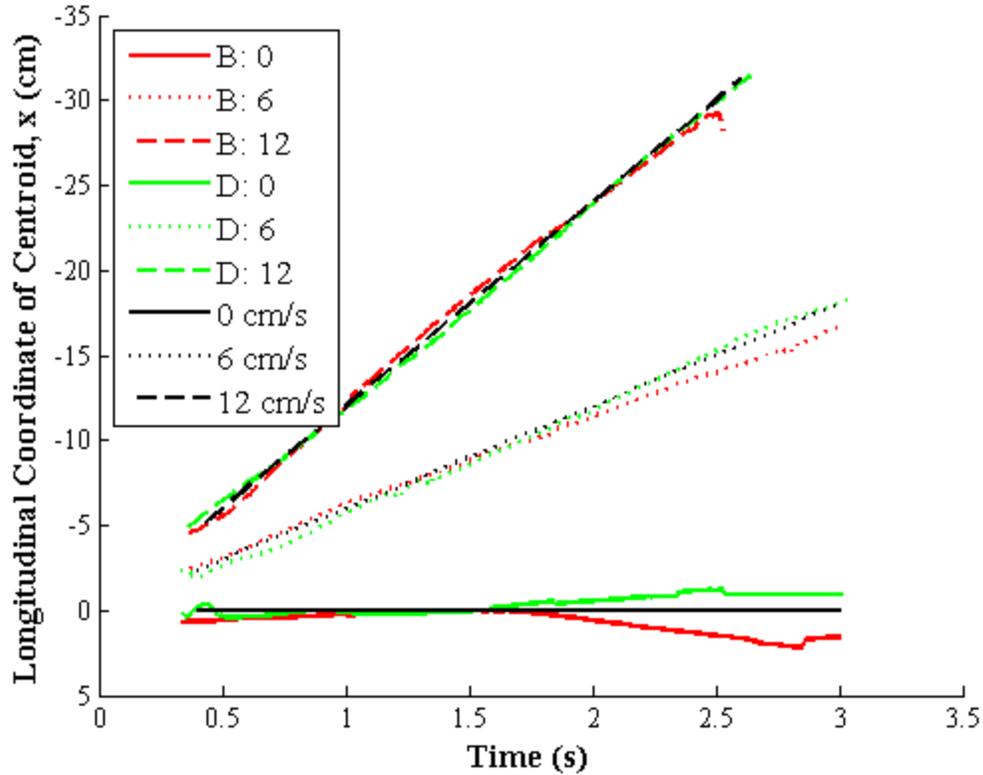
Figure 4-8: Longitudinal coordinate of the centroid of a descending particle cloud versus time for when particles were released below the surface into ambient currents of different magnitudes (two different particle sizes).

For "transitional" and "strong" ambient currents, $u_{a,crit}/\overline{W_c} > 1$ or

$u_{a,crit}/W_{c,max} > 1$, the qualitative observations are similar to the results documented by

Gu et al. (2008). In Chapter 2, their findings were summarized, and they reported that

particle clouds in cross-flows experienced greater growth (Note: Gu et al. defined a

"longitudinal width," which is similar to twice the radius of the parent cloud as named in

this thesis) and reduced descent velocities because the spherical vortex was either

damaged or destroyed; they also concluded that mixing between the particle cloud and

ambient fluid was enhanced. We are in agreement for observations and the limited data

available for "transitional" and "strong" currents. Gu et al. created currents ranging in magnitude from 8.96 *cm/s* to 26.88 *cm/s*, and as documented in Table 4-7 below, using Equations 4-1 and 4-2, every case qualified as either "transitional" or "strong" currents.

Table 4-7: The case and ambient current velocity, u, for the experimental cases of Gu et al. (2008) compared with the critical ambient current velocities of the weak and strong thresholds, $u_{a,crit,1}$ and $u_{a,crit,2}$, using Equations 4-1 and 4-2.

Case	u [cm/s]	$u_{a,crit,1}$ [cm/s]	$u_{a,crit,2}$ [cm/s]	Classification
1	8.96	7.8	10.8	Transitional
2	8.96	7.4	10.2	Transitional
3	8.96	6.8	9.3	Transitional
4	8.96	5.8	8.4	Strong
5	8.96	5.5	7.9	Strong
6	8.96	5.1	7.3	Strong
7	8.96	3.6	5.6	Strong
8	8.96	3.4	5.3	Strong
9	8.96	3.1	4.9	Strong
10	17.92	7.8	10.8	Strong
11	17.92	7.4	10.2	Strong
12	17.92	6.8	9.3	Strong
13	17.92	5.8	8.4	Strong
14	17.92	5.5	7.9	Strong
15	17.92	5.1	7.3	Strong
16	17.92	3.6	5.6	Strong
17	17.92	3.4	5.3	Strong
18	17.92	3.1	4.9	Strong
19	26.88	7.8	10.8	Strong
20	26.88	7.4	10.2	Strong
21	26.88	6.8	9.3	Strong
22	26.88	5.8	8.4	Strong
23	26.88	5.5	7.9	Strong
24	26.88	5.1	7.3	Strong
25	26.88	3.6	5.6	Strong
26	26.88	3.4	5.3	Strong
27	26.88	3.1	4.9	Strong

The magnitude of the ambient current used by Gu et al. ranged between one and more than eight times the critical ambient current velocity of the weak threshold. They comment that the pattern of greater longitudinal spread and reduced descent velocities were both amplified by continuing to increase the strength of the ambient current. This concurs with the observations made beyond the weak threshold for glass beads similar in size to the particles Gu et al. released. Further, for some of the cases that were barely above the weak threshold, the damage or destruction of the spherical vortex that was observed by Gu et al. could have been partly due to the delay in its formation that was recorded in the present study; this is possible since their channel depth was only 0.3 m (half of the depth used in this study). Unfortunately, they did not present any results for what would qualify as "weak" currents, which would have provided the best comparison between the two studies.

4.3 Parent Cloud Development

Once the threshold between "weak" and "transitional" ambient currents was determined, experiments were predominantly performed with "weak" ambient currents. For currents of these magnitudes, the parent cloud always formed with a spherical vortex. However, the speed of descent and the growth varied considerably when release variables such as elevation and water content were applied in different manners. Before these differences can be discussed, the most important variable that influenced the formation and appearance of the parent cloud was the particle size. Note that in this section, parent cloud characteristics, such as the descent velocity and radius, specifically refer to measurements taken on the parent cloud, but will be referred to as "cloud descent

velocity" and "cloud radius." A complete set of images and data for all releases is included in Appendix B and Appendix C, respectively.

4.3.1 Influence of Particle Type and Size

As briefly mentioned previously, the particle size has a significant influence upon the development of the parent cloud. This is shown by the selection of images in Figure 4-9. Clouds composed of larger particle sizes produced an increase in descent velocity (Figure 4-10) and a decrease in the cloud radius (Figure 4-11). These particle clouds of smaller radii were more coherent and had a more distinguishable separation between the parent cloud and trailing stem; however, the composition of the trailing stem will be discussed later. Deviations from these trends emerged when the particles were not perfectly spherical. The Specialty Glass particles were not spheres or as smoothly polished as the Ballotini Glass Beads, and their alteration in descent and growth is due to the increase in entrainment relative to a comparable sized spherical glass bead (see Table 4-8). The particle clouds created with the silica were so incoherent that difficulties arose while executing the image analysis program for images taken from these experiments, but the trends described above were still confirmed.

The entrainment coefficients for the "turbulent" and "circulating" thermal regimes of descent were defined according to the characteristics that Ruggaber (2000) outlined, specifically the presence of a spherical vortex and the change from a very high rate of entrainment to one that is lower: $\alpha 1$ and $\alpha 2$ respectively. The values of $\alpha 2$ are shown in Table 4-8 together with selected results from Ruggaber for his most-similar releases (all conditions were not identical). The values of $\alpha 1$ are not included here because the orientation of the laser in the water channel made it difficult for the image analysis to

distinguish between the growth of the parent cloud and its descent as it entered the field of view. The entrainment coefficients were found by calculating dr/dz (from Equation 2-4) for the entire descent and separating each region by finding the transitional depth where the values of entrainment alter significantly (or visually, if two linear regression fits were employed, where one would end and another would begin on the plot of radius of the parent cloud with descent; this is shown as a demonstration in Figure 4-12). This transition was observed at depths between 8 *cm* and 12 *cm* below the surface, which coincided with a radius of approximately four times the initial pre-release radius of the sediment; the latter result is consistent with Ruggaber's (2000) findings for non-cohesive sediments. However, Ruggaber did not report a change in entrainment due to particle size, though he did observe the difference in coherency. This may be due to the reduced range of particle sizes that he employed for his detailed analysis, so the trend may have not been as clear. Despite that, this is the lone discrepancy between the present results and his conclusions. These entrainment coefficients were also compared to theoretical values found using Equation 2-18, which was the formula derived by Rahimipour and Wilkinson (1992). This predicted entrainment coefficients between 0.26 and 0.31; however, these investigators did not distinguish between the two different phases of the thermal regime, so the comparison is not applicable.

Table 4-8: The entrainment coefficients for the "circulating" (α2) thermal regimes of descent for particle clouds composed of eight different particle sizes when released in the saturated condition from the surface. Selected results for Ruggaber's (2000) most-similar results are shown in the second row, and are denoted by an "(*)".

	SG 0	SG 00	A	B	D	AE	AH	SIL
α2	0.13	0.15	0.10	0.15	0.21	0.22	0.33	0.72
α2 (*)	-	-	-	-	0.17-0.22	-	0.12-0.20	-
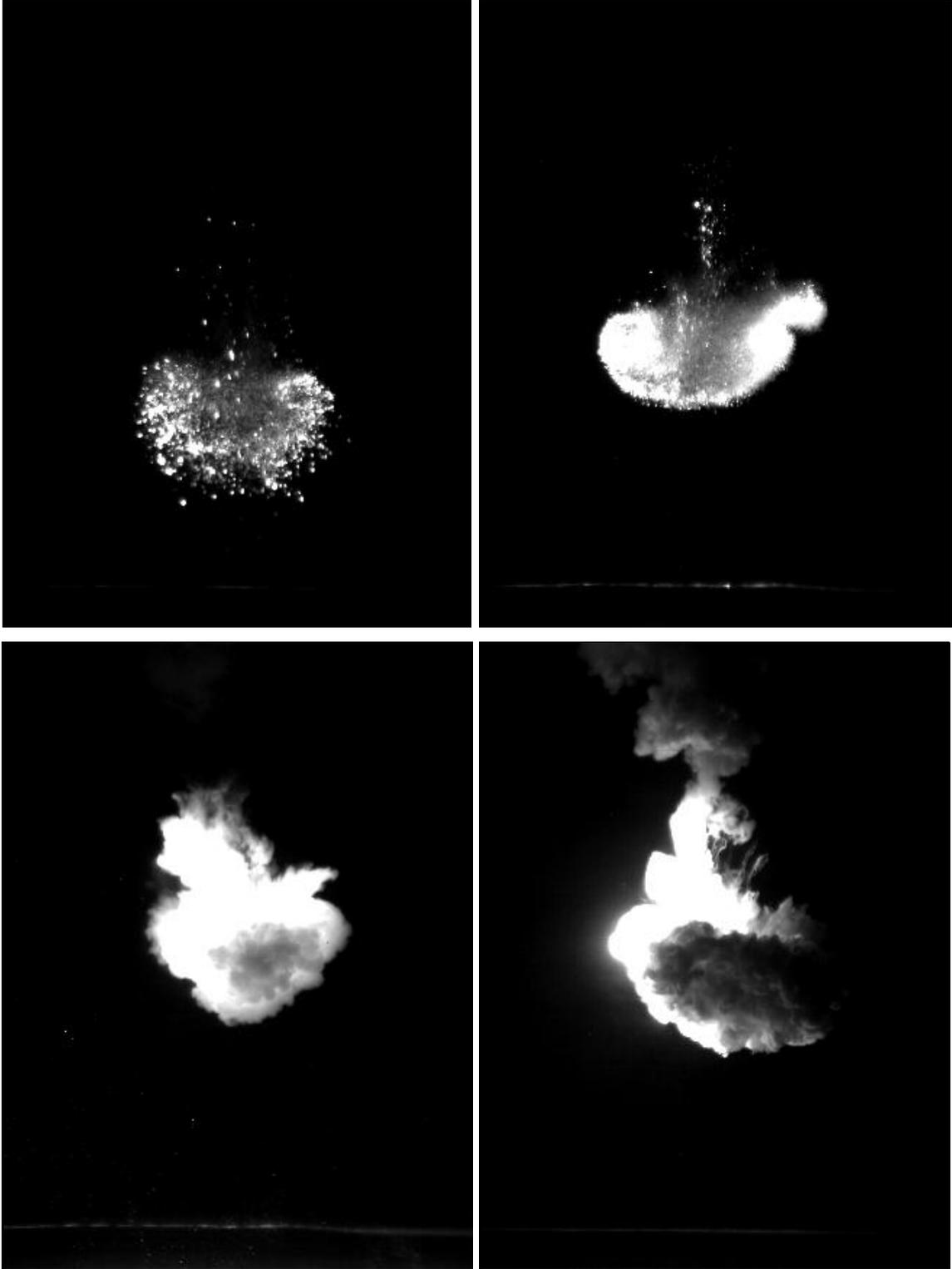
Figure 4-9: Left-to-right from top left: images of Specialty Glass 0, Glass Beads A and AH, and SIL-CO-SIL. The first three are images 1.5 *s* after release, and the silica image is 3.0 *s* after release (all releases are saturated and from the surface). The frame size is approximately 40 *cm* wide x 54 *cm* tall.
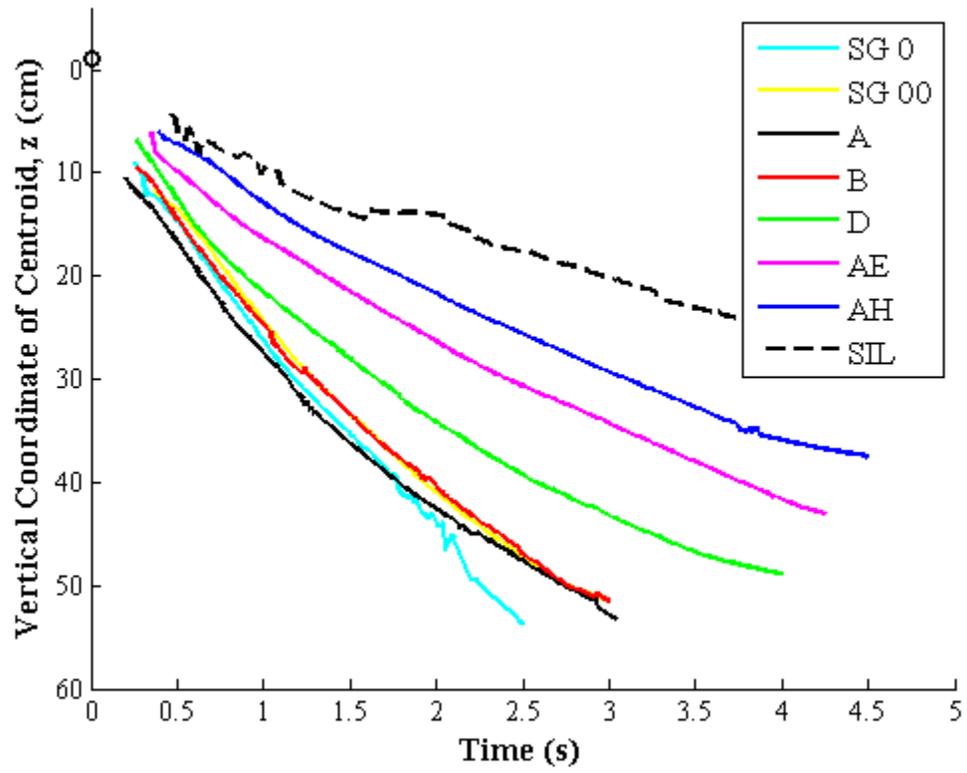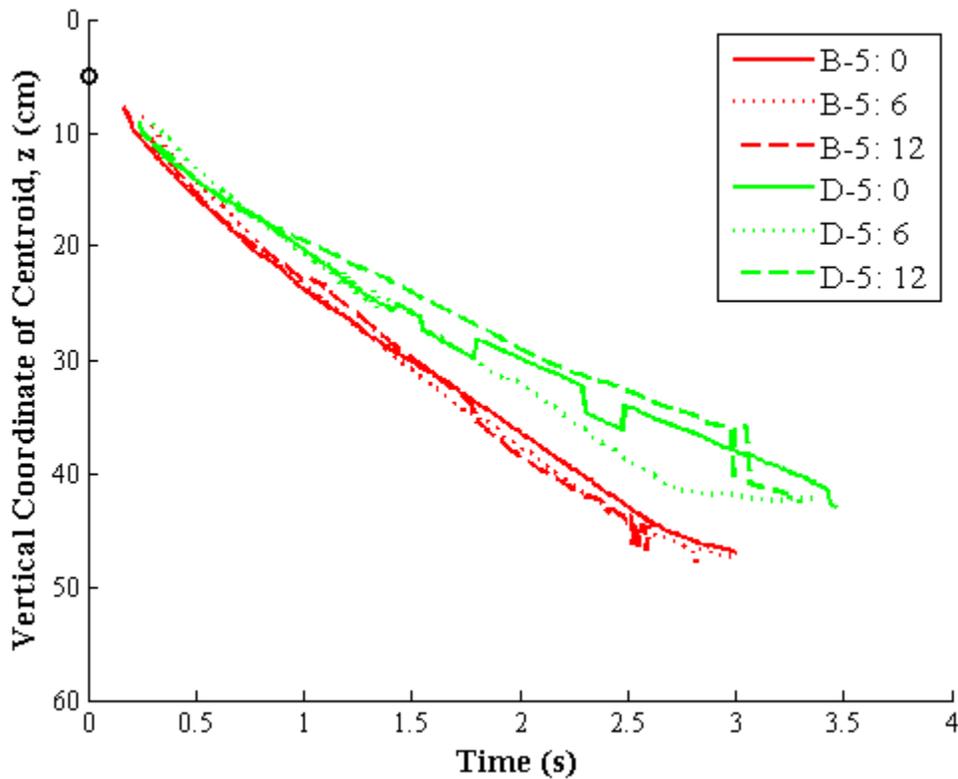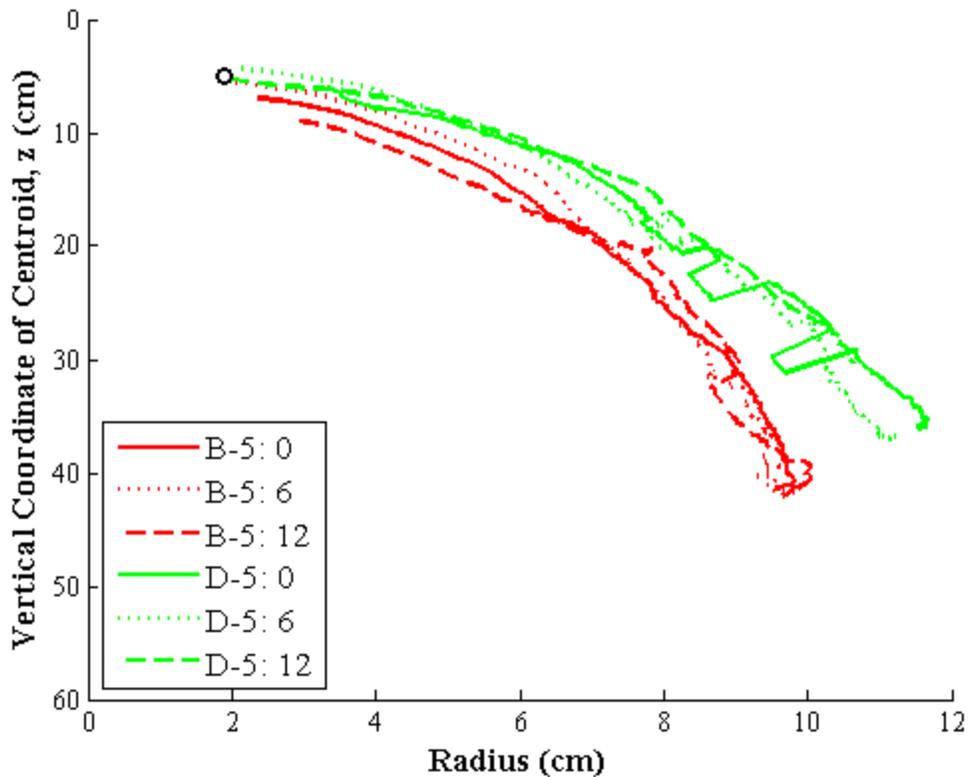
Figure 4-10: Vertical coordinate of the centroid of a descending particle cloud versus time for eight different sizes of particles when released at the surface in a saturated condition. The open circle shows the pre-release height of the sediment.
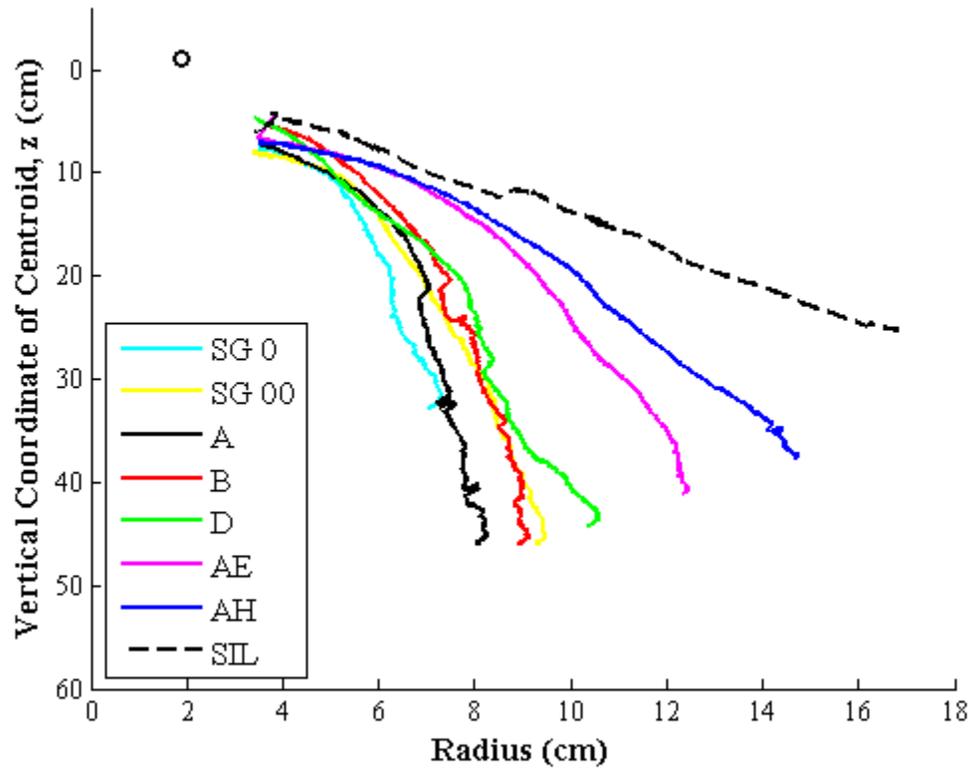
Figure 4-11: Vertical coordinate of the centroid of a descending particle cloud versus cloud radius for eight different sizes of particles when released at the surface in a saturated condition. The open circle shows the pre-release height and radius of the sediment.
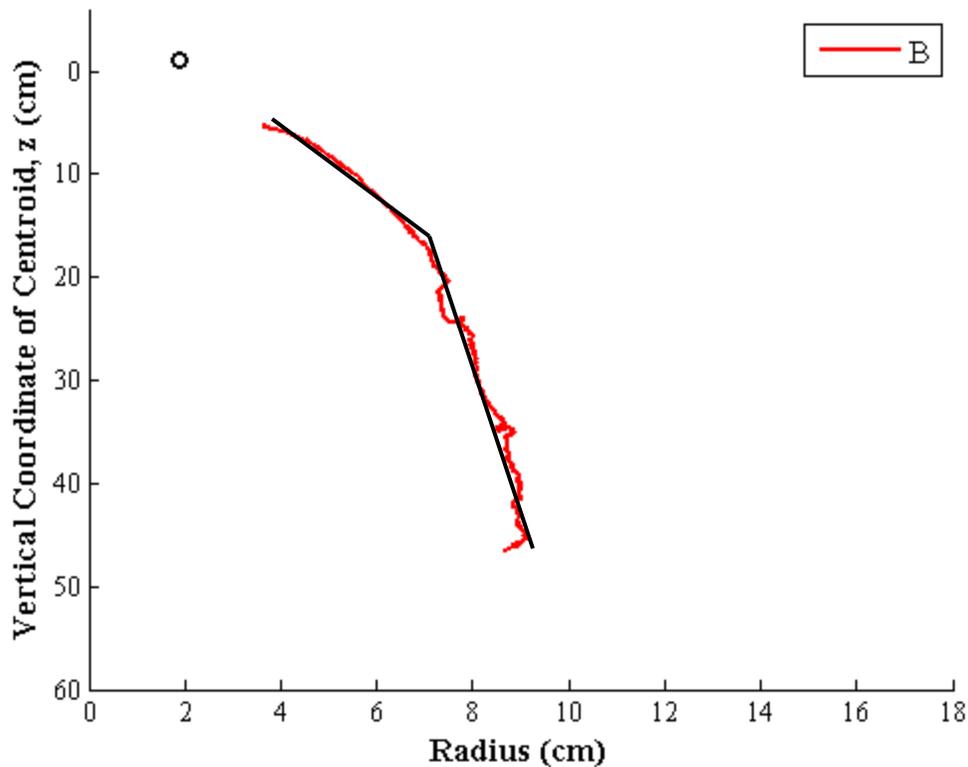
Figure 4-12: Vertical coordinate of the centroid of a descending particle cloud versus cloud radius for B Glass Beads when released at the surface in a saturated condition. The open circle shows the pre-release height and radius of the sediment. The black line shows the two linear regression lines that represent the "turbulent" and "circulating" thermal regimes of descent.

Although the particle clouds that resulted from silica releases were extremely incoherent, their use was explored to continue the investigation of particle size. The exploration of the influence of particle size on the development of the self-preserving thermal also included a brief examination of single phase thermals. To eliminate the multiphase aspect of descent, dense brine (25 % salt by weight) was also utilized to confirm the non-coherency and entrainment of a particle cloud composed of effectively infinitesimal particles. The observations described above were again confirmed, and an image of this type of release is shown in Figure 4-13.

4.3.2 Influence of Elevation

The elevation of the release mechanism above or below the water surface also had a significant impact on the formation of the parent cloud. An increased release elevation correlates with greater initial momentum when the particle cloud enters the water, and this corresponds to an increase in descent velocity (Figure 4-14) and a decrease in the cloud growth (Figure 4-15). For the trials done above the water surface in this study, a direct correlation was found between the release location with respect to the water surface and the resulting entrainment of the particle cloud (see Table 4-9). However, as specified earlier, these observations were made with the "above surface" elevation as 5 *cm* above the water surface. Limited observations so far by researchers at Nanyang Technological University have found that at much larger release elevations above the water surface, the particle cloud will spread in the air before entering the water, and that this "dilution" in the air will cause an increase in entrainment once the particle cloud enters the water, negating the effect of the initial momentum (D. Shao and B. Zhao, Personal Communication, 2010). The critical point where elevation and "dilution" cancel has not yet been determined.

Table 4-9: The entrainment coefficients for the "circulating" ($\alpha2$) thermal regimes of descent for particle clouds composed of two different particle sizes when released at three different elevations: above the surface (dry), at the surface (supersaturated), and below the surface. Selected results for Ruggaber's (2000) most-similar results are shown in the second row, and are denoted by an "(*)".

	B: +5	B: +1	B: -5	D: +5	D: +1	D: -5
$\alpha2$	0.11	0.17	0.20	0.19	0.22	0.24
$\alpha2$ (*)	-	-	-	0.12	0.18	0.18

Figure 4-13: The thermal created by dense brine when released from the surface; it has been colored with rhodamine dye to enhance the visualization of the cloud structure. The frame size is approximately 44 *cm* wide x 55 *cm* tall.
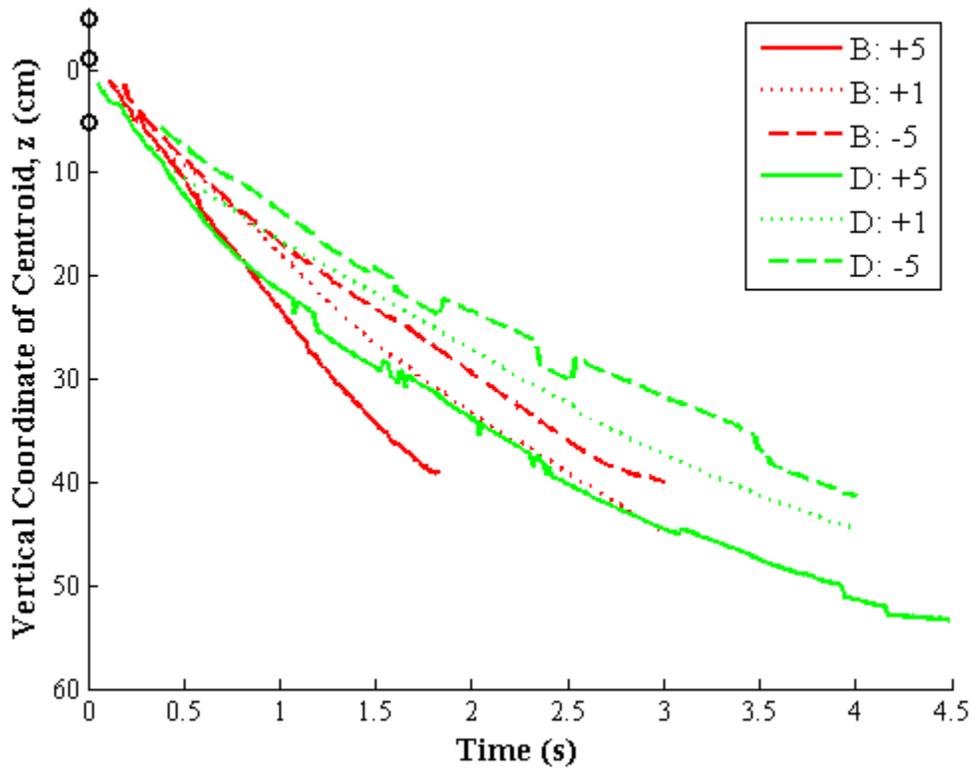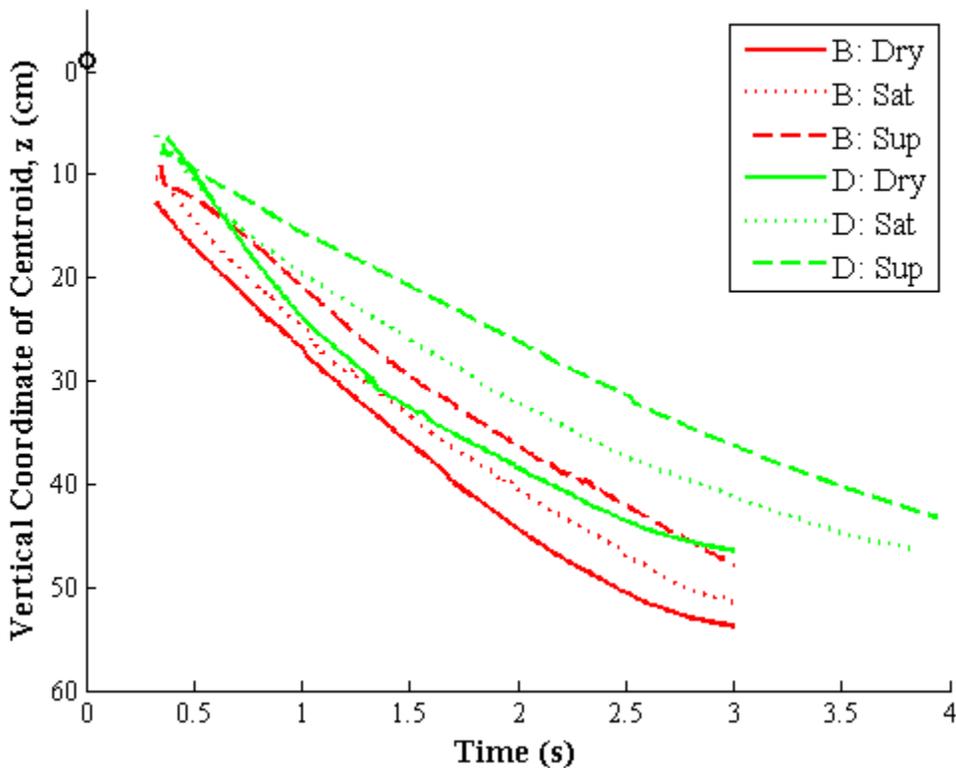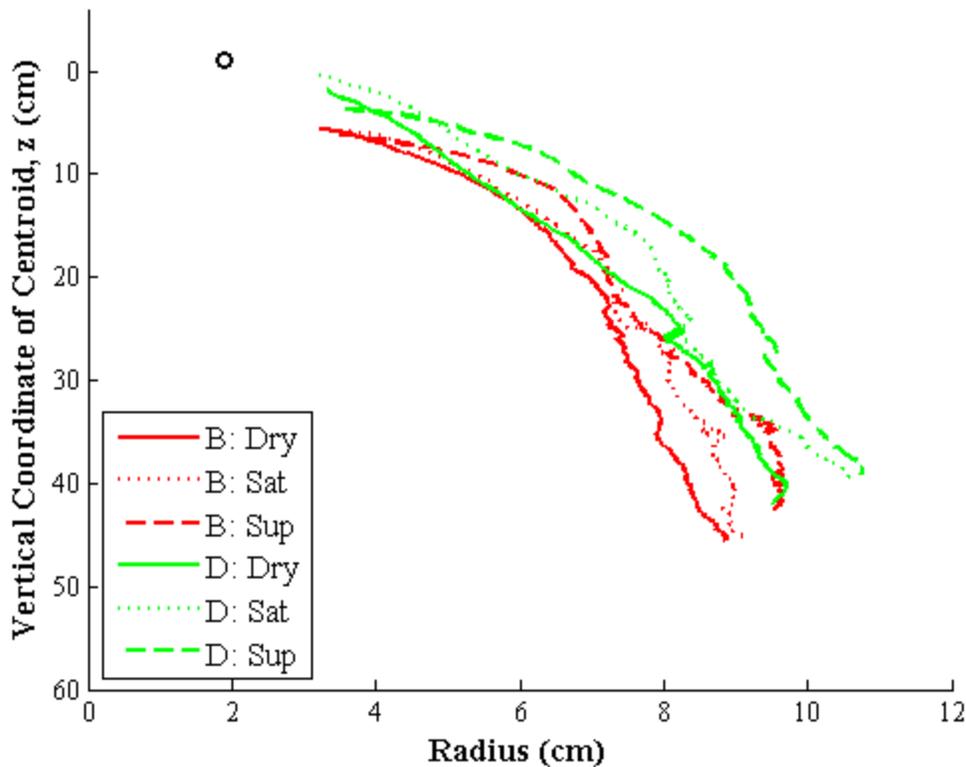
Figure 4-14: Vertical coordinate of the centroid of a descending particle cloud versus time for two different sizes of particles when released above the surface (dry), at the surface (supersaturated), and below the surface. The open circle shows the pre-release heights of the sediment – all the data have been translated to the surface release height for ready comparison.
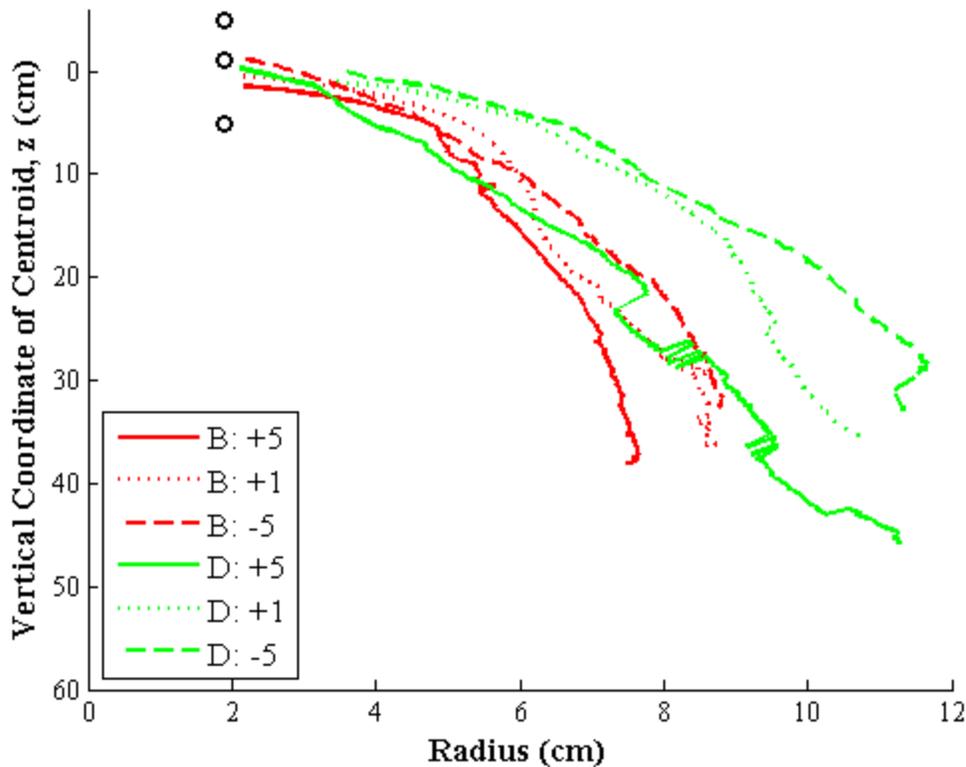
Figure 4-15: Vertical coordinate of the centroid of a descending particle cloud versus cloud radius for two different sizes of particles when released above the surface (dry), at the surface (supersaturated), and below the surface. The open circle shows the pre-release heights and radius of the sediment − all the data have been translated to the surface release height for ready comparison.

A unique aspect of the below surface release that was been noted in previous studies is the delay of the release of the particle cloud, or what Ruggaber (2000) called the "stalling" effect. The calculated increase in entrainment for below surface releases is not due entirely to the removal of the initial momentum, but also due to the action of the ambient water attempting to enter the release cylinder at the same time that the particles are exiting in order to maintain equilibrium between the water levels inside and outside the cylinder. This action slows the release and leads to a decrease in descent velocity and corresponding increase in cloud growth. With the introduction of ambient currents, it

was thought that the "stalling" effect might actually be reduced by the action of the ambient currents in removing the particles from the release cylinder, thus freeing up more area for water to exchange places with the particles. However, as Figure 4-16 and Figure 4-17 show, even with "weak" ambient currents, the growth of particle clouds released below the surface remains nearly identical between the flowing and stagnant cases (and larger than surface and above surface releases). It is important to note, however, that much of this "stalling" effect would be reduced in the field because a split-hull barge, for example, would float higher in the water as the sediment was released, reducing the volume of water required to enter the release vessel. The degree to which the results would change is unknown.

Figure 4-16: Vertical coordinate of the centroid of a descending particle cloud versus time for two different sizes of particles when released below the surface in quiescent and flowing conditions. The open circle shows the pre-release heights of the sediment.

133

Figure 4-17: Vertical coordinate of the centroid of a descending particle cloud versus cloud radius for two different sizes of particles when released below the surface in quiescent and flowing conditions. The open circle shows the pre-release height and radius of the sediment.

4.3.3 Influence of Water Content and Particle Condition

A release variable nearly as important as the elevation of the release mechanism was the moisture content of the sediment prior to being released. By introducing water and creating a sediment/fluid mixture, the two substances interact in a unique manner, creating the multiphase thermal (as seen in Figure 4-18). Once the mixture has entered the water channel, the water that was initially in the release cylinder is separated from the particle front, but it is still within the parent cloud (i.e., has largely not been left behind in the wake or trailing stem). The water fills the voids between particles prior to being
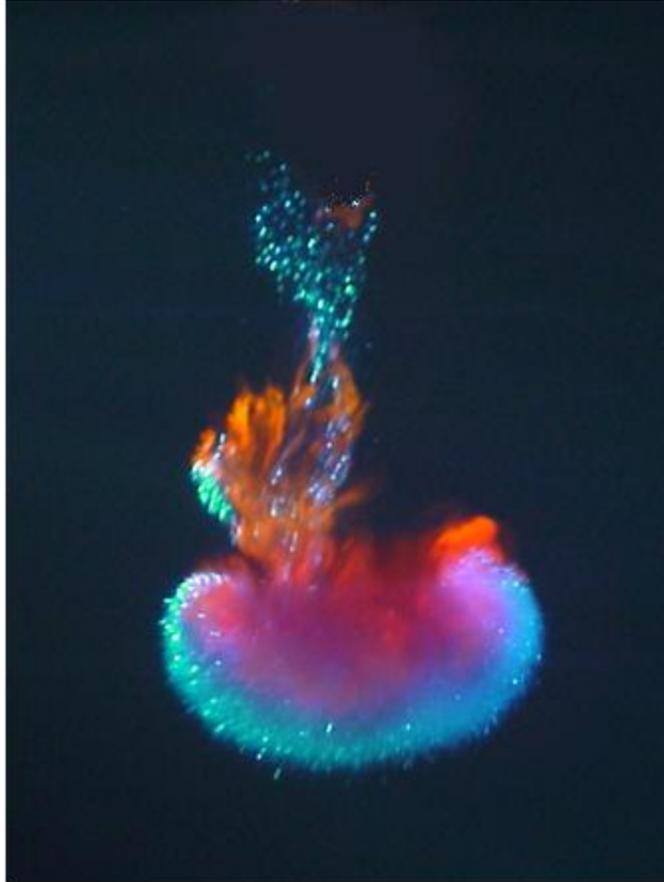
Figure 4-18: The thermal created by B Glass Beads when released from the surface in the saturated condition (with rhodamine dye), into a 6 cm/s current. Note the trailing stem as well as the separation of the fluid and particles. The frame size is approximately 31 *cm* wide x 55 *cm* tall.

released and reduces the friction among individual particles after the release. In the thermal phases of descent, this corresponds to an increase in the entrainment of the particle cloud, and the corresponding decrease in descent velocity (Figure 4-19) and increase in cloud growth (Figure 4-20). The trends are in agreement with the results that Ruggaber (2000) reported. The actual entrainment values are shown for surface releases with all three water conditions in Table 4-10. A notable difference between the saturated and supersaturated condition, with the latter creating a supernatant layer of fluid on top of the particles when they are settled in the release mechanism, is that the excess fluid acts to not only fill the voids, but also drives the particles out of the cylinder and forces them

135

to spread in the water channel. The effects that this has on the trailing stem and predicting the material "lost" to the ambient environment will be discussed in the next two sections.

Table 4-10: The entrainment coefficients for the "circulating" ($\alpha2$) thermal regimes of descent for particle clouds composed of two different particle sizes when released with three different water contents from the surface: dry, saturated, and supersaturated. Selected results for Ruggaber's (2000) most-similar results are shown in the second row, and are denoted by an "(*)".

	B: Dry	B: Sat	B: Sup	D: Dry	D: Sat	D: Sup
$\alpha2$	0.13	0.15	0.17	0.16	0.21	0.22
$\alpha2$ (*)	-	-	-	0.14-0.16	0.08-0.14	0.18

Figure 4-19: Vertical coordinate of the centroid of a descending particle cloud versus time for two different particle sizes when released with three different water contents from the surface: dry, saturated, and supersaturated. The open circle shows the pre-release height of the sediment.

Figure 4-20: Vertical coordinate of the centroid of a descending particle cloud versus cloud radius for two different particle sizes when released with three different water contents from the surface: dry, saturated, and supersaturated. The open circle shows the pre-release height and radius of the sediment.

Finally, the effect of the particle condition (i.e., settled or suspended) was not independently investigated because suspended sediment is highly unlikely in surface and above surface releases involving back hoe type dredges. Suspended conditions were created for the below surface releases, but without varying any other release variables, the effect of particle condition on the parent cloud could not be determined.

4.4 Quantifying Mass within the Trailing Stem

Sediment in the trailing stem is more likely to be transported away from a disposal site by ambient currents, potentially resulting in economic losses and negative

environmental consequences. Thus, it is important to be able to quantitatively distinguish the mass of sediment between the parent cloud and the trailing stem. In order to perform this task, the patterns and traces of the particles on the bottom of the water channel were analyzed and collected according to the grid described in Chapter 3. The deposition patterns from particle cloud experiments performed in ambient currents of various magnitudes were compared to the deposition outlines for similar release conditions in quiescent conditions. The fraction of mass that was found in the trailing stem was compared to the results found by Ruggaber (2000) using his sediment trap in quiescent conditions. Although "weak" currents were used for all experiments (implying similar sized parent clouds), it was discovered that the distribution of mass between the parent cloud and trailing stem varies with current speed, and this is discussed in this section.

4.4.1 Distinguishing the Parent Cloud and Trailing Stem

The trailing stem is of particular interest when studying particles clouds because the mass in this structure is most likely to be lost to the ambient environment; this is important given the economic and environmental considerations of open-water sediment disposal. The bottom depositions were used to quantify the mass that was originally part of the trailing stem; to do this, the shape of the descending particle cloud needed to be modeled. To simplify this process, the typical particle cloud (Figure 4-21) was characterized with a square cross-section, creating a rectangular parent cloud and trailing stem (Figure 4-22). In the presence of an ambient current, the front (lowest edge) of a descending parent cloud touches the bottom while the remainder of the parent cloud above the front edge is still advecting downstream with a speed approximately equal to

the ambient current velocity. Therefore, in an ambient current, the depositions on the bottom that belong to the parent cloud will be longitudinally larger than the depositions collected under quiescent conditions (refer to Figure 3-5). This required a correction factor to distinguish the particles collected from the bottom that originally belonged to the parent cloud and trailing stem, respectively.

Figure 4-22 shows the particle cloud at the time when the bottom half of the parent cloud has landed on the bottom, while the top half is still descending. The regions that are colored green on the corners of the parent cloud (Areas (D) and (E) of Figure 4-22) represent the sections of the parent cloud that land on the bottom outside of an area equal to the deposition area under quiescent conditions (Area (1) of Figure 3-5). Therefore, a correction factor (Area (2) of Figure 3-5) can be applied to the characteristic deposition length by using the images of the particle clouds to determine the length of time from the moment the parent cloud touches the bottom to when the entire parent cloud has settled out of suspension. This correction factor is the sum of Δx_a and Δx_f in Figure 4-22. Using the velocity of the ambient current, the required correction length is easily determined and added to the deposition length in quiescent conditions to designate the depositional area of mass that was originally part of the parent cloud (Areas (1) and (2) of Figure 3-5).

In general, ~ 99 % of the mass that landed within the grid was collected, so by using this system, all other mass that was collected further downstream can be assumed to have formerly been within the trailing stem (Area (3) of Figure 3-5 and Area (C) of Figure 4-22); however, part of the trailing stem (the region colored red, or Areas (A) and (B) on the trailing stem in Figure 4-22) also lands within the area designated as the parent

cloud. Thus, this estimate for the mass of particles included within the trailing stem is an underestimate. A second (or "best") estimate attempts to account for the fraction of the trailing stem that landed within the parent cloud by adjusting the correction factor to eliminate Δx_f. By eliminating Δx_f from the correction factor, the mass in Area (B) of the trailing stem is now properly accounted for. However, mass in Area (A) is still approximated. The approximation is tantamount to assuming that Area (D) of Figure 4-22 is equal to Area (A), i.e., counting mass on the outskirts of the parent cloud (D) as part of the trailing stem in exchange for counting mass within the trailing stem (A) as part of the parent cloud. For both estimates, the correction factor is adjusted for each set of release variables and the current speed by looking directly at the images and extracting the time required for the particles to settle. The next section will discuss the influence of the release variables on the formation of the trailing stem.
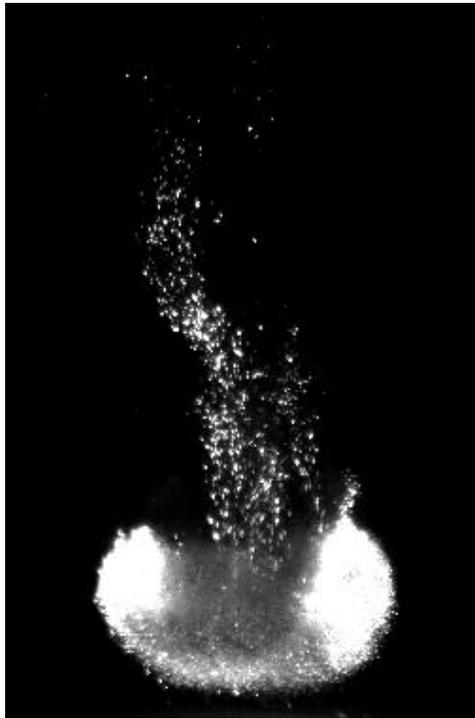
Figure 4-21: An example of a descending particle cloud created with dry, B Glass Beads that were released at the surface in a 6 *cm/s* ambient current.
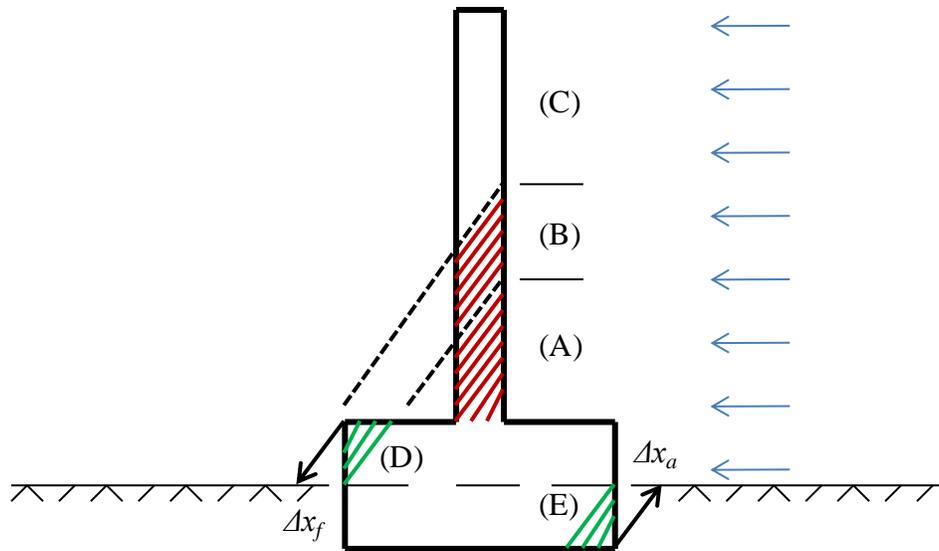
Figure 4-22: A simple model of a descending particle cloud. The green regions indicate the parts of the parent cloud that land outside the deposition area with a characteristic length equal to a particle cloud descending in quiescent conditions. The red region indicates the part of the trailing stem that will be included in the area designated as the parent cloud, and thus not counted in the first estimate of particle mass in the trailing stem. A "best" estimate of the total mass within the trailing stem is calculated by adding Area (B), as well Area (D) of the parent cloud in exchange for neglecting Area (A).

4.4.2 Influence of Release Variables

Using the analytical methods described in the previous section, Table 4-11 and Table 4-12 summarizes the fraction of mass that was within the trailing stem using an underestimate ("1") and a best estimate ("2"), shown as a percentage of the total mass initially released. The most important conclusion is that releases in ambient currents cause more mass to be left out of the parent cloud and be part of the trailing stem, and the mass increases sharply as the velocity of the ambient current increases, regardless of the combination of release variables. In terms of other release variables, Table 4-11 and Table 4-12 indicate a strong sensitivity to particle size and release height, but the results do not show as clear of a trend with variations in water content. Particle clouds composed of larger particles incorporate more of the initial mass into the parent cloud.

143

Particle clouds released from the surface also incorporate more of the initial mass into the parent cloud. The vertical dispersion of particles in the air that occurs for releases above the surface appears to contribute to more mass being left behind in the trailing stem. Similarly, the "stalling" effect of the subsurface releases slows the release enough to prevent a large portion of the mass from becoming included in the parent cloud. The best release height, or the elevation that resulted in the lowest percentage of mass in the trailing stem, was at the surface.   Unfortunately, the results for including different

Table 4-11: The total mass collected within the grid and the percentage of mass in the trailing stem using an underestimate ("1") and best estimate ("2") for all Group 2 experiments.   Results annotated by (*) are from Ruggaber (2000) for experiments performed with comparable conditions. Results annotated by (**) are overestimates and indicate an upper bound for material in the stem, but the exact amount is unknown because too many particles advected beyond the grid.

Experiment Designation	Mass Within Grid	Total Trailing Stem (1)	Total Trailing Stem (2)
D+5RT 0	99.4%	-	-
D+5RT 12	80.7%	19.3%	N/A
D+1RT 0	99.4%	$5.8 \pm 1.5\%$ (*)	
D+1RT 6	97.8%	5.7%	6.9%
D+1RT 12	87.1%	15.4%	16.8%
D+1AT 0	99.8%	$1.9 \pm 0.4\%$ (*)	
D+1AT 6	95.1%	8.2%	9.3%
D+1AT 12	71.2%	$< 28.8\%$ (**)	21.8%
D+1PT 0	99.9%	-	-
D+1PT 6	96.6%	9.0%	10.6%
D+1PT 12	74.3%	$< 25.8\%$ (**)	22.8%
D-5PS 0	99.8%	$9.2 \pm 1.8\%$ (*)	
D-5PS 6	94.3%	11.8%	13.9%
D-5PS 12	71.9%	28.1%	30.5%

Table 4-12: The total mass collected within the grid and the percentage of mass in the trailing stem using an underestimate ("1") and best estimate ("2") for all Group 3 experiments.

Experiment Designation	Mass Within Grid	Total Trailing Stem (1)	Total Trailing Stem (2)
B+5RT 0	99.9%	-	-
B+5RT 12	98.6%	7.4%	9.9%
B+1RT 0	99.9%	-	-
B+1RT 6	99.9%	1.8%	3.3%
B+1RT 12	99.3%	4.9%	6.9%
B+1AT 0	99.4%	-	-
B+1AT 6	99.9%	1.6%	3.6%
B+1AT 12	98.9%	5.7%	8.3%
B+1PT 0	100.0%	-	-
B+1PT 6	99.5%	3.4%	6.5%
B+1PT 12	97.8%	5.9%	7.4%
B-5PS 0	99.9%	-	-
B-5PS 6	99.8%	5.6%	8.1%
B-5PS 12	97.3%	14.4%	19.3%

amounts of water content in the sediment/fluid mixture are not conclusive; the greater circulation of the parent cloud with wet sediment releases should draw more mass into the parent cloud, but the results do not convincingly show this result. More discussion on the practical implications of these results is contained in Chapter 5, and the figures showing the mass collected in each grid interval for all trials are included in Appendix D.

4.5 Predicting "Losses"

The particles collected from the bottom were also used for a related purpose, independent of whether or not they were originally in the parent cloud or trailing stem. In order to provide a practical recommendation for the optimal conditions under which open-water sediment disposal can take place, it is desirable to know the total percentage of mass "lost" to the ambient environment during disposal. In this context, the mass "lost" is not necessarily mass that will never settle out of suspension, but mass that does not fall within a given "target." This was determined using two approaches: 1) reporting the percentage of mass that deposits outside a circle with a radius equal to the water depth that is centered at the drop site; and 2) reporting the percentage of mass that deposits outside the same size circle but centered at the predicted impact location of the parent cloud. For the second method, estimates had to be made on the spread of particles beyond the grid for the equivalent of one to two grid intervals, because for several trials, too many particles advected beyond the grid. This was done by comparing multiple trials and looking at characteristic deposition patterns, and the appropriate deduction was made from the "losses" computation. These two methods of reporting the mass lost to the ambient environment are shown in Figure 4-23. The results of these two methods are shown in Figure 4-13 and Figure 4-14.

.
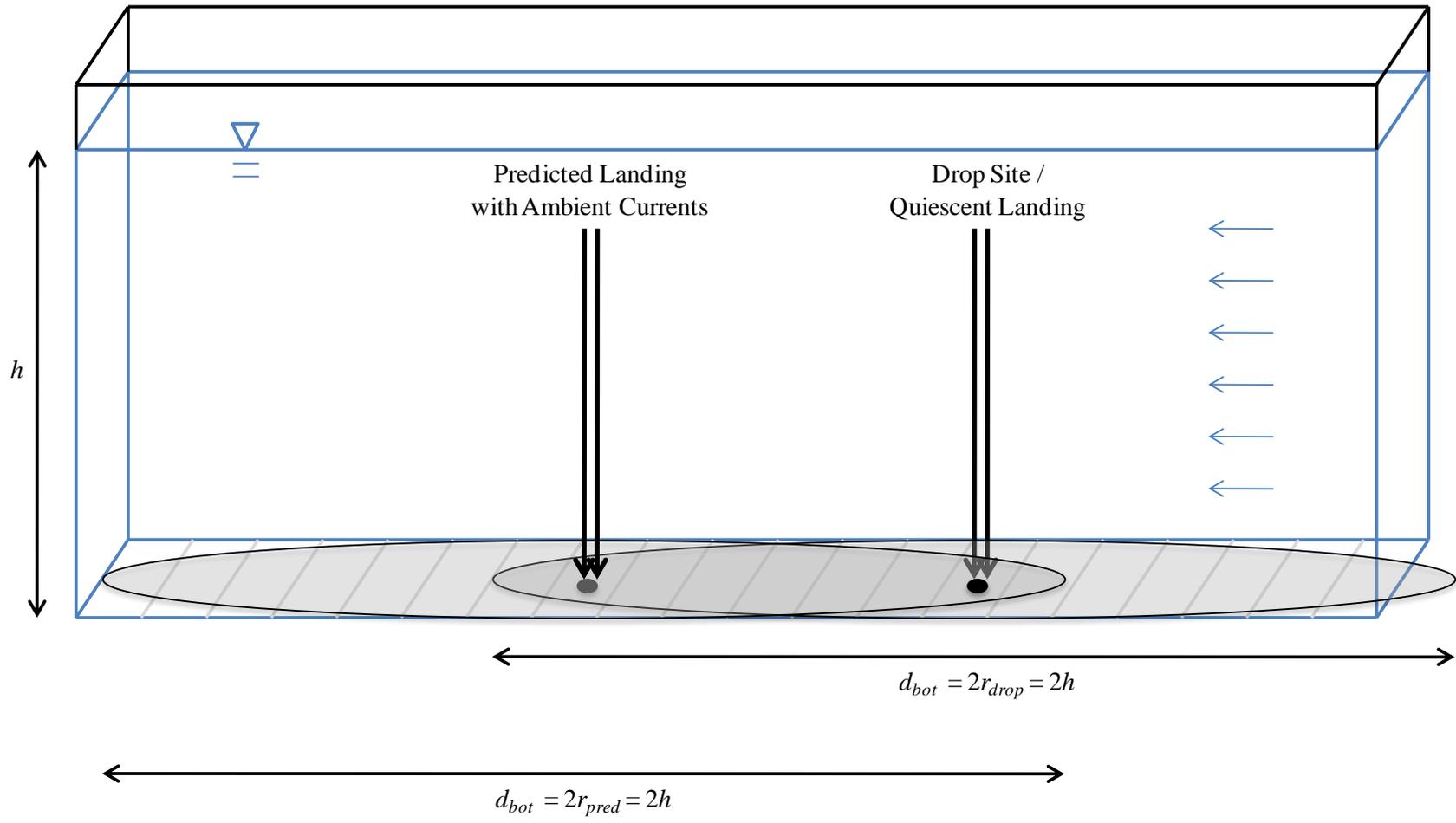
Figure 4-23: Schematic of the two methods of reporting sediment lost to the ambient environment using the deposition pattern of particles collected from a longitudinal grid on the bottom of the water channel.

Table 4-13: The percentage of mass lost to the ambient environment for Group 2 experiments using two definitions for the center of the disposal area. The trials repeated with an (*) are the below surface results that have been adjusted for a change in descent to 55 *cm* rather than the 60 *cm* used in other trials.

Experiment Designation	Mass Lost, $r_{drop} = h$	Mass Lost, $r_{pred} = h$
D+5RT 0		
D+5RT 12	N/A	15.3%
D+1RT 0		
D+1RT 6	11.2%	2.9%
D+1RT 12	39.9%	9.9%
D+1AT 0		
D+1AT 6	25.4%	9.3%
D+1AT 12	82.9%	21.8%
D+1PT 0		
D+1PT 6	24.4%	5.3%
D+1PT 12	70.3%	20.8%
D-5PS 0		
D-5PS 6	21.8%	7.4%
D-5PS 12	73.2%	21.1%
D-5PS 0 (*)		
D-5PS 6 (*)	29.96%	9.1%
D-5PS 12 (*)	83.60%	24.1%

Table 4-14: The percentage of mass lost to the ambient environment for Group 3 experiments using two definitions for the center of the disposal area. The trials repeated with an (*) are the below surface results that have been adjusted for a change in descent to 55 *cm* rather than the 60 *cm* used in other trials.

Experiment Designation	Mass Lost, $r_{drop} = h$	Mass Lost, $r_{pred} = h$
B+5RT 0		
B+5RT 12	23.9%	1.4%
B+1RT 0		
B+1RT 6	0.9%	0.2%
B+1RT 12	16.7%	0.8%
B+1AT 0		
B+1AT 6	1.6%	0.2%
B+1AT 12	35.3%	1.1%
B+1PT 0		
B+1PT 6	1.6%	0.6%
B+1PT 12	28.0%	2.2%
B-5PS 0		
B-5PS 6	1.9%	0.4%
B-5PS 12	24.2%	2.7%
B-5PS 0 (*)		
B-5PS 6 (*)	3.05%	0.65%
B-5PS 12 (*)	38.14%	3.54%

The most important conclusion for "weak" ambient currents is that the landing location of the particle cloud can be predicted, significantly reducing the mass of sediment "lost" to the ambient environment. Not surprisingly, the observed percentage of mass lost beyond the drop site exhibits similar trends with release conditions as does the previously observed percentages made with the trailing stem. Smaller particles, with

their much lower individual particle settling velocities and reduced descent velocities of particle clouds composed of them, are more likely to be advected greater distances in ambient currents. The releases above the water surface cause a dilution of the particles in the air prior to entering the water, but their horizontal transport is limited by the greater momentum when entering the water. Although the time required to impact the bottom is reduced when compared to surface releases, the enhanced spreading negates this advantage. The losses for the subsurface releases initially appear to be less than the corresponding surface releases, but when the difference in depth of descent is accounted for (they must travel 5 cm less), the losses are actually larger than the other modes of release. Finally, the surface releases with varying degrees of moisture shows a clear trend for predicting losses that originate as mass within the parent cloud and trailing stem. Dry releases are the best; because of the reduced circulation, particle clouds that are released dry spread less. Saturated releases are the worst because the circulation is increased to its maximum and gains no benefit from the added momentum. The supersaturated releases are in the middle because the supernatant excess water layer helps push more of the particles down immediately after release, and this partly offsets the enhanced spreading. Additional discussion with implications for the field is added in Chapter 5.

5 Conclusions, Significance, and Suggestions for Future Research

This chapter summarizes the conclusions of this study, discusses the practical interpretations of these results, and also outlines the areas which require additional attention for research in the future.

5.1 Conclusions

The following conclusions can be made from the experimental study on particle clouds in ambient currents, as presented in this thesis:

- Particle clouds released into ambient currents exhibit three regimes of behavior, which are dependent upon the strength of the ambient current. A weak threshold distinguishes "weak" and "transitional" currents, where particle clouds in the former are advected with the current but otherwise behave as though they were descending in quiescent conditions. In the latter case, the spherical vortex that is characteristic of the "circulating" thermal stage of descent begins to be damaged, and the cloud will appear to spread more widely and to slow its descent as its mixing with the ambient surroundings is enhanced. The threshold depends on particle size and the ambient current velocity. Equation 4-1 was derived so that the critical ambient current velocity at the weak threshold can be determined using non-dimensional parameters found from properties of the released material

(i.e., the particle size, mass, and volume of sediment released). A strong threshold separates "transitional" and "strong" currents, where the latter causes the complete destruction of the spherical vortex or prevents it from ever forming. Equation 4-2 is a similar non-dimensional relationship that can determine the strong threshold based on the sediment properties; this latter threshold is also particle size dependent.

- When experiments were performed in "weak" ambient currents, the parent cloud always formed and its growth and descent depended heavily upon the initial set of release variables; it exhibited the greatest dependence on particle size. For the particles used in these experiments (0.040 mm to 3.18 mm), the entrainment coefficient in the "circulating" thermal regime ($\alpha2$) ranged between 0.10 and 0.72. However, for the glass beads that represented "clumps" and "particles" in the field, the range was less significant: between 0.11 and 0.20 for the "clumps;" and between 0.16 and 0.24 for the "particles." This meant that an increase in particle size increased the coherency and the descent velocity of the parent cloud and decreased its size. An increase in the release elevation above the water surface produced a similar trend, and the opposite was true with the introduction of water to create a sediment/fluid mixture; however elevation and moist sediment did not produce the same range of entrainment coefficients that resulted from changes in particle size. Particles that were not perfectly spherical also caused small deviations from these trends, but were not significant.

- The behavior of the trailing stem (in "weak" ambient currents) was also dependent upon the release variables, with the greatest sensitivity again due to

particle size. For experiments that simulated the release of field-sized particles, the trailing stem accounted for up to nearly 30 % of the pre-release mass. For experiments that simulated the release of field-sized clumps but were otherwise similar, the trailing stem accounted for up to nearly 15 % of the pre-release material. The mass that was incorporated into the trailing stem for all experiments also showed a strong dependence on the velocity of the ambient current, even if within the domain of "weak" currents. With all other conditions held constant, doubling the current speed would more than double the amount of mass that was left out of the parent cloud and included in its wake.

- Mass that was "lost" to the ambient environment, or in other words, deposited outside an acceptable range from the targeted disposal site, possessed similar trends as outlined with the trailing stem. A significant difference is that the mass which can advect away from a disposal site may originate in either the parent cloud or the trailing stem. Results show that the location of the impact of the particle cloud on the bottom can be predicted, and that increasing the ambient current velocity increases the likelihood of losing more mass (i.e., causes a greater spread of bottom deposits from the drop site). The particle size dependence was exhibited again, and when the modeled field-sized particles were released, up to 84 % was lost outside a circle with a radius equal to the water depth and centered at the disposal site; when a circle of the same size is translated to account for the ambient current velocity, the losses were reduced to less than 28 %. For the laboratory particles that represented field-sixed clumps, the corresponding losses were 38 % and 3.5 %, respectively.

5.2 Implications for Open-Water Sediment Disposal

The results on the three current regimes and the "losses" that result for "weak" ambient currents can be used to guide policy and regulations regarding open-water sediment disposal. It is desirable to limit open-water sediment disposal operations to time windows in which currents are "weak" because the resulting clouds are more coherent and much more predictable. Equation 4-1 can be used for predicting the weak threshold based on the material being disposed. By using current measurements, a time window could be determined where sediment disposal was allowed (if, for example, the currents are largely due to the tides). It is recommended that disposal not be conducted in "transitional" or "strong" currents because of the high percentage of mass that will advect well beyond the disposal site.

This experimental study also showed that particle clouds composed of larger particles incorporated more of the initial mass into the parent cloud; this suggests that when performing open-water sediment disposal in the field, clumps of particles (e.g., clay) may have a positive effect on minimizing mass in the trailing stem. If the sediment being disposed is cohesive, it would be advantageous to leave the sediment moist and in clumps instead of attempting to break down the clumps into individual particles. A caution should be issued, though, against blindly wetting down all particles prior to release because of the potential for them to spread more if saturated; however, if enough of a supernatant layer of excess water can be created on top of the sediment, then having the ability to pump water into the release vessel prior to disposal could be a method to reduces losses.

These considerations can be applied to dredged material that has been disposed in Boston Harbor. The Federal Navigation Channel has a depth of 12.2 *m* at MLLW, and it is approximately 3 *m* deeper at high tide. The maximum recorded currents in the navigation channels of Boston Harbor were 1.10 *m/s* during flood flow and 1.17 *m/s* during ebb flow during a post-disposal monitoring period (Tubman, 2007). These scale to 19.2 *cm/s* and 20.5 *cm/s* respectively in the laboratory. By assuming a repeating standing wave with a semi-diurnal period, a maximum percentage of losses to the ambient environment can be chosen that will correspond with a particular amount of time prior to or following slack water. The results indicate that at one hour before or after slack water, less than 1 % (0.2 to 0.7 %) of the initial mass, if clumps, would be lost outside a circle with a radius equal to the depth, and less than 10 % (2.9 to 9.1 %) of the initial mass, if particles, would be lost. If the disposal window is extended to two hours before or after slack water, then less than 5% (0.8 to 3.5 %) of the initial mass, if clumps, would be lost outside a circle with a radius equal to the depth, and less than 30 % (19.3 to 28.8 %) of the initial mass, if particles, would be lost. These results use the ambient current velocity to predict the deposit location of the particle cloud. Therefore, the existing acceptable practice of allowing disposal operations one hour prior to and two hours following slack water appears appropriate. However, the range of results shows that regulations should take into account the size of the sediment being disposed, and if possible in the future, the expected condition of the sediment as well. Oversight agencies could also encourage the practice of predicting the landing sites of the particle clouds based on the speed of the ambient current, because it reduces the losses by more than a factor of two.

5.3 Recommendations for Future Research

In addition to the work which state and federal agencies can do to regulate open-water sediment disposal, there are several areas of research that could be continued to better understand the behavior of particle clouds:

- Improvements and changes could be made to parts of the release mechanism to better understand several processes and focus the comparison between releases in the lab and the field.

  o If the focus of the experimental study is to calibrate a numerical model, such as one that uses forcing similar to a piston to simulate the release, then experiments could be done with different cylinder sizes (ideally smaller ones) to create different release cylinder aspect ratios. This also makes the release time longer, and not so instantaneous, which is similar to the conditions of the real world. Unfortunately, the repeatability of experiments decreases substantially if the release time is increased too much.

  o If the focus of the experimental study is one specific type of release in the field, such as a back hoe dredge, then more work could be done with a release mechanism similar to a hemispherical cup, rather than a cylinder. This type of release introduces the axial rotation of the real release. This introduces asymmetry, so once again there is a tradeoff between the accurate modeling of release in the real world and repeatability in the lab; some processes may be quite random, but that can be documented as well.

- o A final element of the release mechanism can be improved if the focus of the experimental study is on one specific type of release in the field. For example, if considering a split-hull barge, then the subsurface releases could be equipped so that the release mechanism can float instead of being fixed at a particular depth. This would allow the release mechanism to rise in the water column as sediment is disposed, which would be similar to the way that a barge's draft would decrease in the field as it disposes of its dredge material.

- Additional experiments could be performed that vary the condition of the sediment for different sets of other release variables. This would not be limited to allowing the particles to settle or stirring them into suspension, but different combinations of sediment of various sizes could also be used to simulate non-homogeneous sediments in the field.

- The work on the ambient current threshold between "weak," "transitional," and "strong" currents could be continued, particularly between "transitional" and "strong" currents, as a function of particle size. This has practical consequences for determining the amount of sediment that is lost to the ambient environment in more extreme field operations.

- Experiments could also be performed in a recirculating water channel that focuses more on the long-term fate of dredged material. One way to do this could be to eliminate the smooth glass bottom and create a natural bottom of non-homogeneous sediment (that can even have some ripples). This would introduce more variables, including the second phase of descent: dynamic collapse. This is

important because if a particle cloud impacts with sufficient energy, then sediment that is on the bottom prior to release can be resuspended and transported away in an ambient current. This gap of knowledge was noted by Tavolaro (1984), and little has occurred since then. In this study, minimal resuspension was observed for particle clouds composed of silica, and these were not included in the analysis of the bottom depositions. The effect would be clearer for all sediment sizes on a natural bed. Further, this would require a change in the documentation of losses. Currently, only the mass lost during descent is quantified, and the dynamic collapse would expand the tally of "losses" to include the mass that is resuspended and transported away from the disposal site as well.

- Finally, in addition to being able to predict losses and recommend particular time windows for disposal, the optimal release location and conditions could be determined by more detailed sensitivity between different sets of experiments. However, practical considerations of field releases must always be retained when doing these, such as the likelihood of having a large amount of excess water present with any dredging that uses an environmental dredge, and the efficiency of lowering a back hoe dredge, for example, well below the deck of a barge to release closer to the surface.

A MATLAB® Image Analysis Code

```matlab
%particle_cloud_analysis.m
%updated by Jim Gensheimer


%%%%%%%%%%%%%%%%%%%%%%%%%%%%%%%%%%%%%%%%%%%%%%%%%%%%%%%%%%%%

% Color CCD: scale = 0.07148438
%%% Frame rate = 10 fps
% Black and White CCD: scale = 0.12616633
%%% Frame rate = 80 fps

close all;
fclose all;
clear;
clc;


[filename1, path] = uigetfile('C:\Research - Trial
Pictures\20100205\B001\*.*','Select the first file to analyze');
%ask for the location of the first image
[filename2, path] = uigetfile('C:\Research - Trial
Pictures\20100205\B001\*.*','Select the last file to analyze');
%ask for the location of the last image

if (filename1(end-7)=='_'||filename1(end-7)=='a')
    nf=3;
else
    nf=4;
end
startframe=str2num(filename1(end-nf-3:end-4));
endframe=str2num(filename2(end-nf-3:end-4));

framerate=80;

scale= 0.12616633;    %ratio of length (cm) per pixel

top=10;%30;       %where to begin top; starts at 1
bottom=450;%450;   %where to end bottom; ends at 485

jumpframes=1;    %how many interval frames are dumped for analysis

cen=144.3;    %location of the centerline in pixel value

mov_ave=13.3333;    %moving-average points

dummy=1 %figure plot iter
```

```matlab
delta_dummy=8 % frames to save as figure

dt = 1/framerate;    %time interval of the selected images
time=startframe:jumpframes:endframe+1;
time=time.*dt;    %time line
fig=figure(1);
aviobj = avifile('new2.avi','fps',1);


%%%%%%%%%%%%%%%%%%%%%%%%%%%%%%%%%%%%%%%%%%%%%%%%%%%%%%%%%%%%%%%%%%%
for i=1:jumpframes:endframe-startframe+2
    ffm=strrep('%0xd\n','x',num2str(nf));
    fname1=strcat(filename1(1:end-nf-4),num2str(i,ffm));
    fname1=strcat(fname1,'.BMP');
    mov=imread(strcat(path,fname1));    %read images from bmp frames

    IB = squeeze(mov(top:bottom,:,1));      %generate matrix from image
    F = IB-min(min(IB));                     %subtract the background level
    F = double(F)/double(max(max(F)));    %normalize the grayscale level

    threshold = graythresh(F);   % global image threshold using Otsu's
method
    adjust=0.625;
    bw = im2bw(F,threshold*adjust);

    % tune the threshold through comparing BW against IB from Segout
below

    se=strel('disk',2);
    I1=imopen(bw,se);         % eliminate the small noise points

    BW=bwperim(I1);      % find the edge of the blob
    Segout=IB;
    Segout(BW)=255;

    BWfill = imfill(BW,'holes');    % fill the inside of the blob

    L = bwlabel(BWfill);    % label the blob by identifying the objects
individually
    stats = regionprops(L, {'centroid','area'});
    % calculate centroid and area for the individual objects
    areaArray = [stats.Area];
    [areamax,idx] = max(areaArray);   % identify the object with the
largest area as the cloud
    y_centroid_cloud(i) = stats(idx).Centroid(:,2);    % centroid of
the determined cloud
    x_centroid_cloud(i) = stats(idx).Centroid(:,1);
    area_cloud(i)=areamax; % area of the determined cloud

    L_bulk = double(BWfill);     % label the blob indiscriminately
    bulk  = regionprops(L_bulk, {'centroid','area'});
    y_centroid_bulk(i)=bulk.Centroid(:,2);
    x_centroid_bulk(i)=bulk.Centroid(:,1);
    area_bulk(i)=bulk.Area;  % calculate the bulk centroid and area

    area_stem(i)=area_bulk(i)-area_cloud(i);
```

162

```matlab
    radius_cloud(i)=(area_cloud(i)/pi)^(1/2)*scale;
    radius_bulk(i)=(area_bulk(i)/pi)^(1/2)*scale;

    figure(1);clf;
    %imshow(Segout,'InitialMagnification','fit'); hold on;  %show
original image and the edge
    imagesc(IB); hold on;  %show color image and the edge
    grid on
    plot(x_centroid_cloud(i),y_centroid_cloud(i),'b*');
    plot(x_centroid_bulk(i),y_centroid_bulk(i),'ro');
    title(strcat('time=',num2str(time(i)),' s'));
    drawnow;pause(0);
    if i>dummy
        saveas(gcf,['C:\Users\James Gensheimer\Documents\Graduate -
MIT\Research - Trial Pictures\20100205\B001/plumecolorpic'
num2str(i)],'bmp');
        dummy=dummy+delta_dummy;
    end

    Frame = getframe(fig);
    aviobj = addframe(aviobj,Frame);

    Z_bulk(i)=y_centroid_bulk(i)*scale;
    X_bulk(i)=(x_centroid_bulk(i)-500+cen)*scale;

    Z_cloud(i)=y_centroid_cloud(i)*scale;
    X_cloud(i)=(x_centroid_cloud(i)-500+cen)*scale;

end

%%%%%%%%%%%%%%%%%%%%%%%%%%%%%%%%%%%%%%%%%%%%%%%%%%%%%%%%%%%%%%%%%

close(fig);
aviobj = close(aviobj);

cpp_bulk = spline(time,Z_bulk);
dcpp_bulk=fnder(cpp_bulk); % generate first derivative
Vel_bulk=ppval(dcpp_bulk,time);
AveVel_bulk=smooth(Vel_bulk,mov_ave)';

cpp_cloud = spline(time,Z_cloud);
dcpp_cloud=fnder(cpp_cloud); % generate first derivative
Vel_cloud=ppval(dcpp_cloud,time);
AveVel_cloud=smooth(Vel_cloud,mov_ave)';

x_bulk=[time;X_bulk];
y_bulk=[time;Z_bulk];
G_bulk=[Z_bulk;radius_bulk];
R_bulk=[time;radius_bulk];
V_bulk=[time;AveVel_bulk];

x_cloud=[time;X_cloud];
y_cloud=[time;Z_cloud];
```

```matlab
G_cloud=[Z_cloud;radius_cloud];
R_cloud=[time;radius_cloud];
V_cloud=[time;AveVel_cloud];


A=[time;area_bulk*scale^2;area_cloud*scale^2;area_stem*scale^2];


fid = fopen('Z_centroid_bulk.dat', 'wt');
fprintf(fid,'time(s)  Z_centroid_bulk(cm)  \n');
fprintf(fid,'%6.3f   %8.4f\n',y_bulk);
fclose(fid);


fid = fopen('Z_centroid_cloud.dat', 'wt');
fprintf(fid,'time(s)  Z_centroid_cloud(cm)  \n');
fprintf(fid,'%6.3f   %8.4f\n',y_cloud);
fclose(fid);


fid = fopen('X_centroid_bulk.dat', 'wt');
fprintf(fid,'time(s)  X_centroid_bulk(cm)  \n');
fprintf(fid,'%6.3f   %8.4f\n',x_bulk);
fclose(fid);


fid = fopen('X_centroid_cloud.dat', 'wt');
fprintf(fid,'time(s)  X_centroid_cloud(cm)  \n');
fprintf(fid,'%6.3f   %8.4f\n',x_cloud);
fclose(fid);


fod = fopen('growth_rate_bulk.dat', 'wt');
fprintf(fod,'Z_centroid_bulk(cm)  Cloud_radius_bulk(cm)\n');
fprintf(fod,'   %8.4f           %8.4f\n',G_bulk);
fclose(fod);


fod = fopen('growth_rate_cloud.dat', 'wt');
fprintf(fod,'Z_centroid_cloud(cm)  Cloud_radius_cloud(cm)\n');
fprintf(fod,'   %8.4f           %8.4f\n',G_cloud);
fclose(fod);


fad = fopen('Cloud_radius_bulk.dat', 'wt');
fprintf(fad,'time(s)  Cloud_radius_bulk(cm)\n');
fprintf(fad,'%6.3f   %8.4f\n',R_bulk);
fclose(fad);


fad = fopen('Cloud_radius_cloud.dat', 'wt');
fprintf(fad,'time(s)  Cloud_radius_cloud(cm)\n');
fprintf(fad,'%6.3f   %8.4f\n',R_cloud);
fclose(fad);


fud = fopen('Descendant_velocity_bulk.dat', 'wt');
fprintf(fud,'time(s)  Velocity_bulk(cm/s)\n');
fprintf(fud,'%6.3f   %8.4f\n',V_bulk);
fclose(fud);


fud = fopen('Descendant_velocity_cloud.dat', 'wt');
fprintf(fud,'time(s)  Velocity_cloud(cm/s)\n');
fprintf(fud,'%6.3f   %8.4f\n',V_cloud);
fclose(fud);
```

```matlab
fed = fopen('Cloud_area.dat', 'wt');
fprintf(fed,'time(s)  Area_bulk(cm^2)   Area_cloud(cm^2)
Area_stem(cm^2)\n');
fprintf(fed,'%6.3f   %8.4f  %8.4f   %8.4f\n',A);
fclose(fed);


%%%%%%%%%%%%%%%%%%%%%%%%%%%%%%%%%%%%%%%%%%%%%%%%%%%%%%%%%%%%%%%%
linewidth=2;

figure(2);hold all;              %z centoid vs time
plot(time,Z_bulk,'k-');   % linespec for more colors/line options
plot(time,Z_cloud,'k:');
axis ij;
title('z centroid vs time');
legend('bulk','cloud');
xlabel('time (s)');
ylabel('z (cm)');

figure(3);hold all;              %z centoid vs radius
plot(radius_bulk,Z_bulk,'k-');
plot(radius_cloud,Z_cloud,'k:');
axis ij;
title('z centroid vs radius');
legend('bulk','cloud');
xlabel('radius(cm)');
ylabel('z (cm)');

figure(4);hold all;              %x centoid vs time
plot(time,X_bulk,'k-');
plot(time,X_cloud,'k:');
axis ij;
title('x centroid vs time');
legend('bulk','cloud');
xlabel('time (s)');
ylabel('x (cm)');

figure(5);hold all;              %x centoid vs radius
plot(radius_bulk,X_bulk,'k-');
plot(radius_cloud,X_cloud,'k:');
axis ij;
title('x centroid vs radius');
legend('bulk','cloud');
xlabel('radius(cm)');
ylabel('x (cm)');

figure(6);hold all;              %area vs time
plot(time,area_bulk*scale^2,'k-');
plot(time,area_cloud*scale^2,'k:');
plot(time,area_stem*scale^2,'k--');
title('area vs time');
legend('area of bulk (cm^2)','area of cloud (cm^2)','area of stem
(cm^2)');
xlabel('time (s)');
ylabel('area (cm^2)');
```

```matlab
figure(7);hold all;                 %time vs velocity
plot(AveVel_bulk,time,'k-');
plot(AveVel_cloud,time,'k:');
axis ij;
title('time vs descent velocity');
legend('bulk','cloud');
xlabel('velocity(cm/s)');
ylabel('time(s)');

figure(8);hold all;                 %time vs radius
plot(radius_bulk,time,'k-');
plot(radius_cloud,time,'k:');
axis ij;
title('time vs radius');
legend('bulk','cloud');
xlabel('radius(cm)');
ylabel('time(s)');

%%%%%%%%%%%%%%%%%%%%%%%%%%%%%%%%%%%%%%%%%%%%%%%%%%%%%%%%%%%%%%%%%%
```

B Selected Images from Experimental Trials

To review the designations and their corresponding release variables, Tables 4-1, 4-2, and 4-3, and have been reprinted here for the reader's reference. For all images, the frame size is approximately 82 *cm* wide x 61 *cm* tall. The interval of time between images is designated next to the experiment label for each set of images.

Group 1 Experiments.

| Experiment Designation	Particle Type	Release Location [z = 0 at surface]	Water Content	Particle Condition	Current Magnitude
SG 0+1AT 0	SG 0	+ 1 cm	Saturated	Settled	0 cm/s
SG 00+1AT 0	SG 00	+ 1 cm	Saturated	Settled	0 cm/s
A+1AT 0	A	+ 1 cm	Saturated	Settled	0 cm/s
B+1AT 0	B	+ 1 cm	Saturated	Settled	0 cm/s
D+1AT 0	D	+ 1 cm	Saturated	Settled	0 cm/s
AE+1AT 0	AE	+ 1 cm	Saturated	Settled	0 cm/s
AH+1AT 0	AH	+ 1 cm	Saturated	Settled	0 cm/s
SIL+1AT 0	SIL	+ 1 cm	Saturated	Settled	0 cm/s

SG 0+1AT 0 (0.5 s interval)   SG 00+1AT 0 (0.5 s interval)
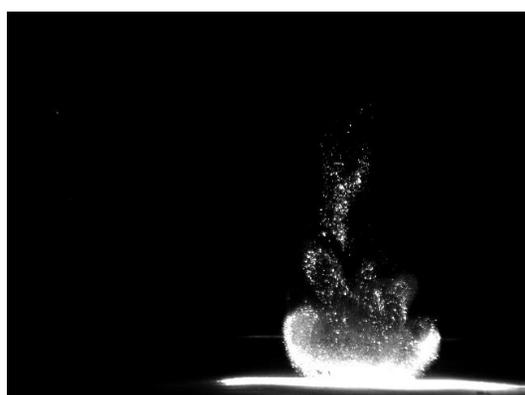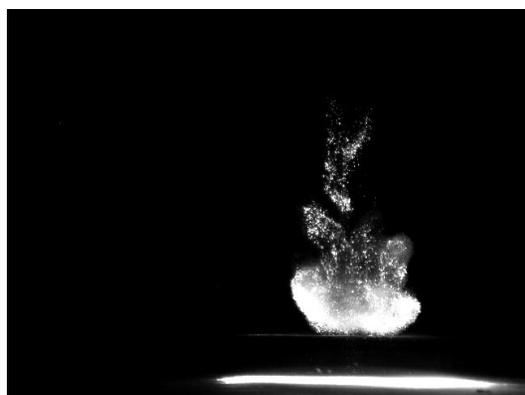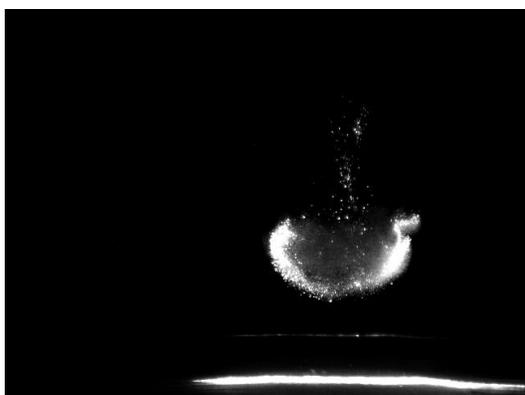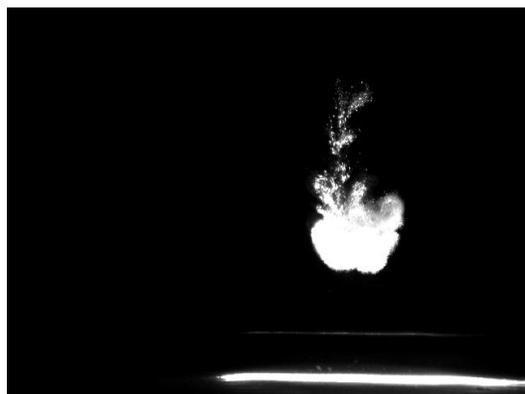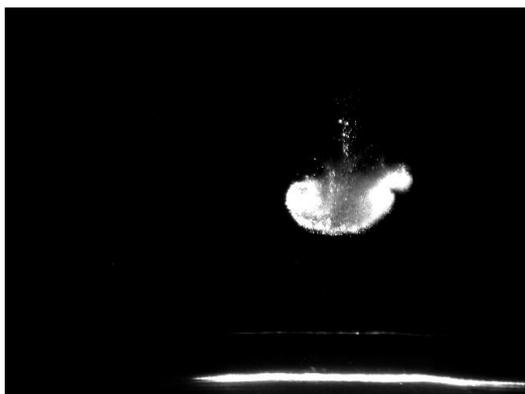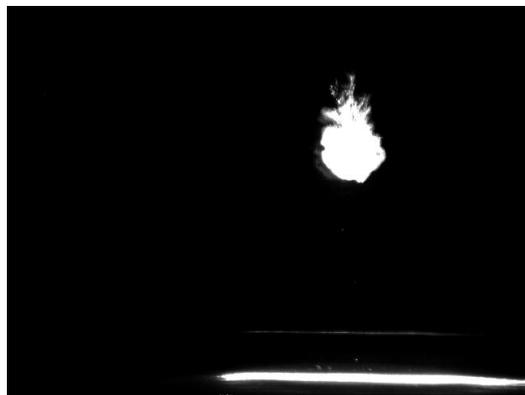
A+1AT 0 (0.75 s interval) B+1AT 0 (0.75 s interval)
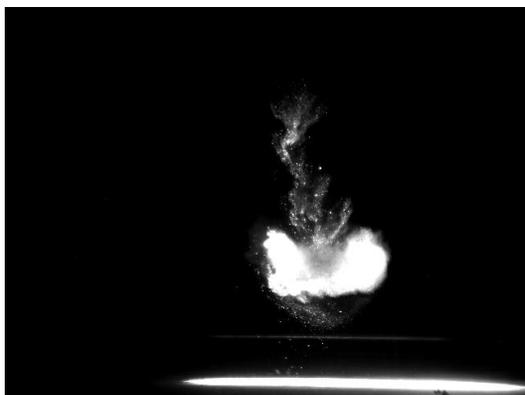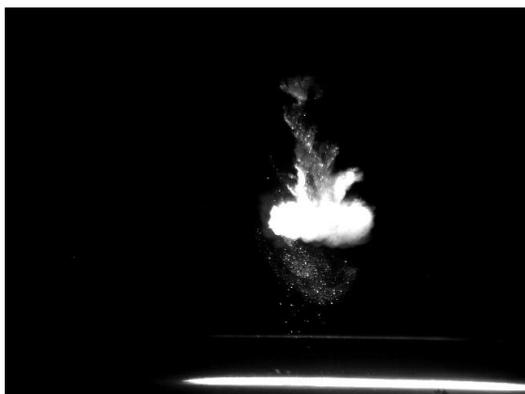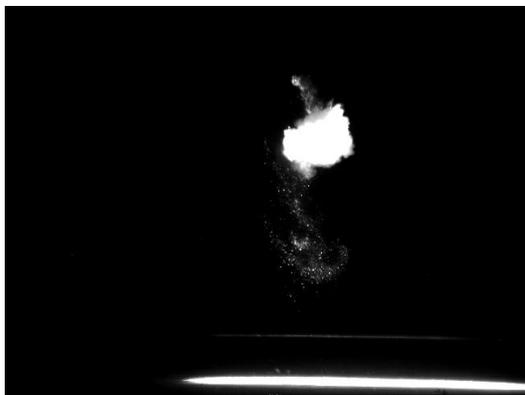
D+1AT 0 (0.75 s interval)   AE+1AT 0 (1.0 s interval)
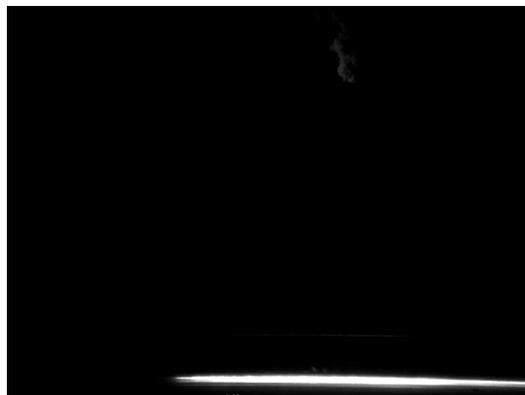
AH+1AT 0 (1.0 s interval)   SIL+1AT 0 (1.5 s interval)

175

Group 2 Experiments.

Experiment Designation	Particle Type	Release Location [z = 0 at surface]	Water Content	Particle Condition	Current Magnitude
D+5RT 0	D	+ 5 cm	Dry	Settled	0 cm/s
D+5RT 12	D	+ 5 cm	Dry	Settled	12 cm/s
D+1RT 0	D	+ 1 cm	Dry	Settled	0 cm/s
D+1RT 6	D	+ 1 cm	Dry	Settled	6 cm/s
D+1RT 12	D	+ 1 cm	Dry	Settled	12 cm/s
D+1AT 0	D	+ 1 cm	Saturated	Settled	0 cm/s
D+1AT 6	D	+ 1 cm	Saturated	Settled	6 cm/s
D+1AT 12	D	+ 1 cm	Saturated	Settled	12 cm/s
D+1PT 0	D	+ 1 cm	Supersaturated	Settled	0 cm/s
D+1PT 6	D	+ 1 cm	Supersaturated	Settled	6 cm/s
D+1PT 12	D	+ 1 cm	Supersaturated	Settled	12 cm/s
D-5PS 0	D	- 5 cm	Supersaturated	Suspended	0 cm/s
D-5PS 6	D	- 5 cm	Supersaturated	Suspended	6 cm/s
D-5PS 12	D	- 5 cm	Supersaturated	Suspended	12 cm/s

D+5RT 0 (0.75 s interval)   D+5RT 12 (0.75 s interval)
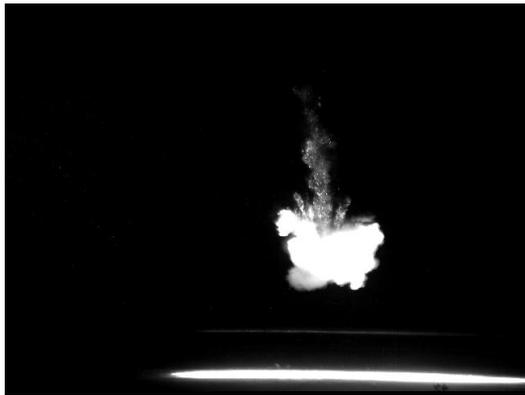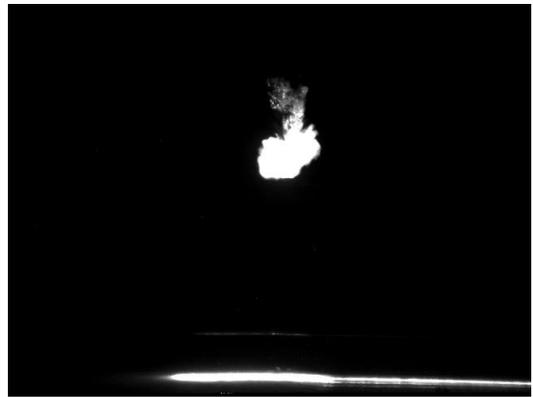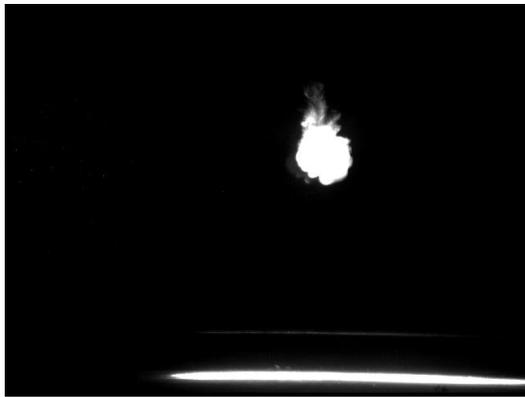
D+1RT 0 (0.75 s interval)   D+1RT 6 (0.75 s interval)
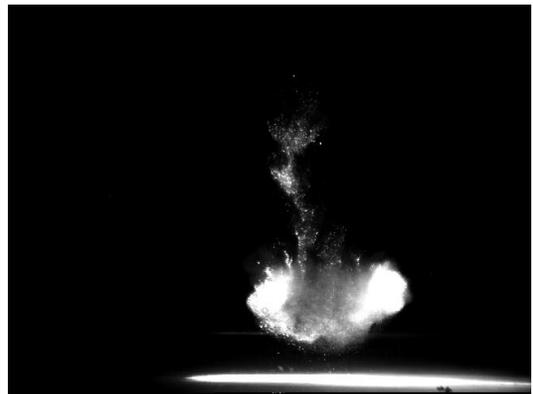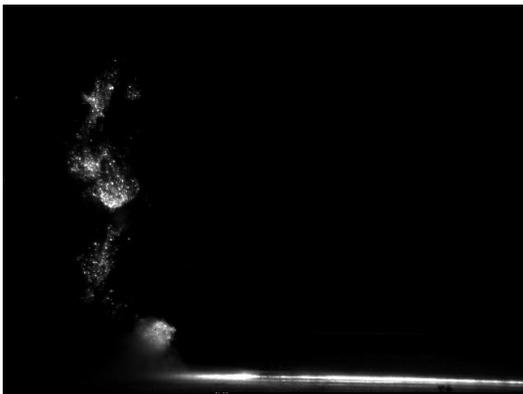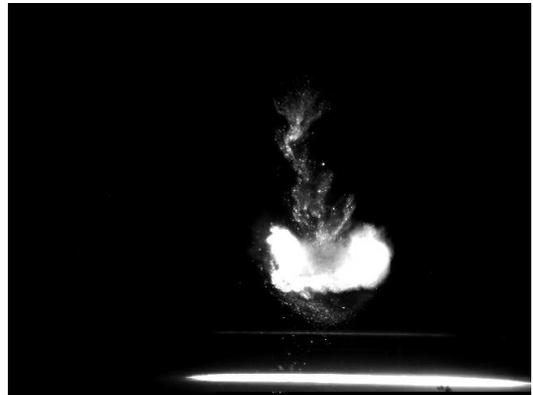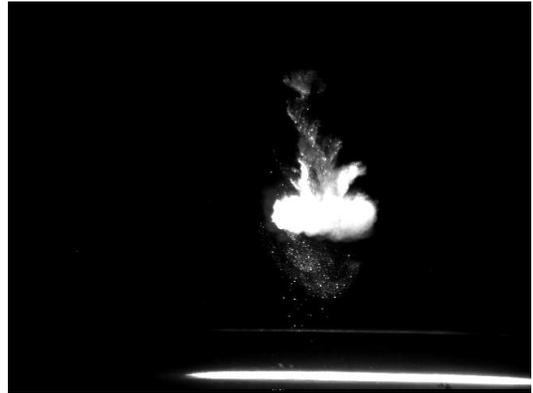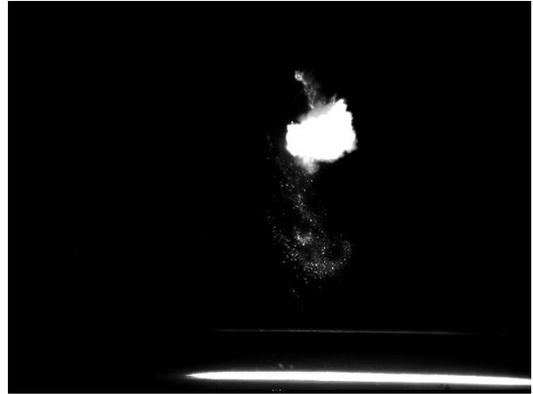
D+1RT 12 (0.75 s interval)   D+1AT 0 (0.75 s interval)
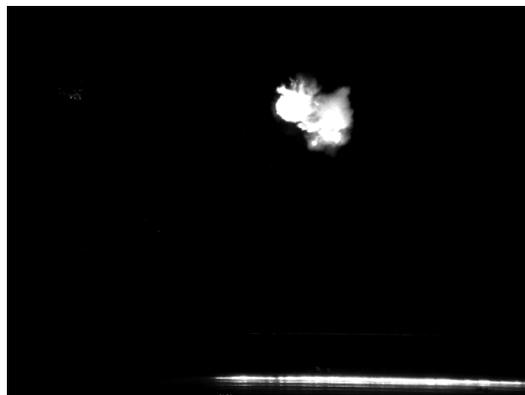
D+1AT 6 (0.75 s interval)   D+1AT 12 (0.75 s interval)
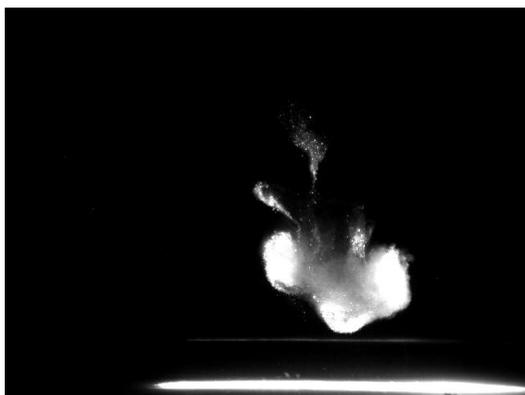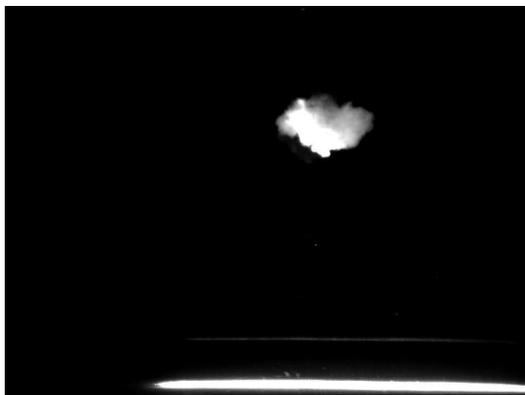
D+1PT 0 (0.75 s interval)   D+1PT 6 (0.75 s interval)

187
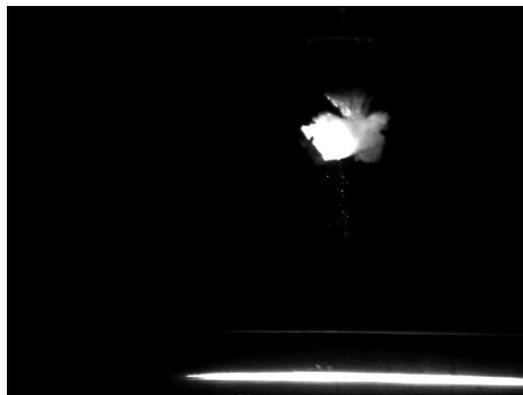
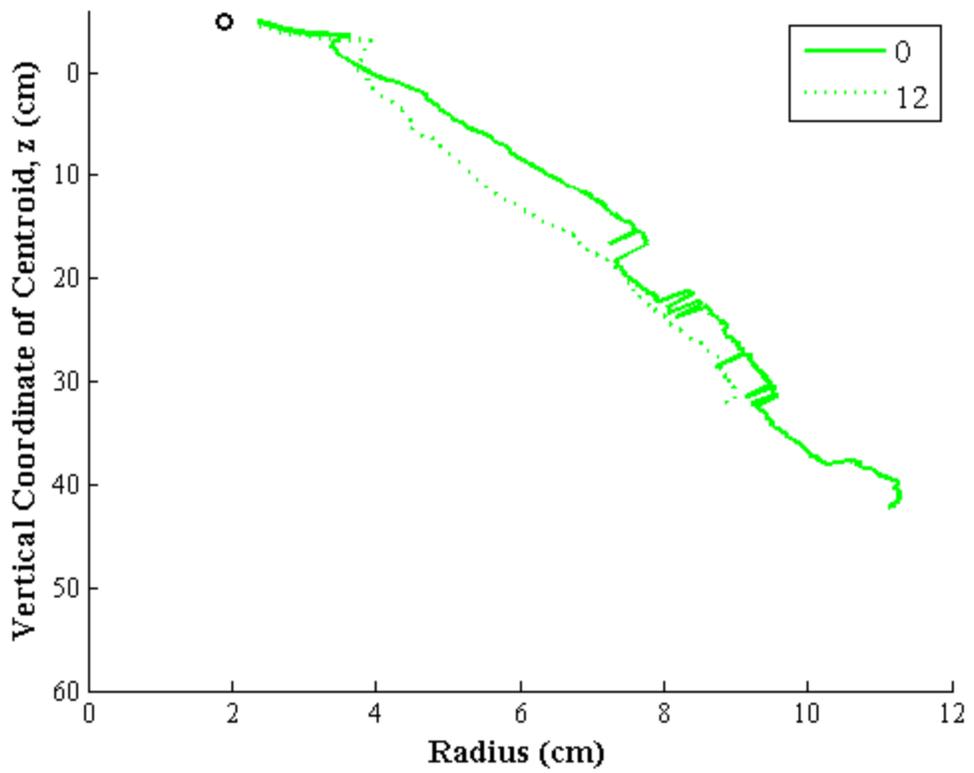D+1PT 12 (0.75 s interval)   D-5PS 0 (0.75 s interval)
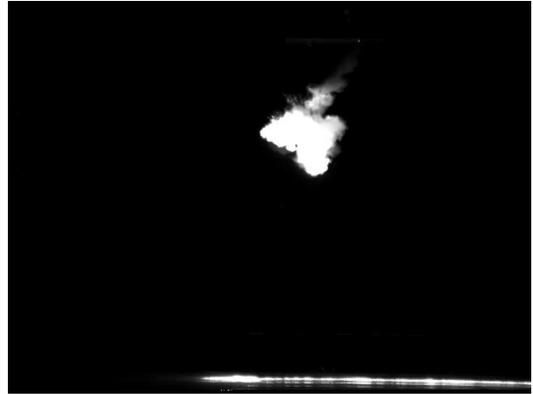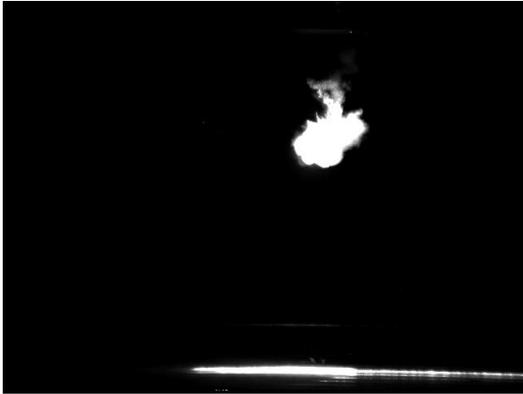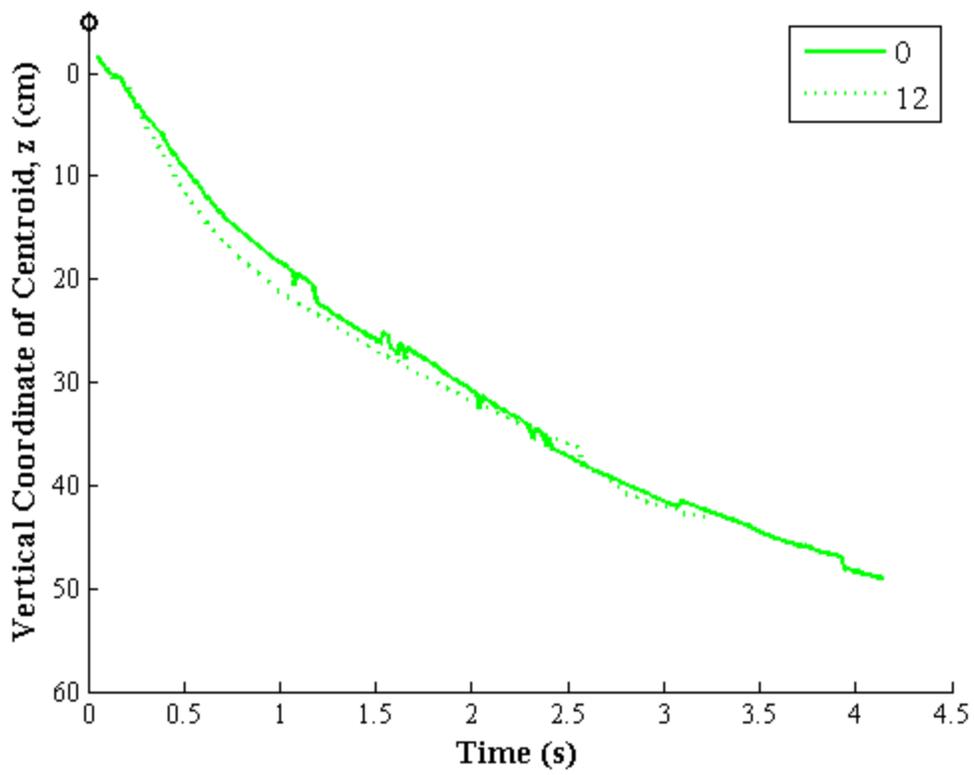
D-5PS 0 (0.75 s interval)   D-5PS 0 (0.75 s interval)

Group 3 Experiments.

Experiment Designation	Particle Type	Release Location [z = 0 at surface]	Water Content	Particle Condition	Current Magnitude
B+5RT 0	B	+ 5 cm	Dry	Settled	0 cm/s
B+5RT 12	B	+ 5 cm	Dry	Settled	12 cm/s
B+1RT 0	B	+ 1 cm	Dry	Settled	0 cm/s
B+1RT 6	B	+ 1 cm	Dry	Settled	6 cm/s
B+1RT 12	B	+ 1 cm	Dry	Settled	12 cm/s
B+1AT 0	B	+ 1 cm	Saturated	Settled	0 cm/s
B+1AT 6	B	+ 1 cm	Saturated	Settled	6 cm/s
B+1AT 12	B	+ 1 cm	Saturated	Settled	12 cm/s
B+1PT 0	B	+ 1 cm	Supersaturated	Settled	0 cm/s
B+1PT 6	B	+ 1 cm	Supersaturated	Settled	6 cm/s
B+1PT 12	B	+ 1 cm	Supersaturated	Settled	12 cm/s
B-5PS 0	B	- 5 cm	Supersaturated	Suspended	0 cm/s
B-5PS 6	B	- 5 cm	Supersaturated	Suspended	6 cm/s
B-5PS 12	B	- 5 cm	Supersaturated	Suspended	12 cm/s

B+5RT 0 (0.75 s interval)   B+5RT 12 (0.75 s interval)
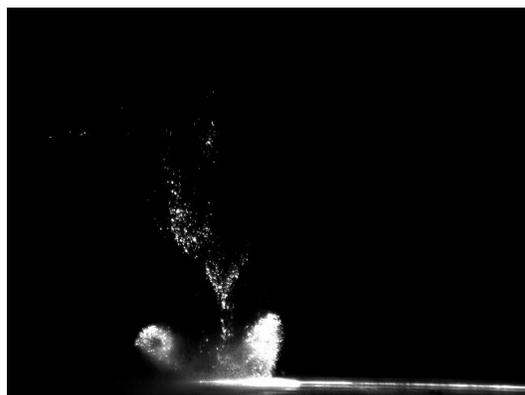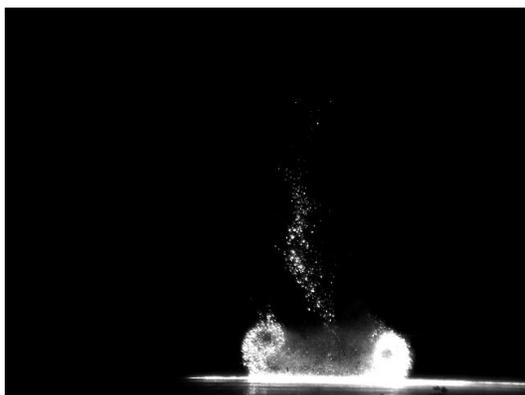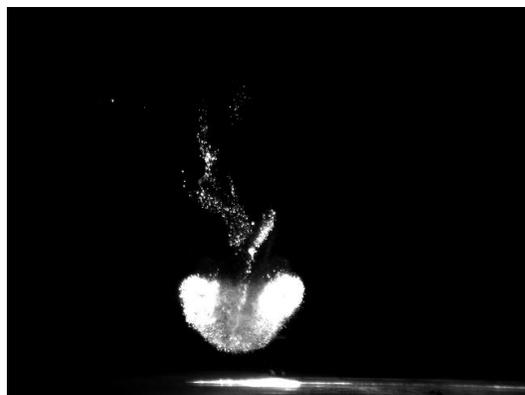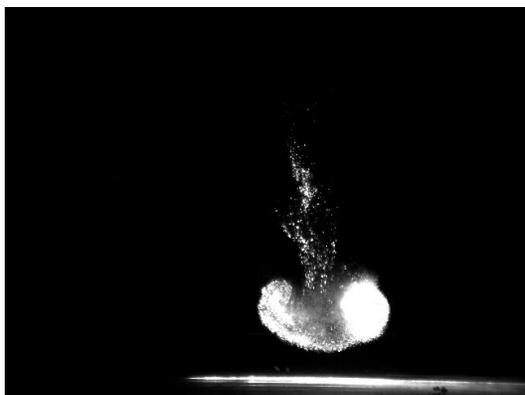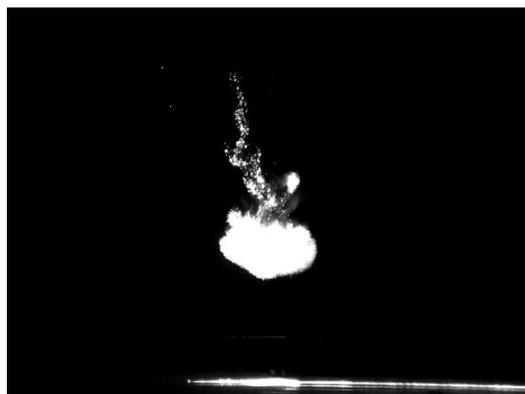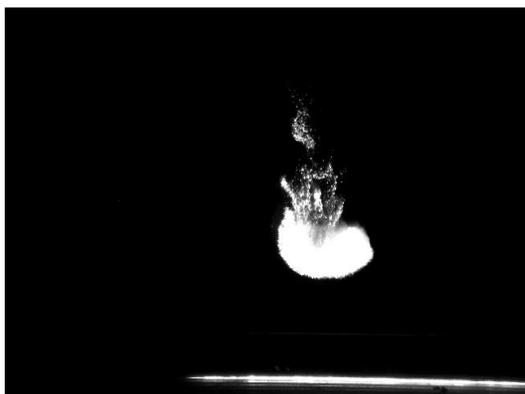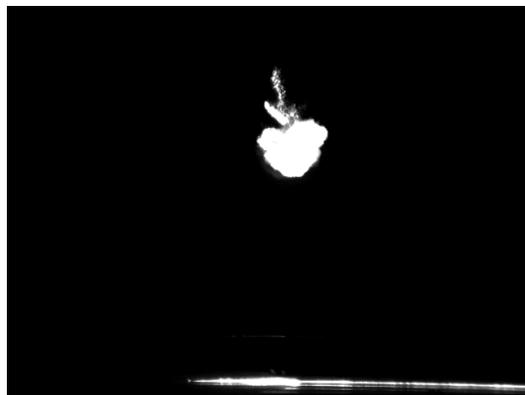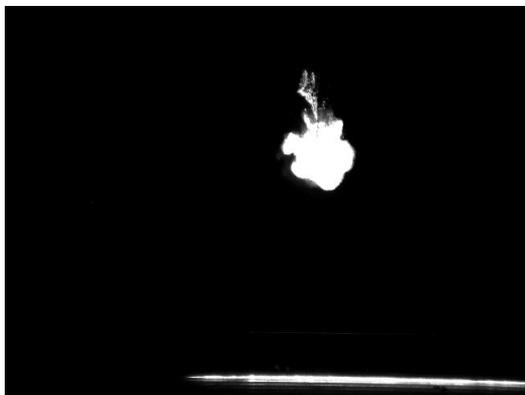
B+1RT 0 (0.75 s interval)   B+1RT 6 (0.75 s interval)
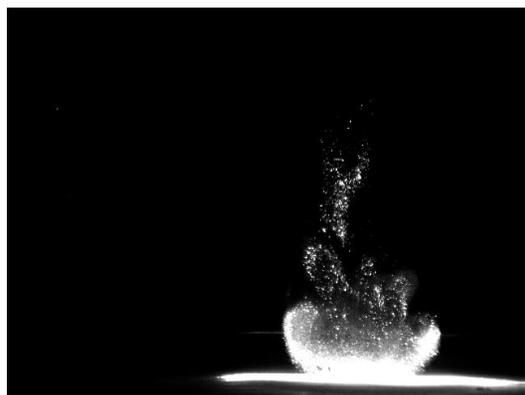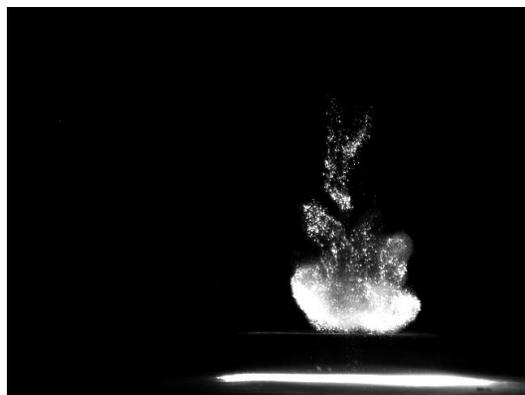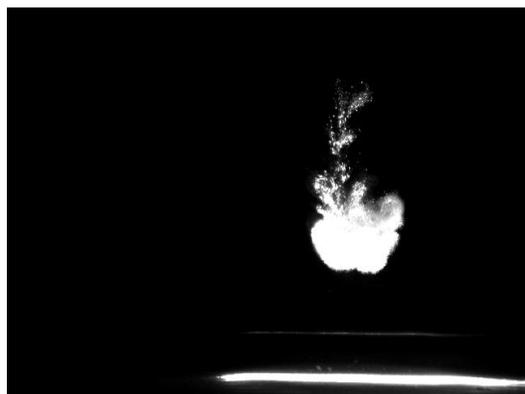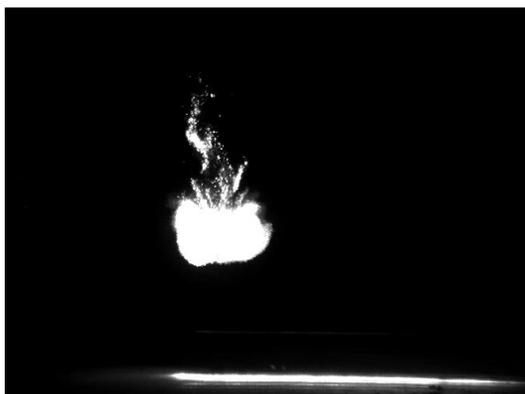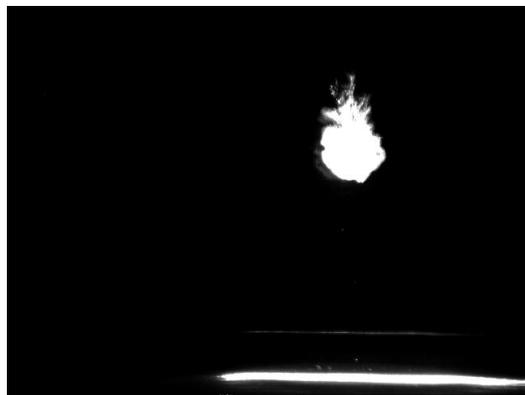
B+1RT 12 (0.75 s interval)   B+1AT 0 (0.75 s interval)
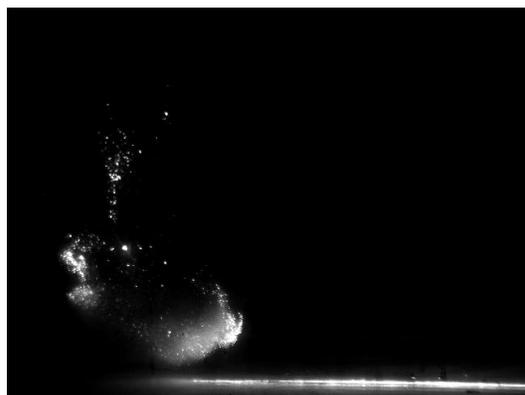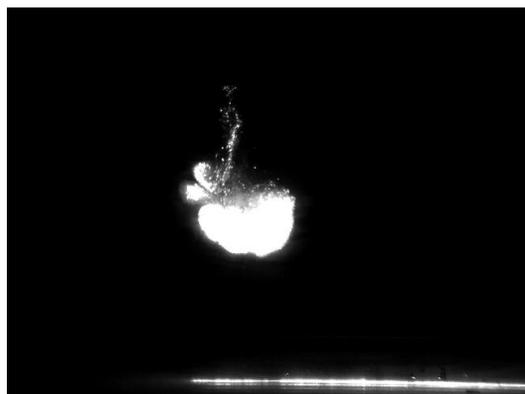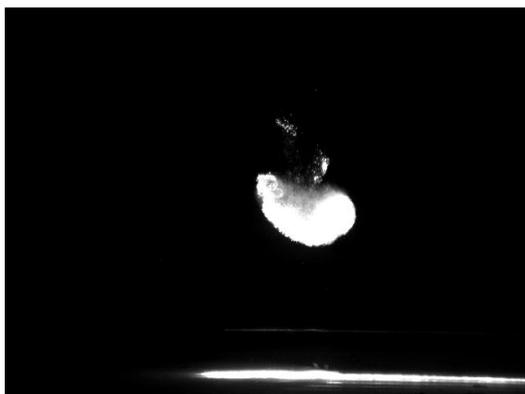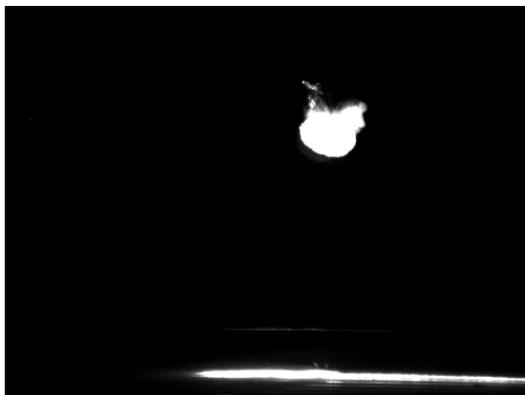
B+1AT 6 (0.75 s interval)   B+1AT 12 (0.75 s interval)
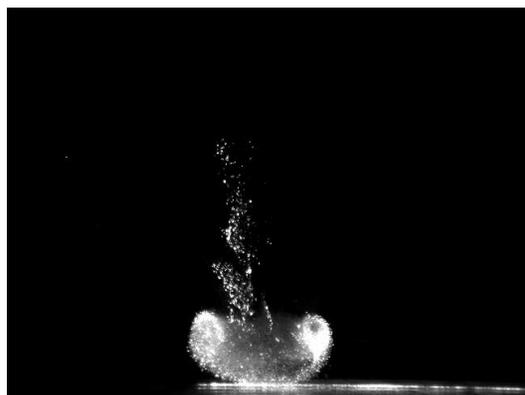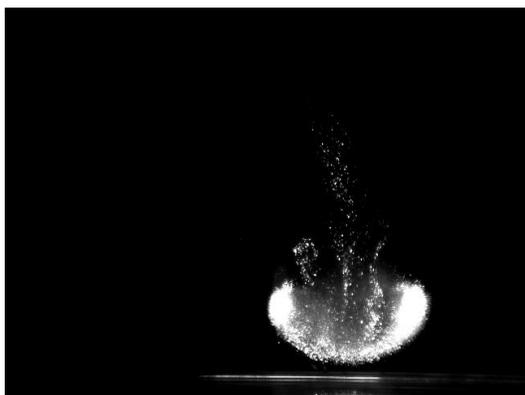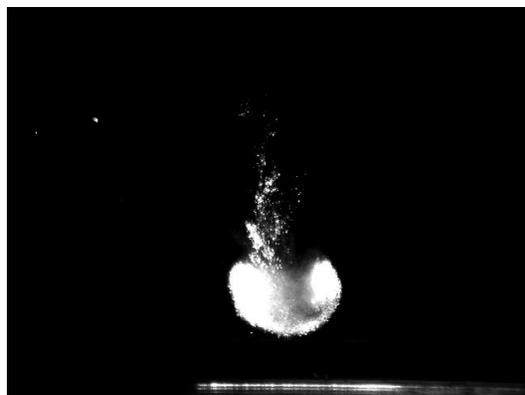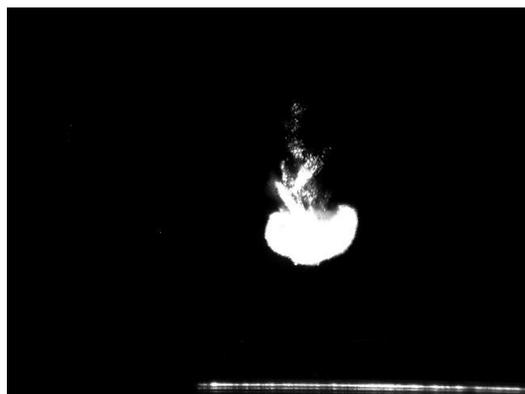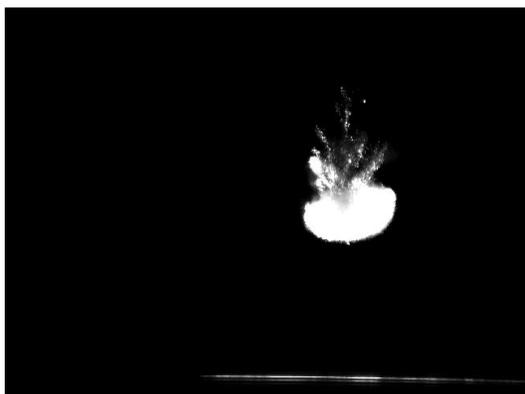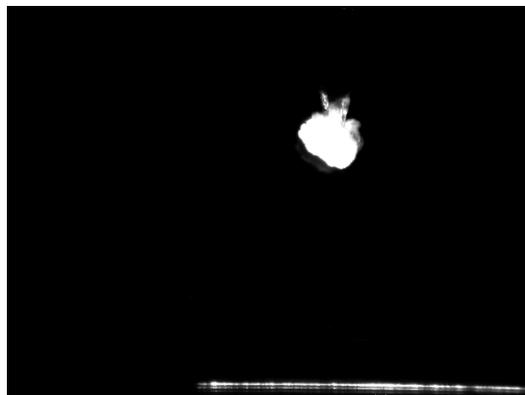
B+1PT 0 (0.75 s interval)   B+1PT 6 (0.75 s interval)
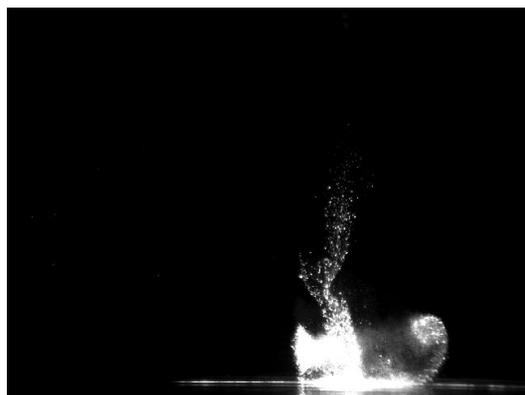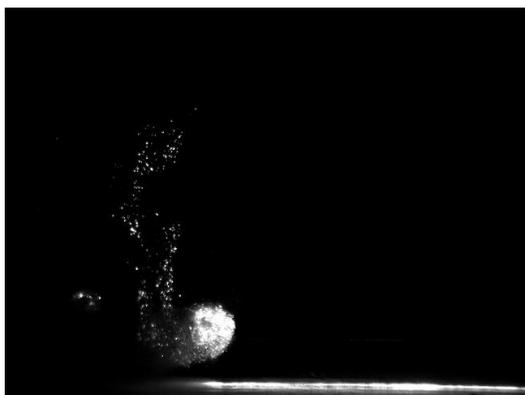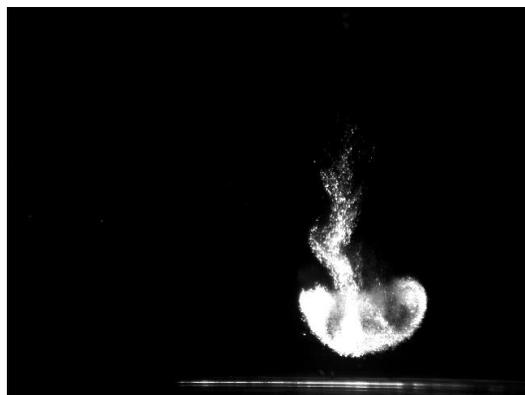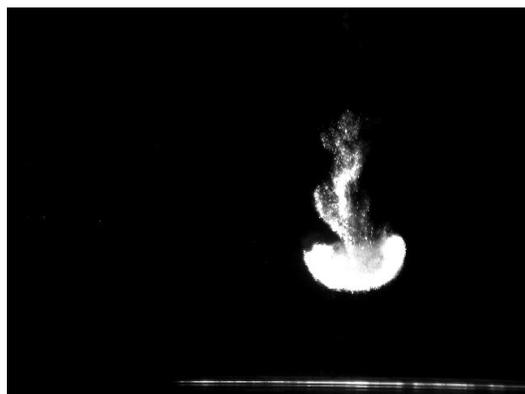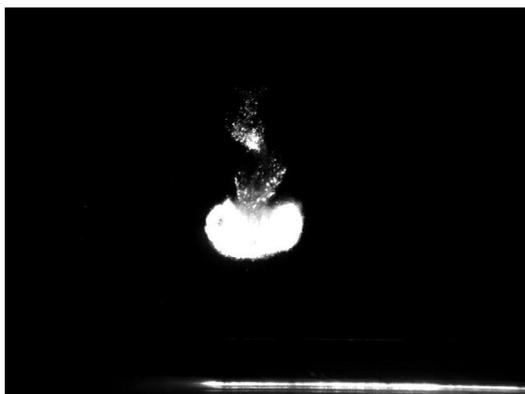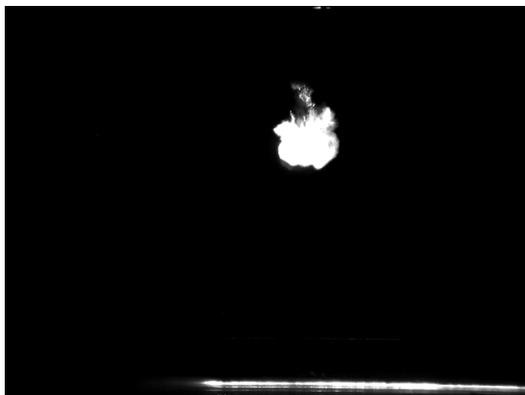
B+1PT 12 (0.75 s interval)   B-5PS 0 (0.75 s interval)
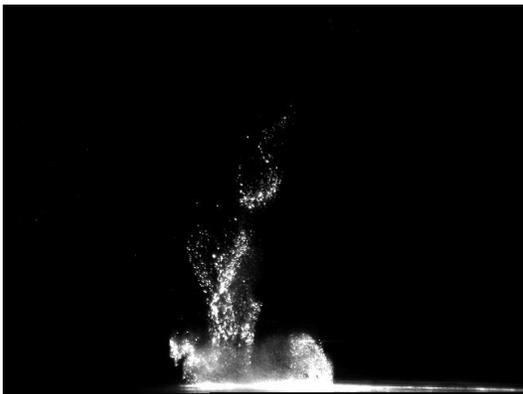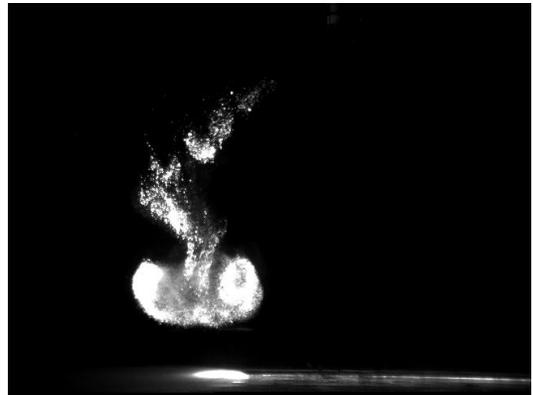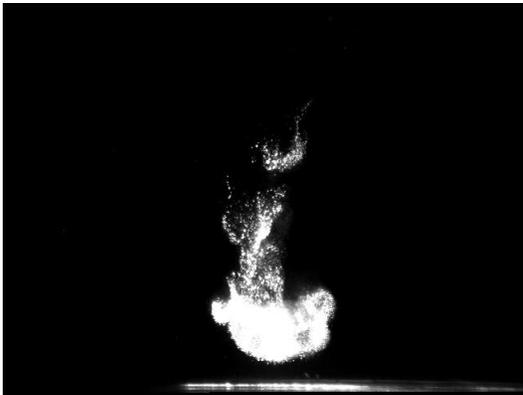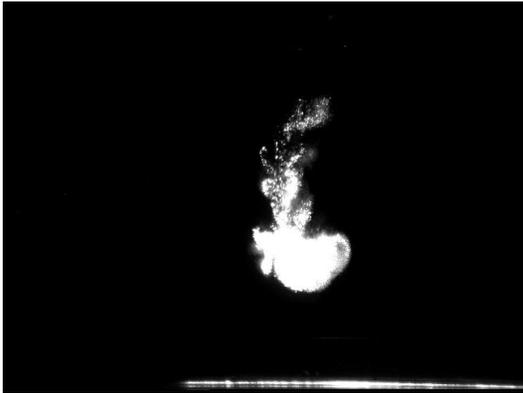
B-5PS 6 (0.75 s interval)   B-5PS 12 (0.75 s interval)

C Output from Image Processing

Plots for all experiment groups of the vertical centroid, *z*, versus time and vertical centroid, *z*, versus radius are shown below. The legends on all plots show the velocity of the ambient current. From these plots, the radius growth over time can be determined, the descent velocity can be determined by dz/dt, and the entrainment coefficient can be directly calculated as well using dr/dz. Refer to Appendix A for experiment designations for the three groups of experiments.
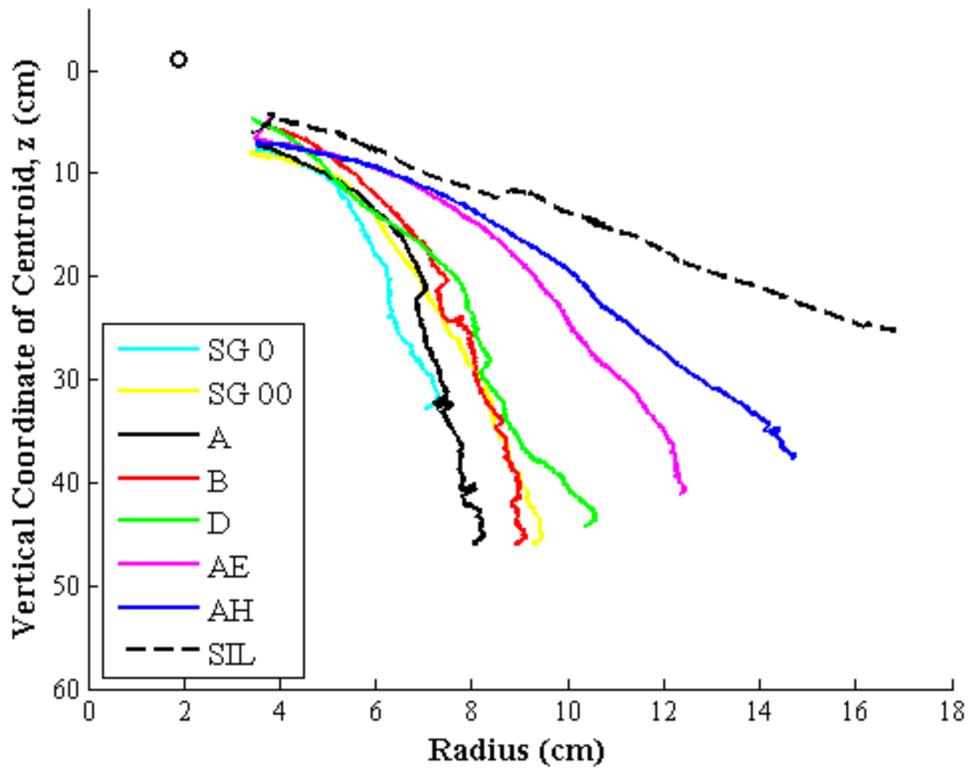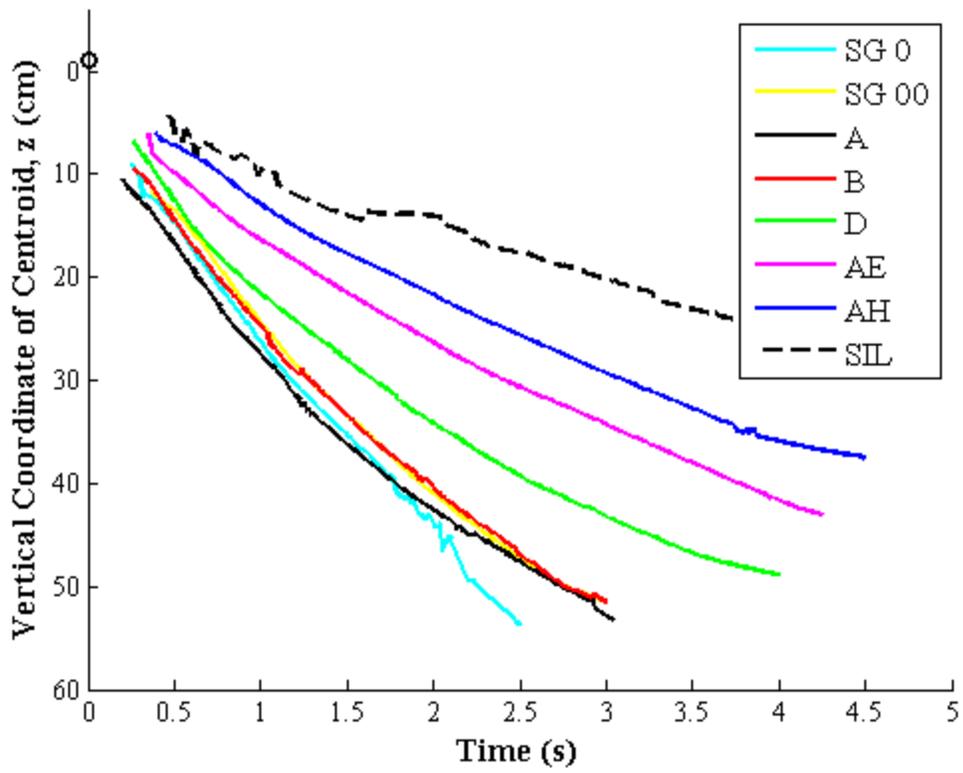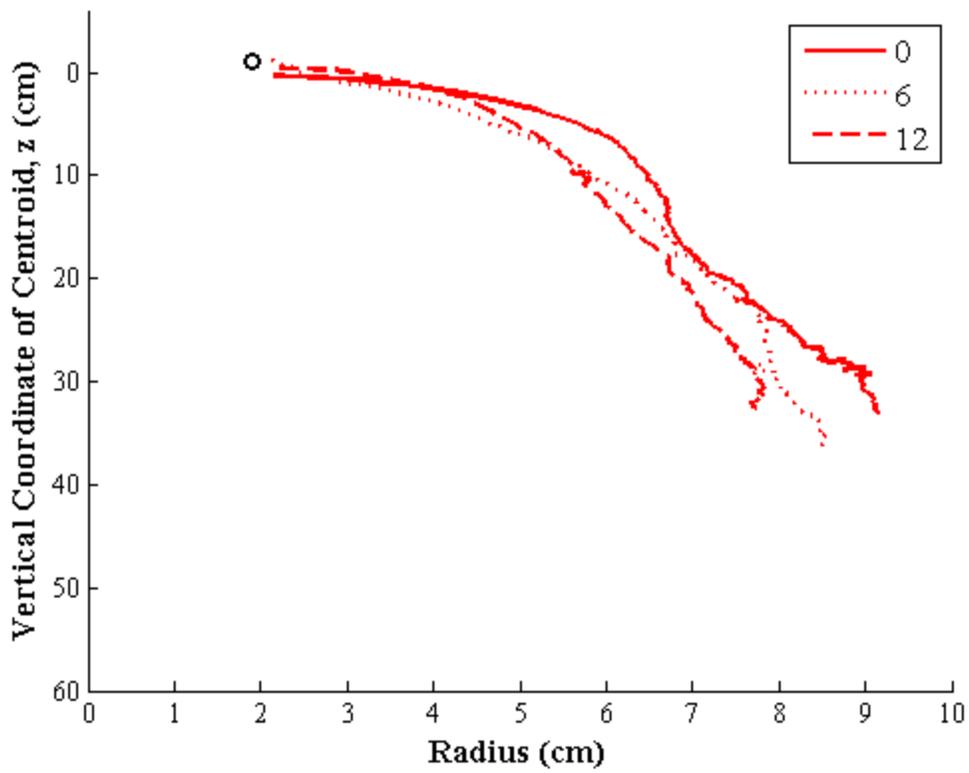
Group 1: All.

Group 2: D+5RT

Group 2: D+1RT
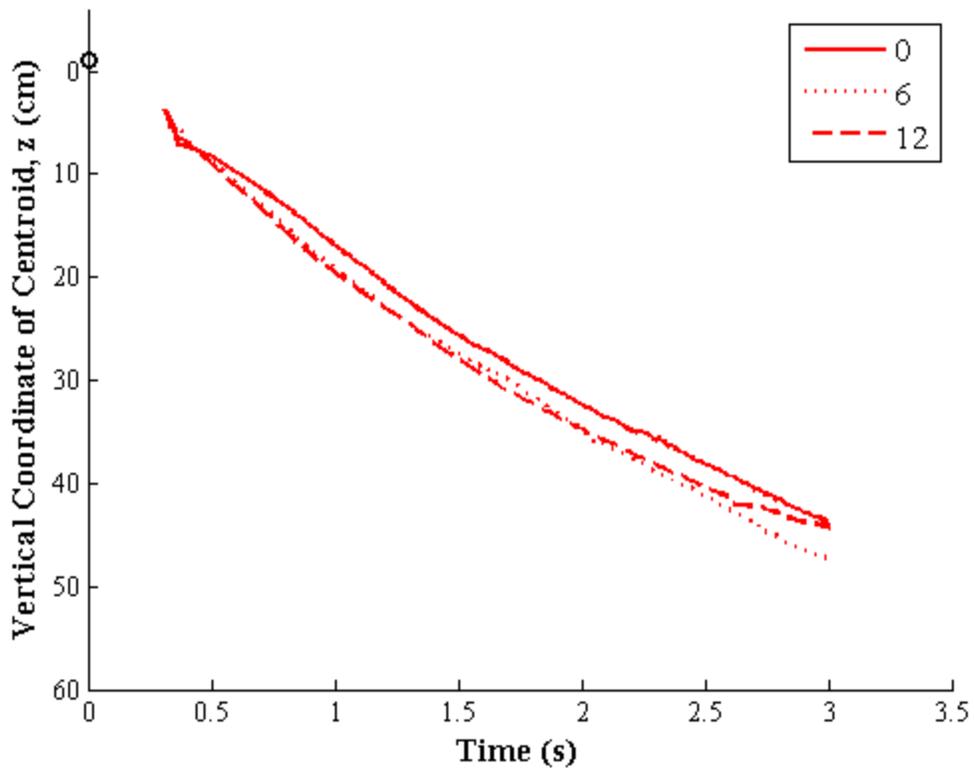
Group 2: D+1AT

217

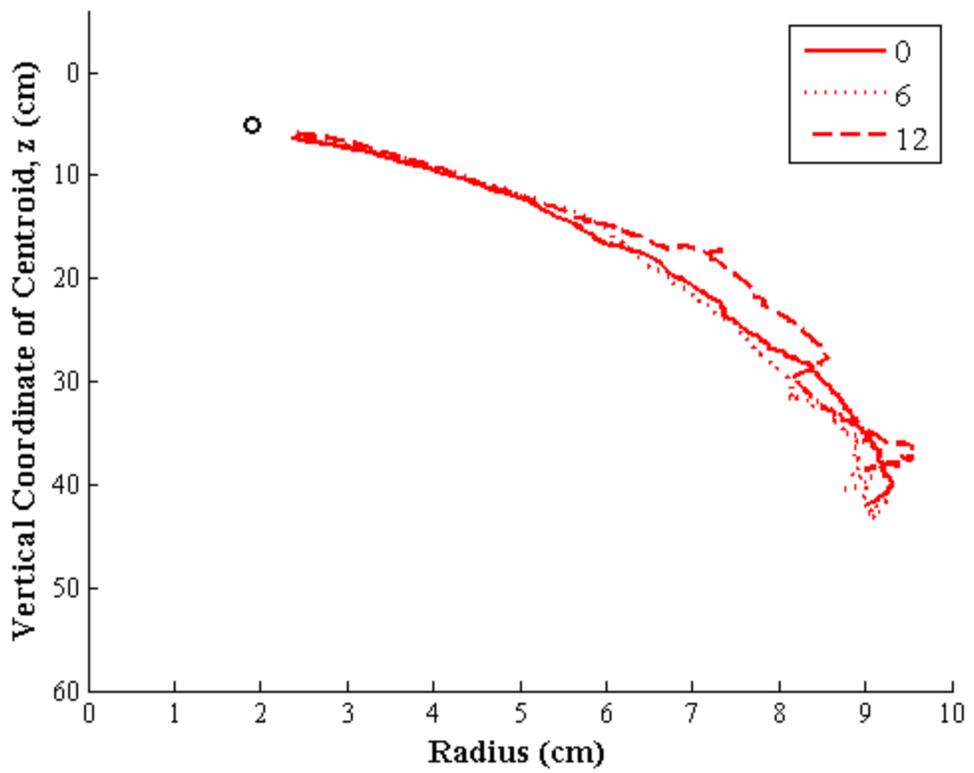Group 2: D+1PT

219

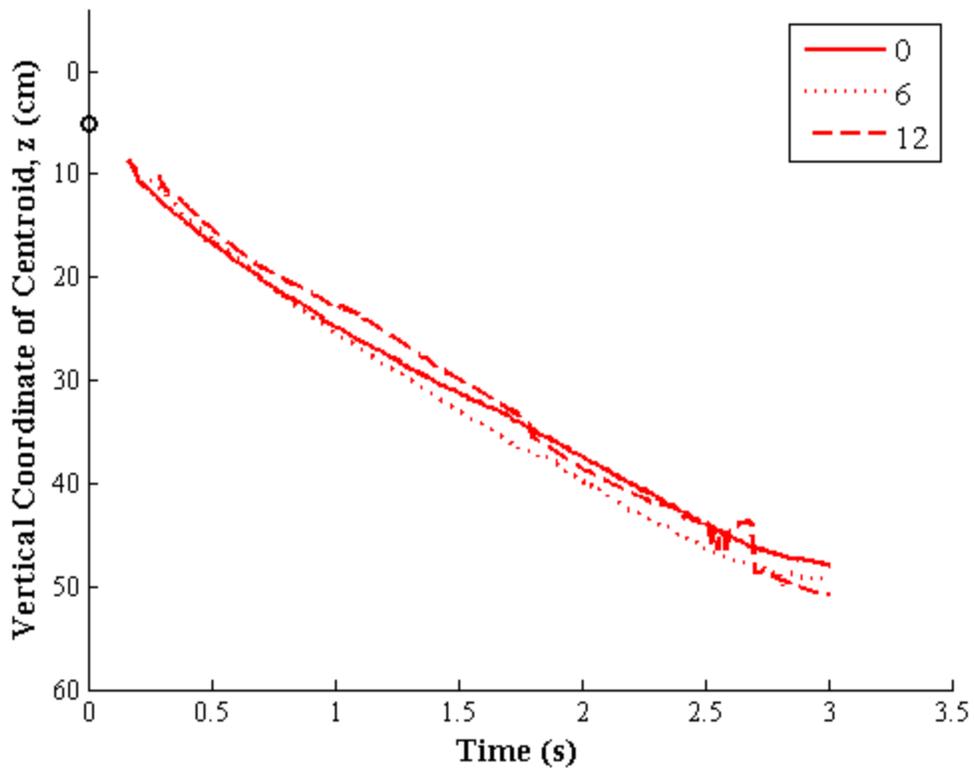Group 2: D-5PS

221

Group 3: B+5RT

223

Group 3: B+1RT

225

Group 3: B+1AT

Group 3: B+1PT

229

Group 3: B-5PS

231

D Bottom Mass Deposits

The following figures show the mass collected for every grid interval for all Group 2 and Group 3 experiments. The legend shows the magnitude of the ambient current velocity.

Group 2: D+5RT

Group 2: D+1RT

237

Group 2: D+1AT
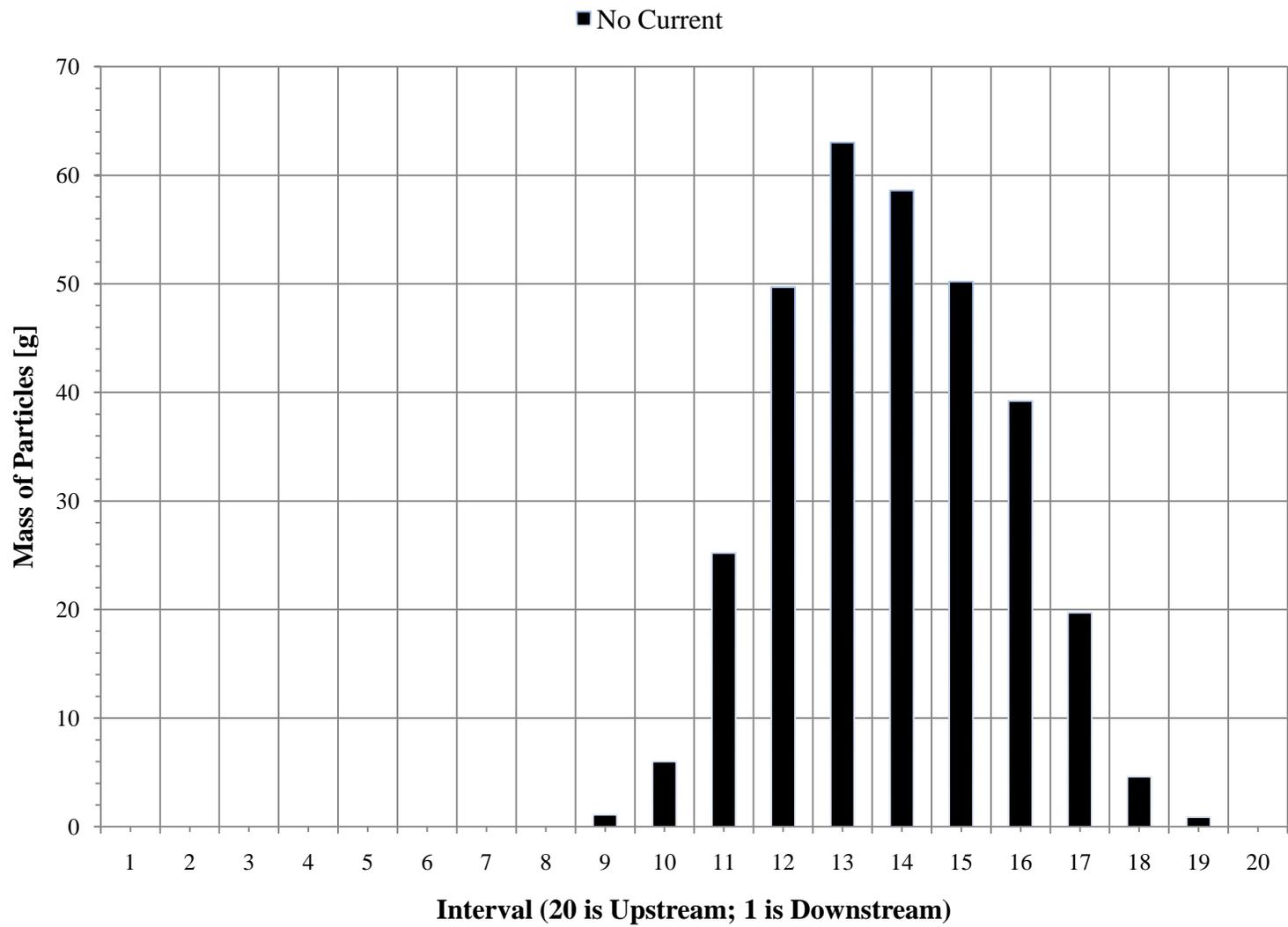
239
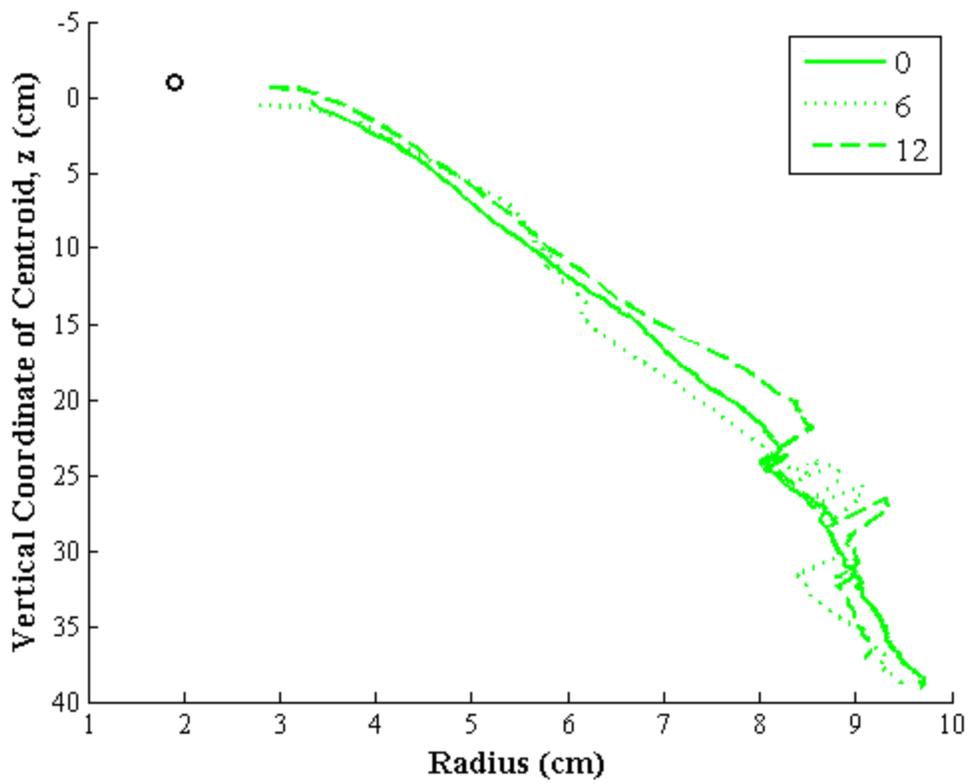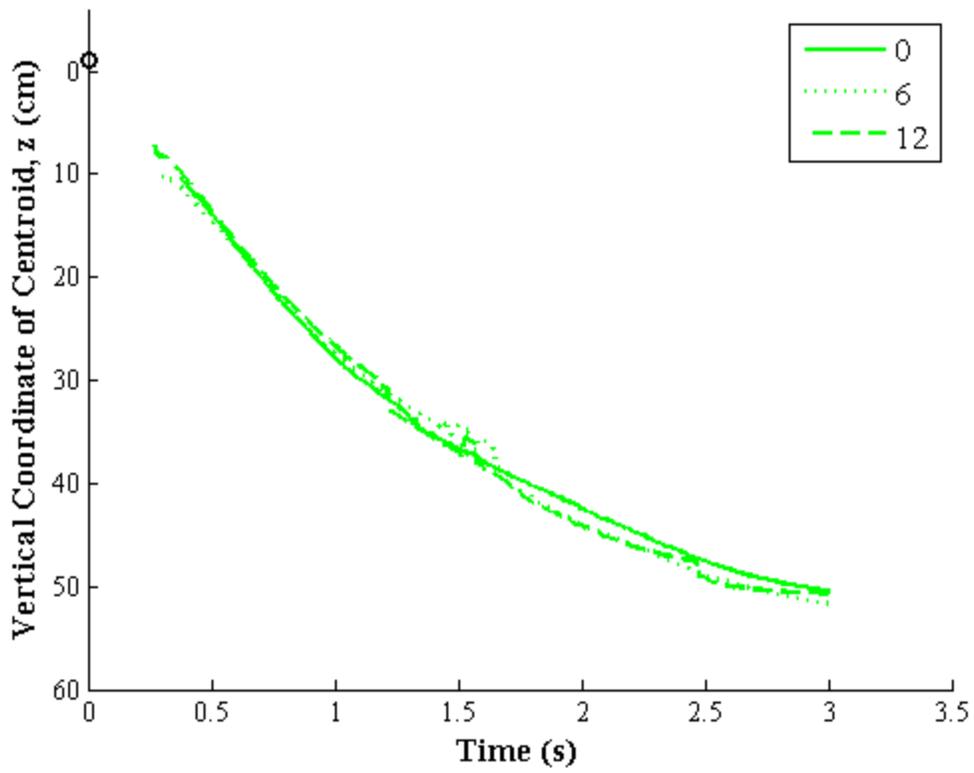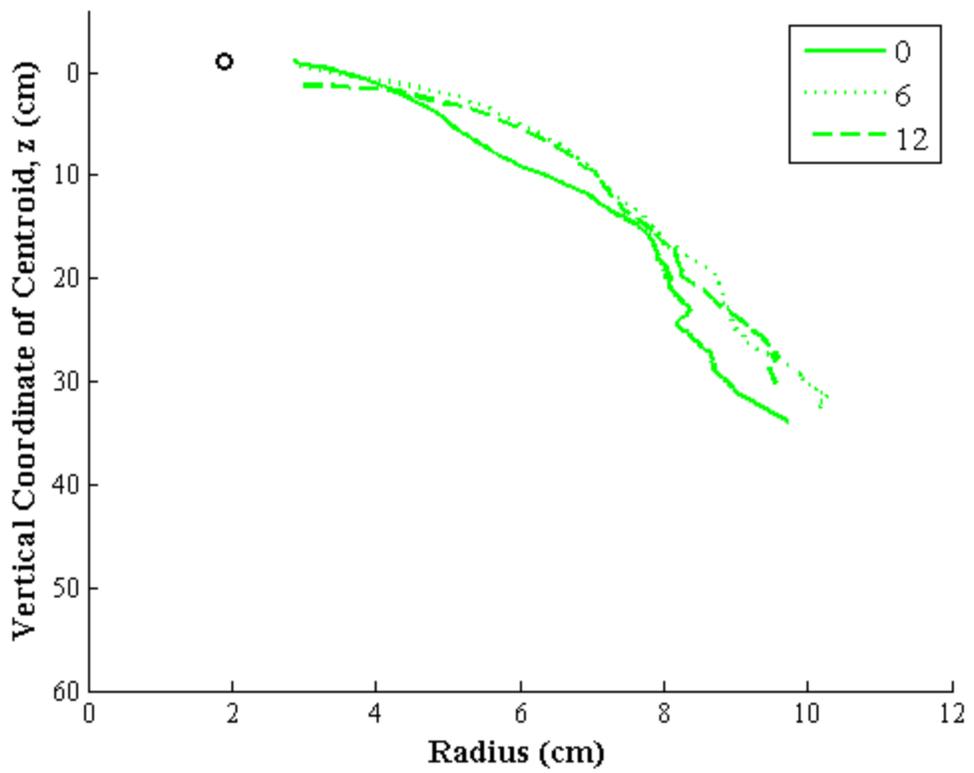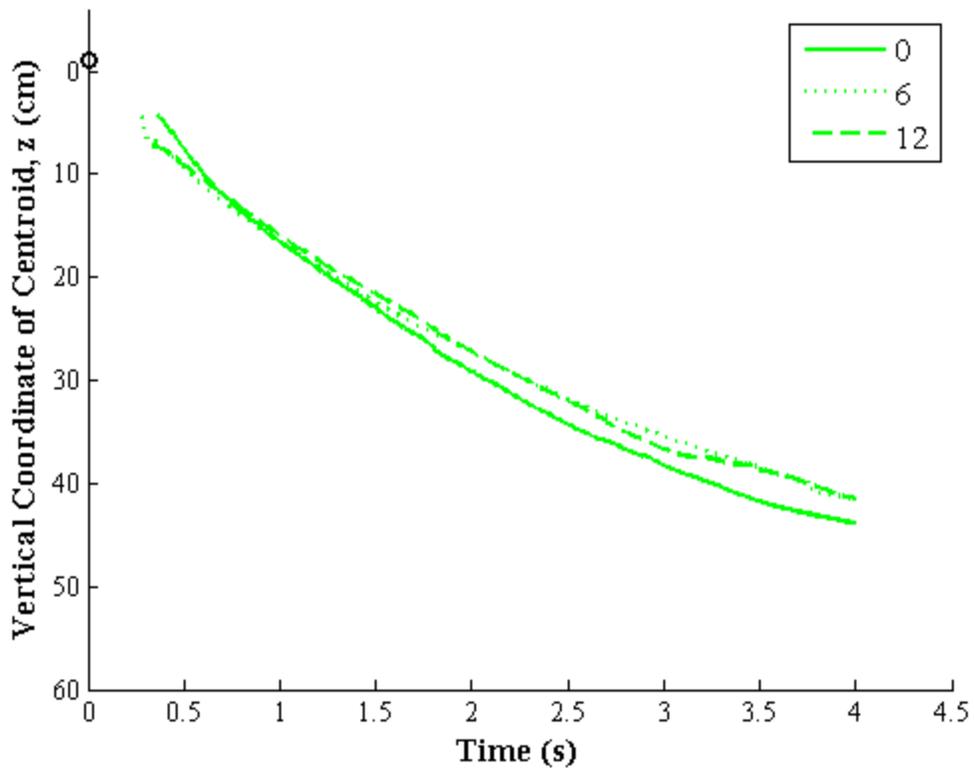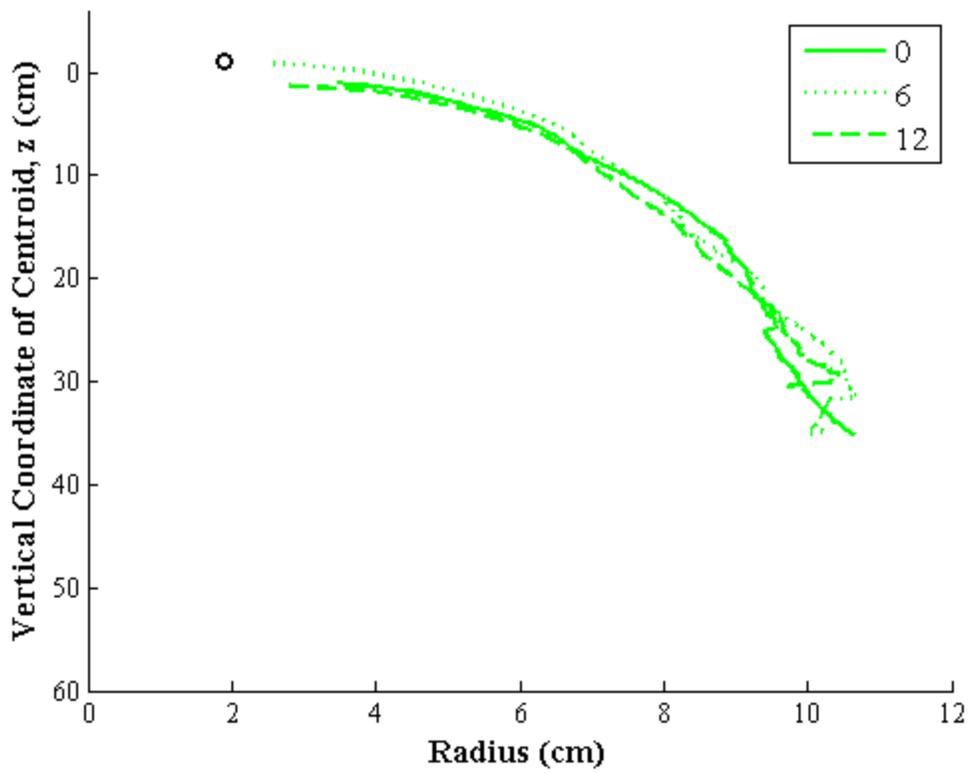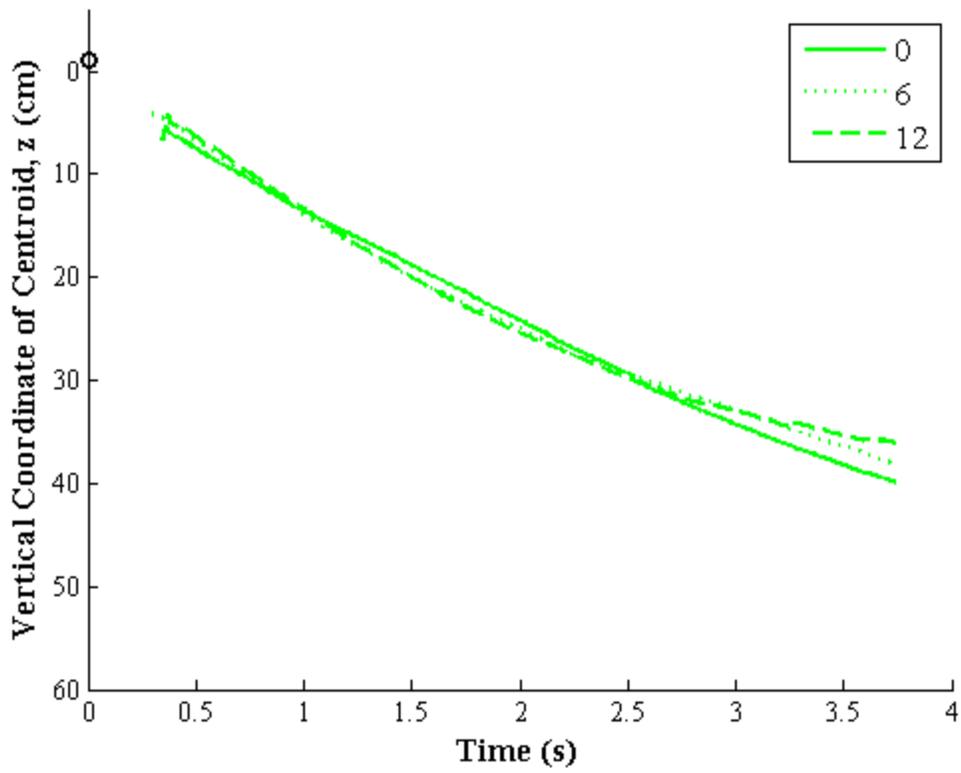
Group 2: D+1PT
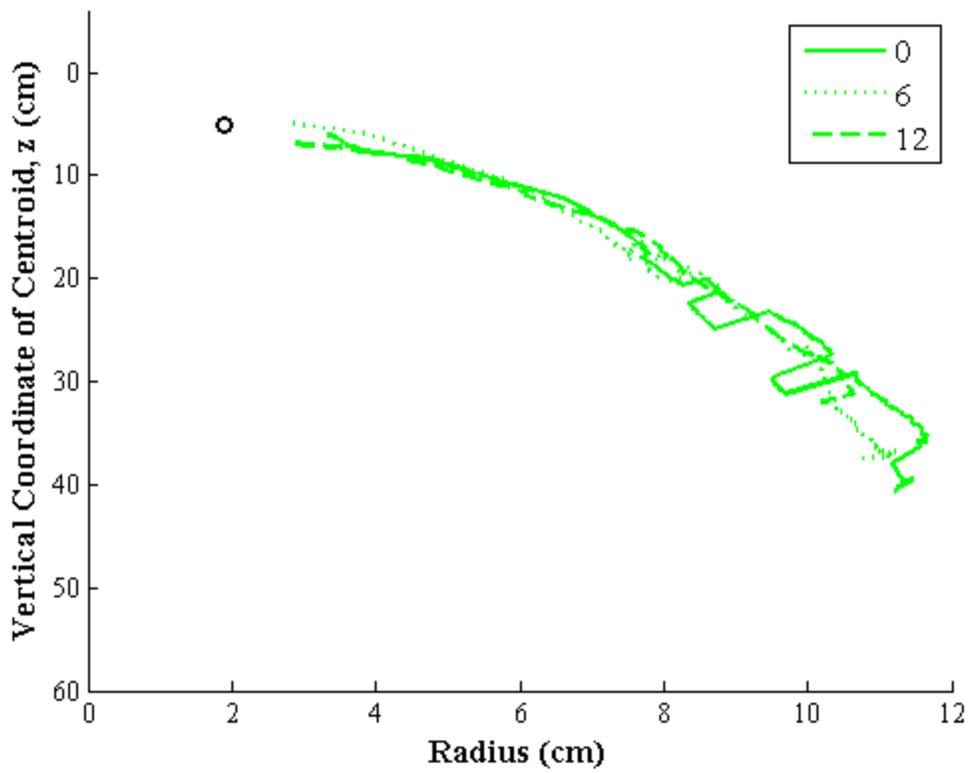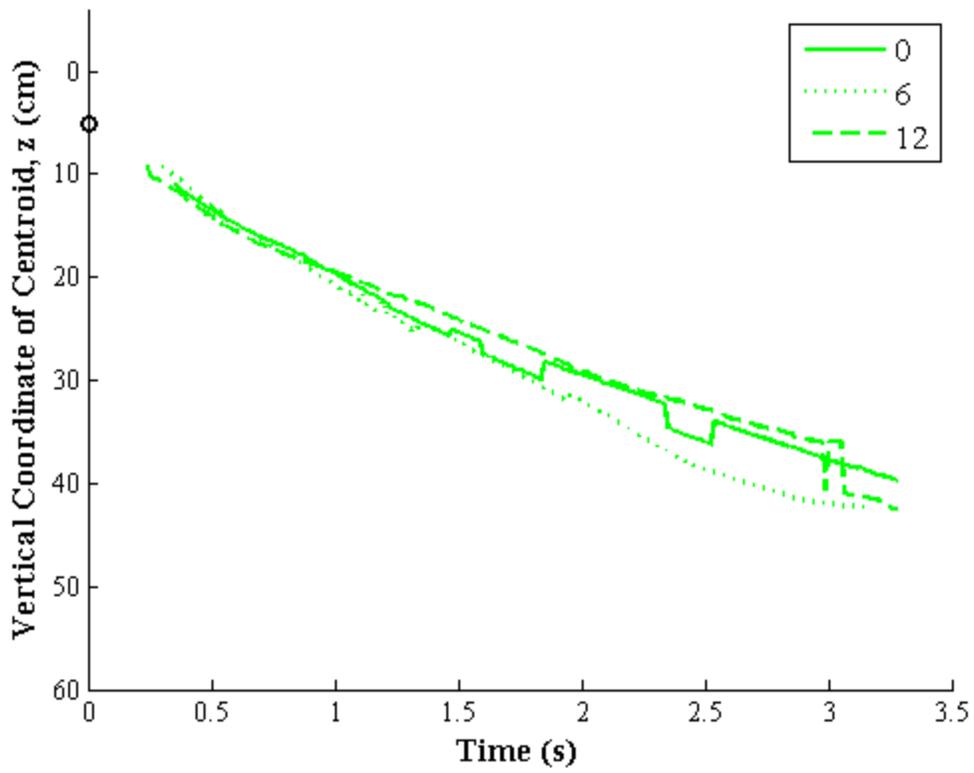
Group 2: D-5PS
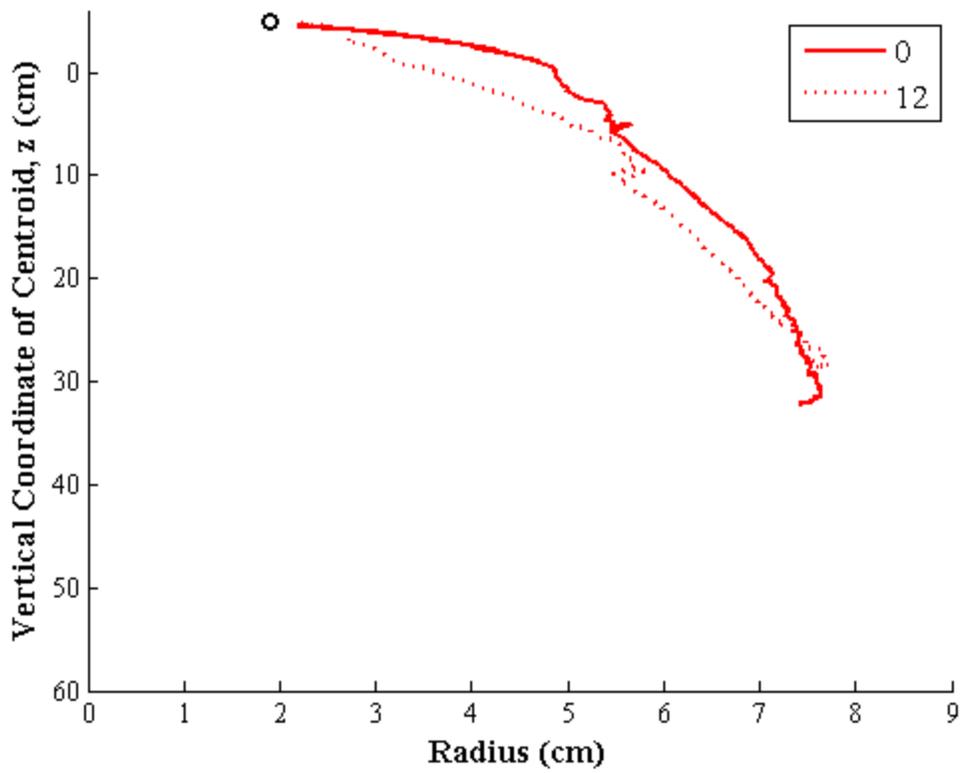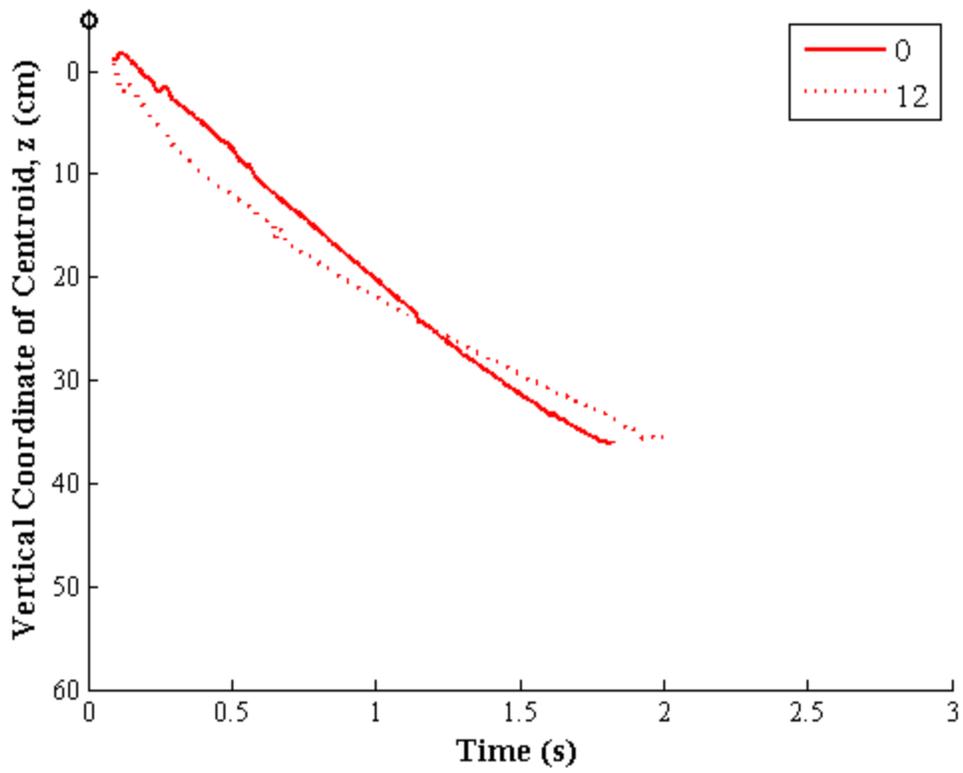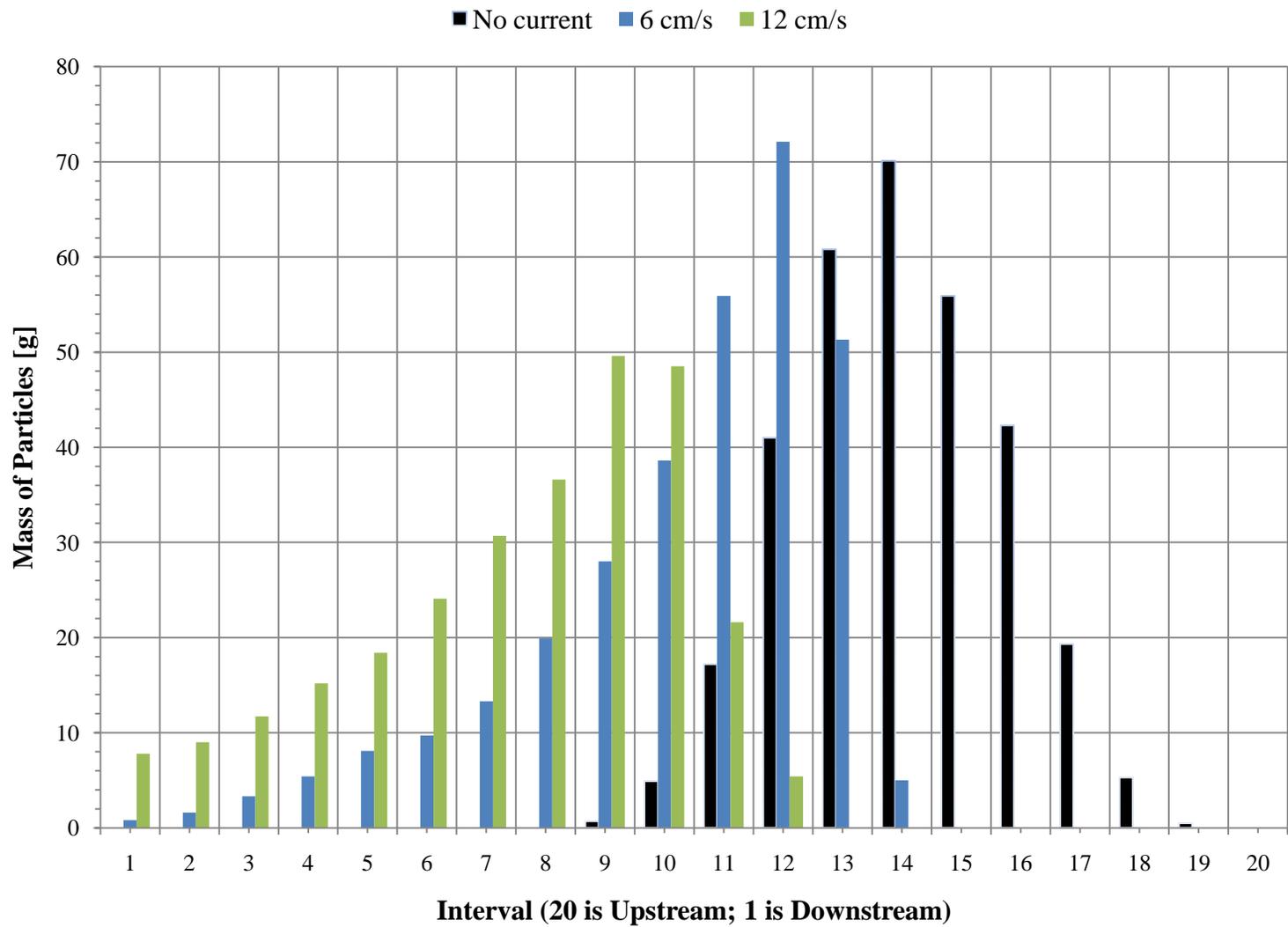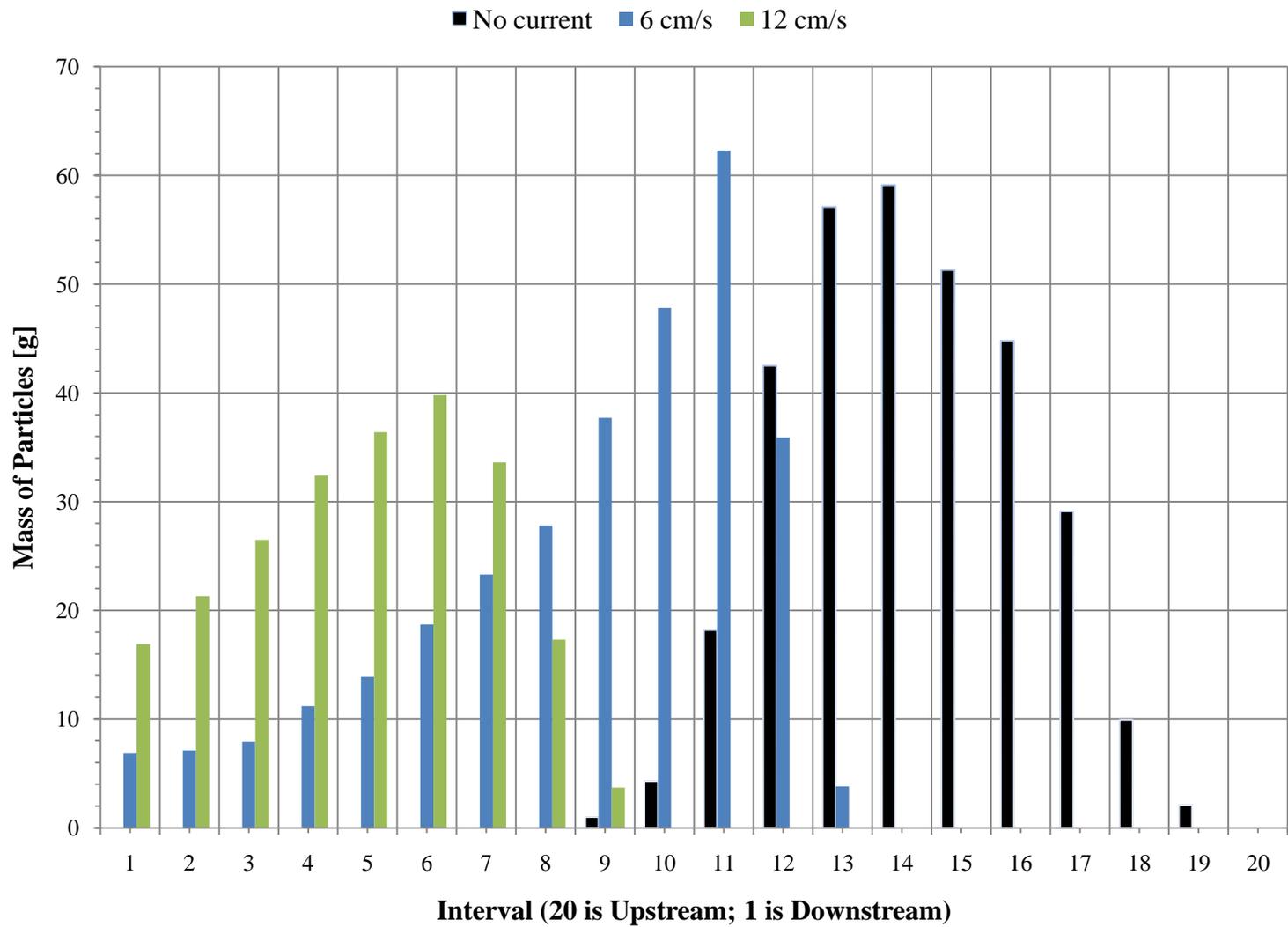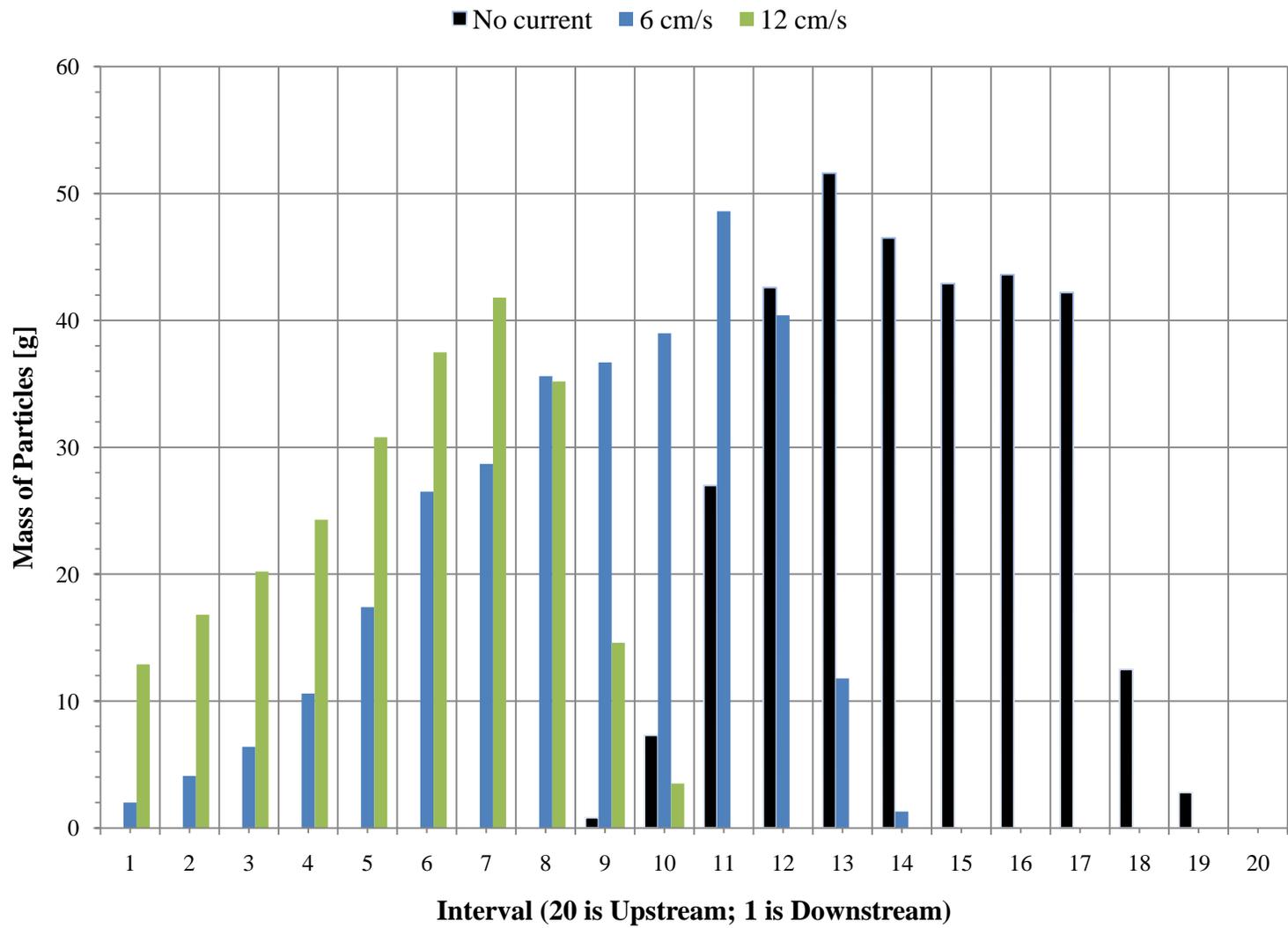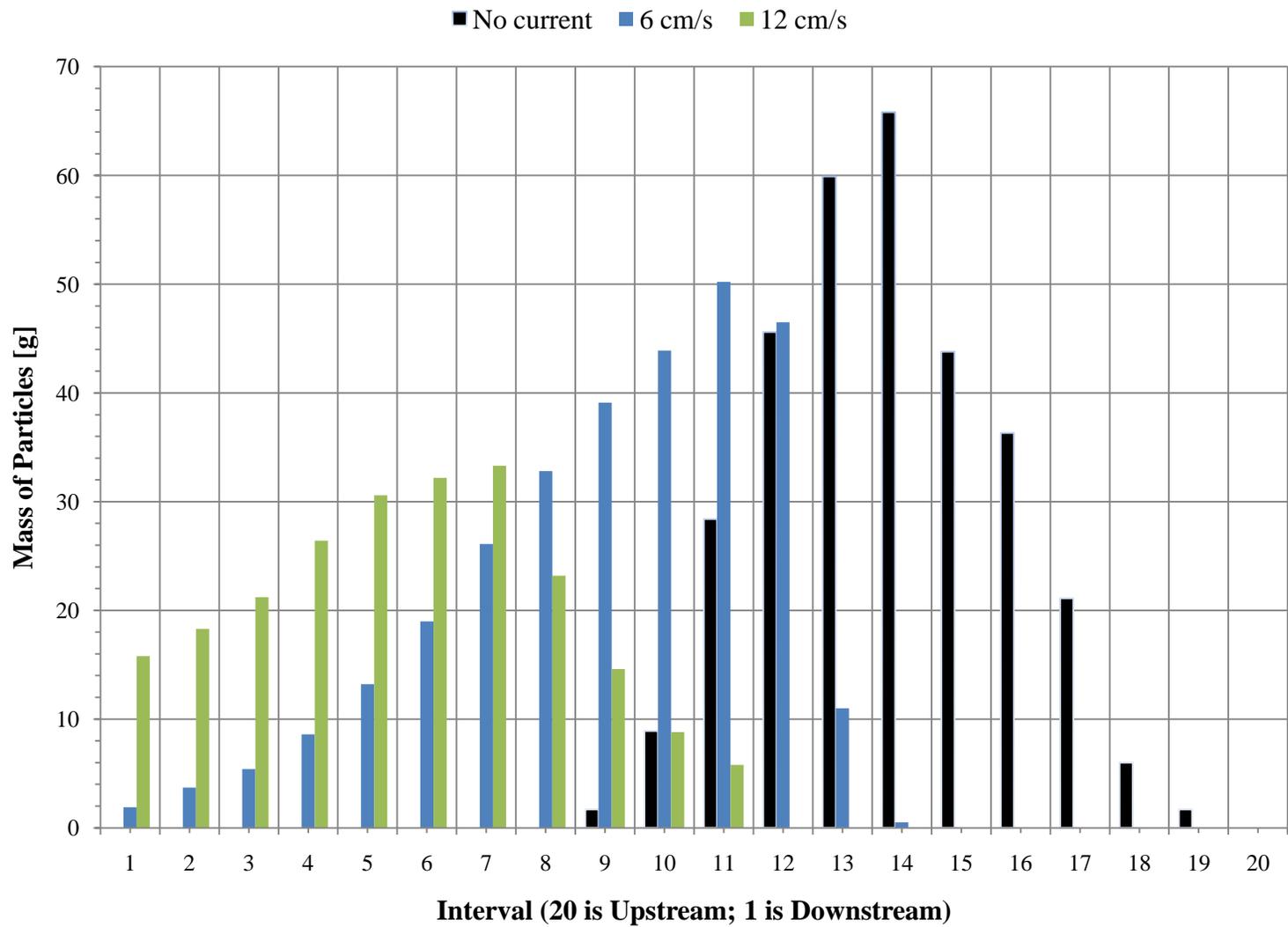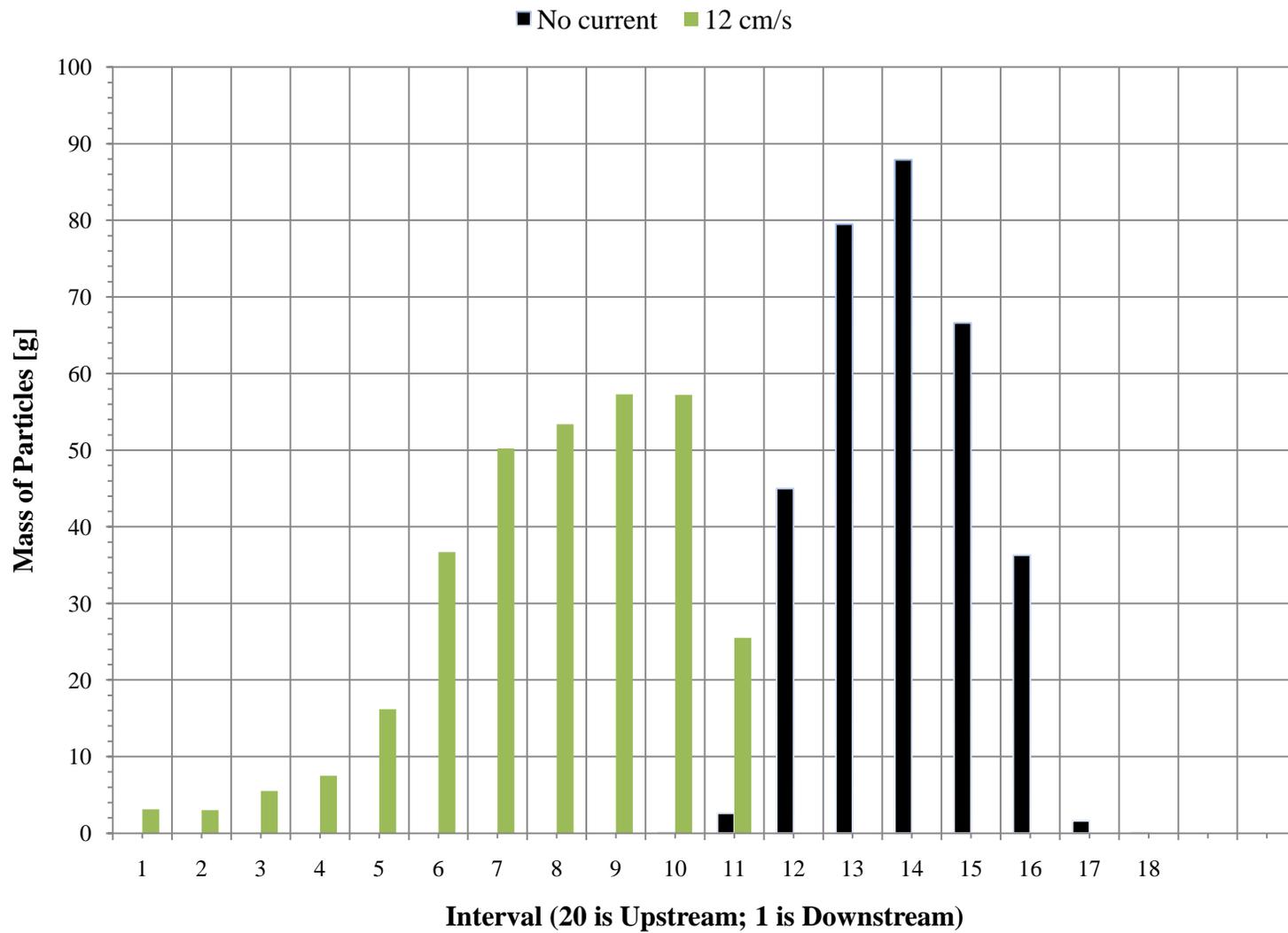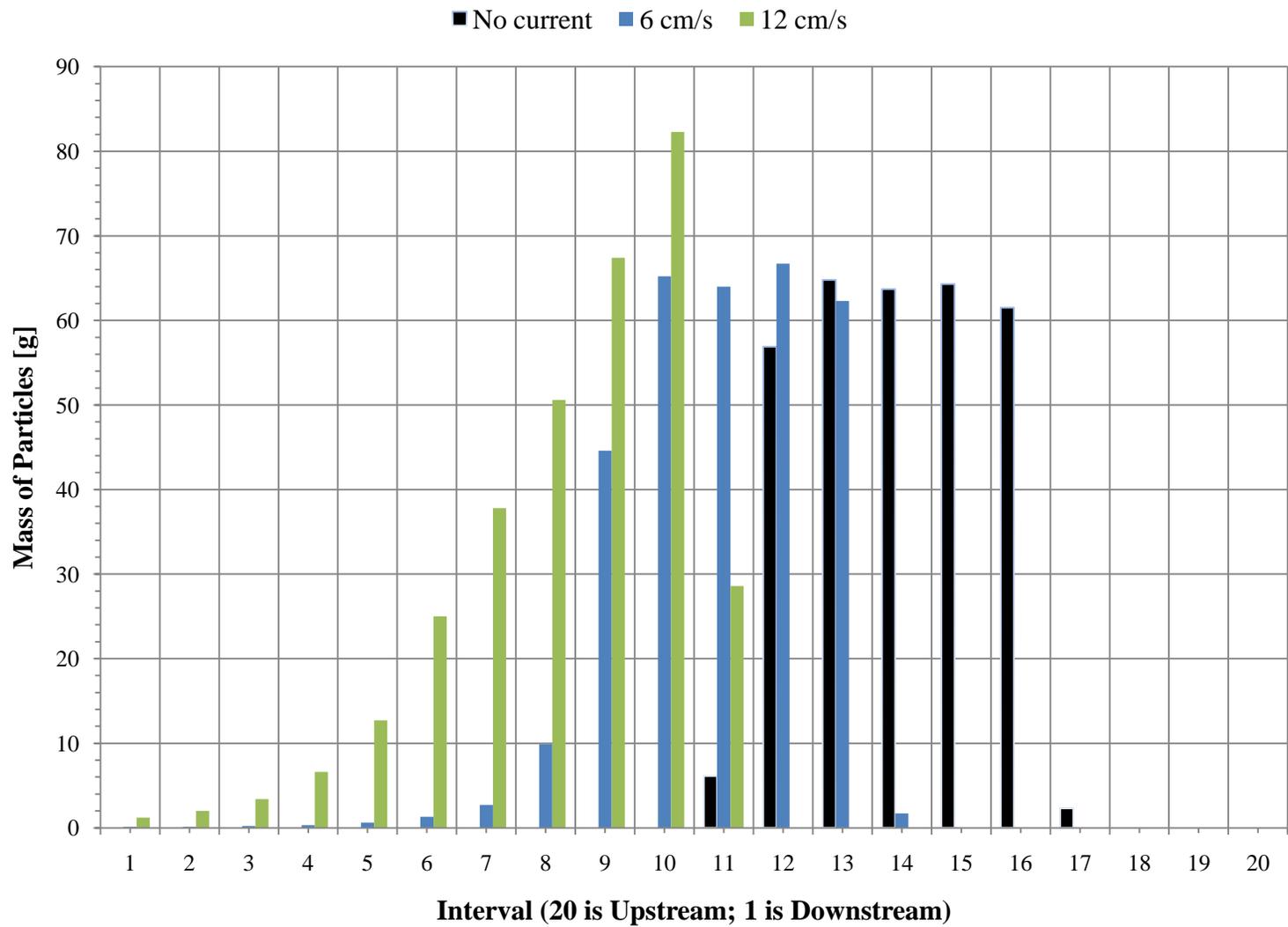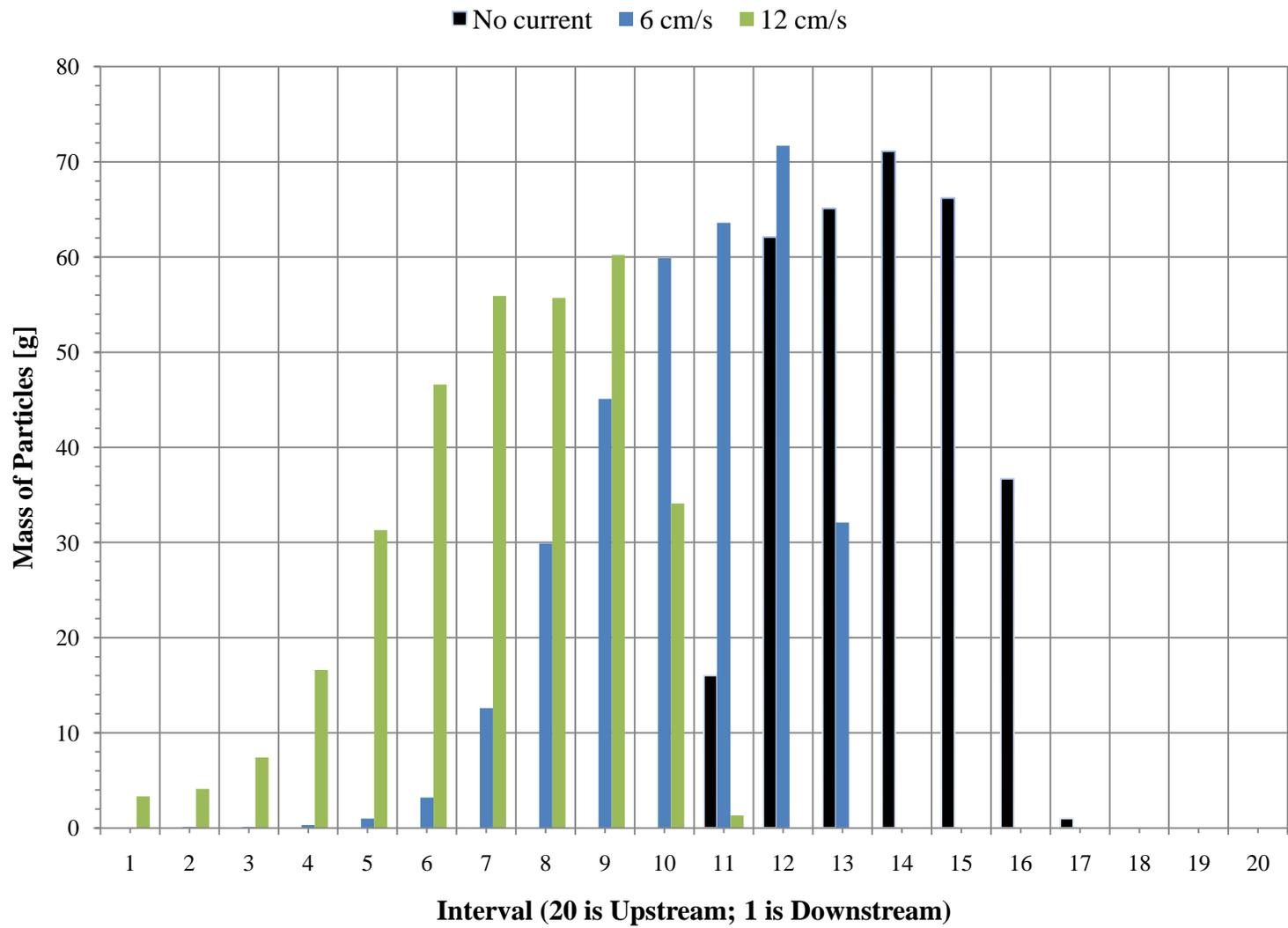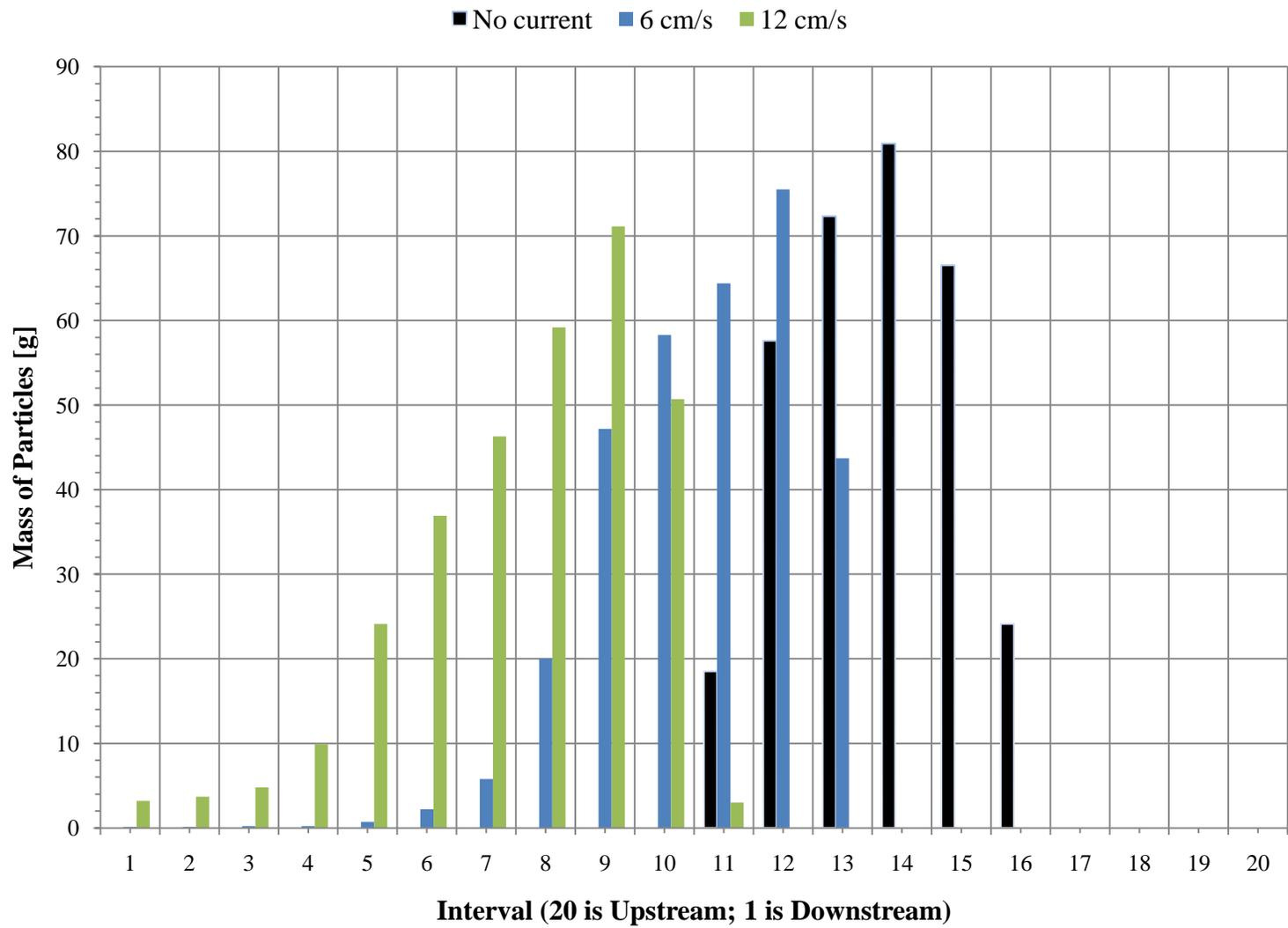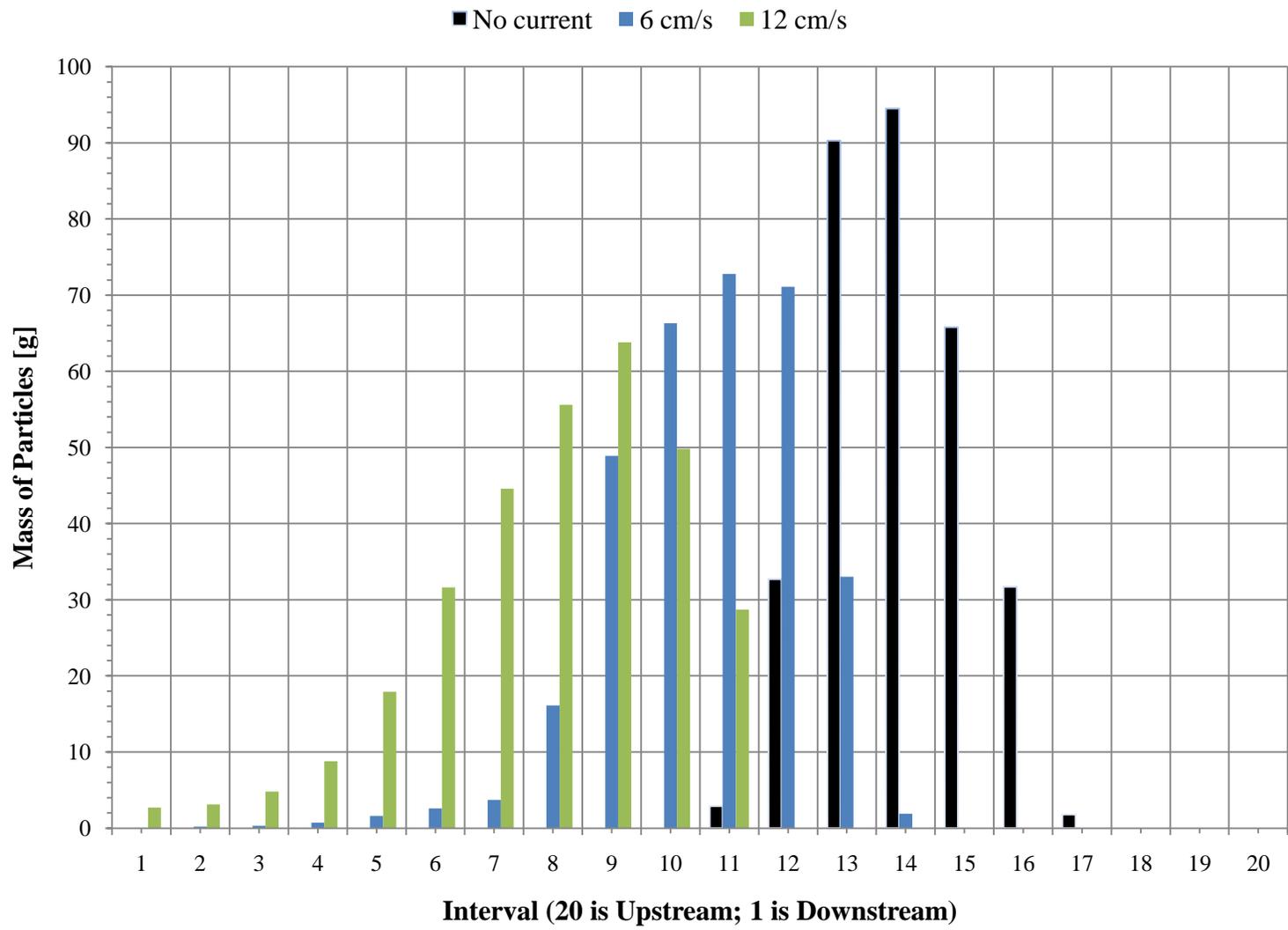
Group 3: B+5RT
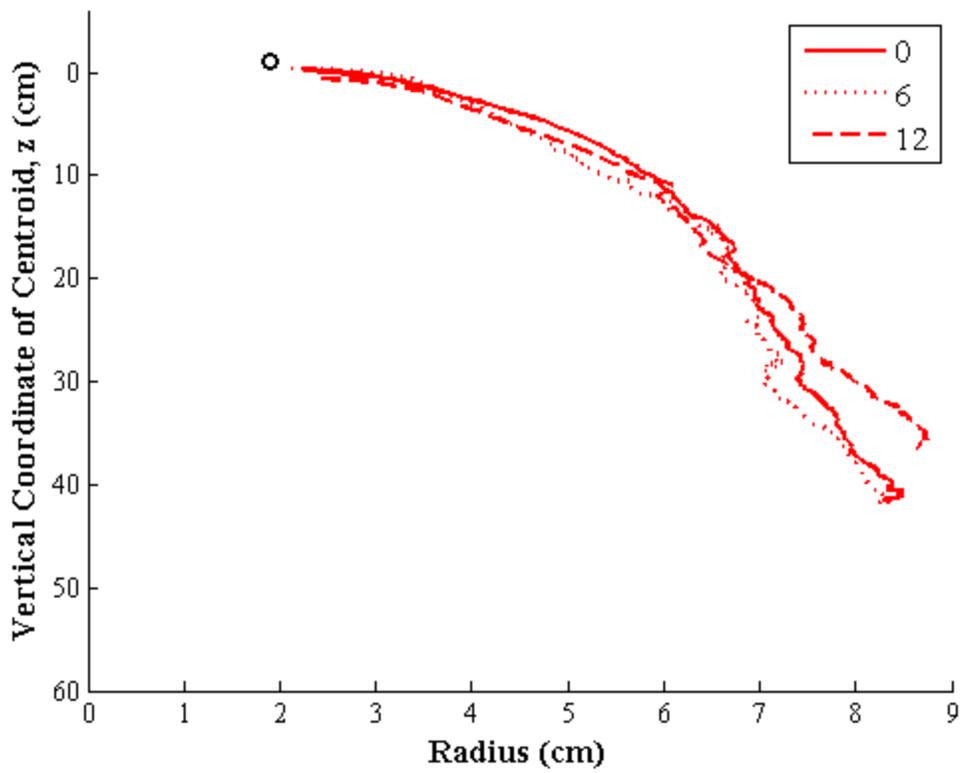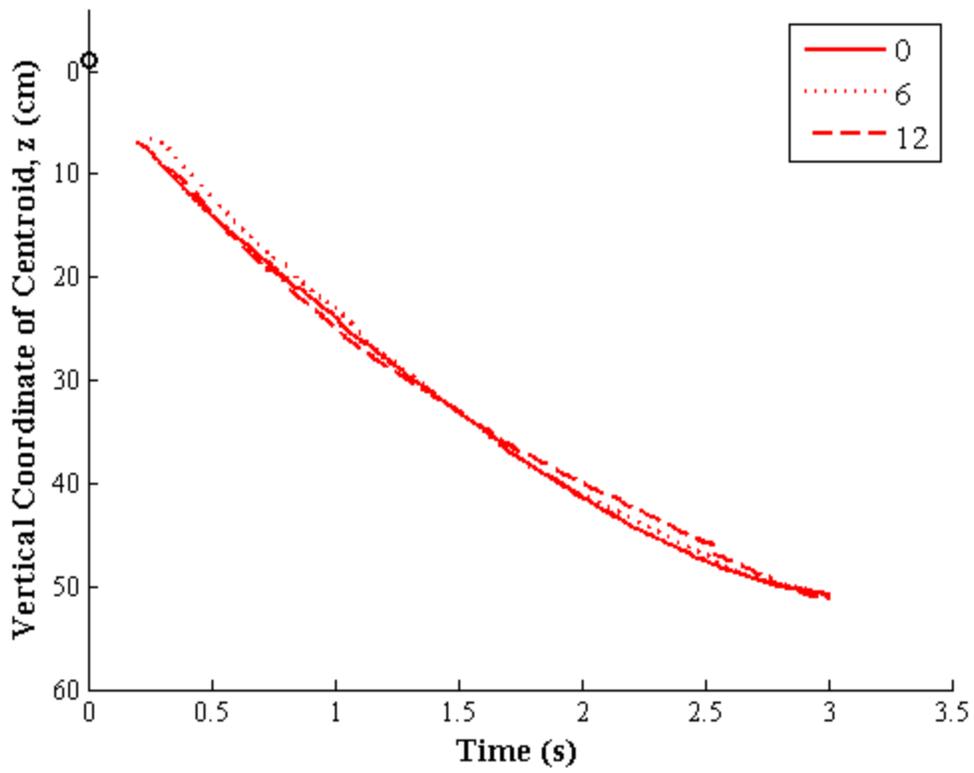
Group 3: B+1RT

Group 3: B+1AT

Group 3: B+1PT

251

Group 3: B-5PS

References

[1] AECOM. 2009a. Monitoring Survey at the New London Disposal Site, July/August 2007. DAMOS Contribution No. 180. U.S. Army Corps of Engineers, New England District, Concord, MA.

[2] AECOM. 2009b. Monitoring Survey at the Portland Sound Disposal Site, August 2007. DAMOS Contribution No. 179. U.S. Army Corps of Engineers, New England District, Concord, MA.

[3] AECOM. 2009c. 2008 DAMOS Data Summary: Massachusetts Bay Disposal Site Capping Demonstration. *Document No. W912WJ-07-D-002, Task Order 6*, prepared for the New England District of the U.S. Army Corps of Engineers, Concord, MA.

[4] Baines, W. D. and Hopfinger, E. J. 1984. Thermals with large density difference. *Atmospheric Environment*. 18(6): 1051-1057.

[5] Batchelor, G. K. 1954. Heat convection and buoyancy effects in fluids. *Quartlery Journal of the Royal Meteorological Society*. 80(245): 339-358.

[6] Bokuniewicz, H. J., Gebert, J., Gordon, R. B., Higgins, J. L., Kaminsky, P., Pilbeam, C. C., Reed, M., and Tuttle, C. 1978. Field Study of the Mechanics of the Placement of Dredged Material at Open-Water Sites. *Technical Report D-78-7*, prepared by Yale University for the U.S. Army Engineer Waterways Experiment Station, Vicksburg, MS.

[7] Brandsma, M. G. and Divoky, D. J. 1976. Development of Models for Prediction of Short-Term Fate of Dredged Material Discharged in the Estuarine Environment. *Contract Report D-76-5*, prepared by Tetra Tech, Inc. for U.S. Army Engineer Waterways Experiment Station, Vicksburg, MS.

[8] Bühler, J. and Papantoniou, D. A. 1991. Swarms of coarse particles falling through a fluid. *Environmental Hydraulics*. J. H. W. Lee and Y. K. Cheung, Eds. Balkema, Rotterdam: 135-140.

[9] Bühler, J. and Papantoniou, D. A. 1999. Barge dumping of rubble in deep water. *Environmental Hydraulics*. J. H. W. Lee, A. W. Jayawardena, and Z. Y. Wang, Eds. Balkema, Rotterdam: 193-198.

[10] Bühler, J. and Papantoniou, D. A. 2001. On the motion of suspension thermals and particle swarms. *Journal of Hydraulic Research*. 39(6): 643-653.

[11] Bush, J. M. W., Thurber, B. A., and Blanchette, F. 2003. Particle clouds in homogeneous and stratified environments. *Journal of Fluid Mechanics*. 489: 29-54.

[12] Clark, B. D., Rittal, W. F., Baumgartner, D. J., and Byram, K. V. 1971. The Barged Disposal of Wastes, A Review of Current Practice and Methods of Evaluation. Pacific Northwest Water Quality Laboratory, Northwest Region, U.S. Environmental Protection Agency, Corvallis, OR.

[13] Dietrich, W. E. 1982. Settling Velocity of Natural Particles. *Water Resources Research*. 18(6): 1615-1626.

[14] Dong, C.-D., Chen, C.-W., Chen, C.-F., and Kao, C.-M. 2007. Mathematical Modeling and Simulation of Ocean Disposal of Harbor Dredged Materials. *Practice Periodical of Hazardous, Toxic, and Radioactive Waste Management*, ASCE. 11(3): 207-213.

[15] ENSR International Corporation. 2002. Boston Harbor Navigation Improvement Project Phase 2 Summary Report. *Document No. 9000-278-000*, prepared for the New England District of the U.S. Army Corps of Engineers, Concord, MA.

[16] Escudier, M. P. and Maxworthy, T. 1973. On the motion of turbulent thermals. *Journal of Fluid Mechanics*. 61(3): 541-552.

[17] Gordon, R. B. 1974. Dispersion of dredge spoil dumped in near-shore waters. *Estuarine and Coastal Marine Science*. 2: 349-358.

[18] Gu, J., Huang, J., and Li, C. W. 2008. Experimental study on instantaneous discharge of unsorted particle cloud in cross-flow. *Journal of Hydrodynamics*. 20(1): 10-16.

[19] Hill, M. J. M. 1894. On a spherical vortex. *Philosophical Transactions of the Royal Society of London, A*. 185: 213-245.

[20] Johnson, B. H. and Fong, M. T. 1995. Development and verification of numerical models for predicting the initial fate of dredged material disposal in open water; Report 2, Theoretical developments and verification results, *Technical Report DRP-93-1*, Final Report, U.S. Army Engineer Waterways Experiment Station, Vicksburg, MS.

[21] Johnson, B. H. and Holliday, B. W. 1978. Evaluation and Calibration of the Tetra Tech Dredged Material Disposal Models Based on Field Data. *Technical Report D-78-47*, U.S. Army Engineer Waterways Experiment Station, Vicksburg, MS.

[22] Koh, R. C. Y. and Chang, Y. C. 1973. Mathematical Model for Barged Ocean Disposal of Wastes. *Environmental Protection Technology Series EPA 660/2-73-029*, U.S. Environmental Protection Agency, Washington, D.C.

[23] Lamb, H. 1932. *Hydrodynamics*, 6th Edition. Cambridge University Press, 738 pp.

[24] Li, C. W. 1997. Convection of particle thermals. *Journal of Hydraulic Research*. 35(3): 363-376.

[25] Maxworthy, T. 1974. Turbulent vortex rings. *Journal of Fluid Mechanics*. 62(2): 227-239.

[26] Maxworthy, T. 1977. Some experimental studies of vortex rings. *Journal of Fluid Mechanics*. 81(3): 465-495.

[27] McDowell, J. E. 1999. Contaminated Sediments in the Marine Environment. *Nor'Easter*.

[28] Montgomery, R. L. and Engler, R. M. 1986. Fate of dredged material during open-water disposal. *Environmental Effects of Dredging Technical Notes*, *Technical Report EEDP-01-2*, U.S. Army Engineer Waterways Experiment Station, Vicksburg, MS.

[29] Morton, B. R., Taylor, G., and Turner, J. S. 1956. Turbulent gravitational convection from maintained and instantaneous sources. *Proc. of the Royal Society of London, Series A*. 234(1196): 1-23.

[30] Neves, M. J. V. and Almeida, P. D. 1991. The influence of density on thermal motion. *Environmental Hydraulics*. Lee and Cheung, Eds. Balkema, Rotterdam: 141-146.

[31] Noh, Y. and Fernando, H. J. S. 1993. The transition in the sedimentation pattern of a particle cloud. *Phys. Fluids A*. 5(12): 3049-3055.

[32] Rahimipour, H. and Wilkinson, D. 1992. Dynamic behavior of particle clouds. *Proc. 11th Australasian Fluid Mechanics Conf.* University of Tasmania, Hobart, Australia: 743-746.

[33] Richards, J. M. 1961. Experiments on the penetration of an interface by buoyant thermals. *Journal of Fluid Mechanics*. 11: 369-384.

[34] Ruggaber, G. J. 2000. Dynamics of particle clouds related to open-water sediment disposal. Ph.D. Thesis, Dept. of Civil and Environmental Engineering, MIT, Cambridge, MA.

[35] Ruggaber, G. J. and Adams, E. E. 2000. Dynamics of Particle Clouds Related to Open-Water Sediment Disposal. *Conference on Dredged Material Management: Options and Environmental Considerations*, MIT Sea Grant College Program, Cambridge, MA: 11-15.

[36] Saffman, P. G. 1995. *Vortex Dynamics*. Cambridge University Press, 311 pp.

[37] Sau, R. and Mahesh, K. 2008. Dynamics and mixing of vortex rings in crossflow. *Journal of Fluid Mechanics*. 604: 389-409.

[38] Science Applications International Corporation (SAIC). 1984. Dredged Material Disposal Operations at the Boston Foul Ground, June 1982 – February 1983. DAMOS Contribution No. 41, prepared for the New England Division of the U.S. Army Corps of Engineers, Waltham, MA.

[39] Science Applications International Corporation (SAIC). 1988. Distribution of Dredged Material at the Rockland Disposal Site, May 1985. DAMOS Contribution No. 50, prepared for the New England Division of the U.S. Army Corps of Engineers, Waltham, MA.

[40] Scorer, R. S. 1957. Experiments on convection of isolated masses of buoyant fluid. *Journal of Fluid Mechanics*. 2: 583-594.

[41] Shariff, K, Leonard, A., and Ferziger, J. H. 1989. Dynamics of a class of vortex rings. *NASA TM-102257*.

[42] Slack, G. W. 1963. Sedimentation of a Large Number of Particles as a Cluster in Air. *Nature*. 200: 1306.

[43] Suedel, B. C., Kim, J., Clarke, D. G., and Linkov, I. 2008. A risk-informed decision framework for setting environmental windows for dredging projects. *Science of The Total Environment*. 403(1-3): 1-11.

[44] Sustar, J. and Wakeman, T. 1977. Dredged Material Study, San Francisco Bay and Estuary – Main Report. U.S. Army Engineer District, San Francisco, San Francisco, CA.

[45] Tamai, M., Muraoka, K., and Murota, A. 1991. Diffusion process of turbidity in direct dumping of soil. *Environmental Hydraulics*. Lee and Cheung, Eds. Balkema, Rotterdam: 147-152.

[46] Tavolaro, J. F. 1982. Sediment Budget Study for Clamshell Dredging and Disposal Activities. U.S. Army Engineer District, New York, New York, NY.

[47] Tavolaro, J. F. 1984. A Sediment Budget Study of Clamshell Dredging and Ocean Disposal Activities in the New York Bight. *Environmental Geology and Water Science*. 6(3): 133-140.

[48] Thalkan, C. L. 2006. Record of Decision for the Boston Harbor Inner Harbor Maintenance Dredging Project. *Document 06-6792*. New England District of the U.S. Army Corps of Engineers, Concord, MA.

[49] Truitt, C. L. 1986. The Duwamish Waterway Capping Demonstration Project: Engineering Analysis and Results of Physical Monitoring. *Technical Report D-86-2*, U.S. Army Engineer Waterways Experiment Station, Vicksburg, MS.

[50] Truitt, C. L. 1988. Dredged Material Behavior During Open-Water Disposal. *Journal of Coastal Research*. 4(3): 489-497.

[51] Tubman, M. W. 2007. Boston Harbor Navigation Channel Improvement Project: Field Data Collection Program Final Report. Coastal and Hydraulics Laboratory, U.S. Army Engineer Research and Development Center, prepared for the New England District of the U.S. Army Corps of Engineers, Concord, MA.

[52] Turner, J. S. 1957. Buoyant vortex rings. *Proc. of the Royal Society of London, Series A*. 239: 61-75.

[53] Turner, J. S. 1960. A comparison between buoyant vortex rings and vortex pairs. *Journal of Fluid Mechanics*. 7: 419-432.

[54] Turner, J. S. 1964. The dynamics of spheroidal masses of buoyant fluid. *Journal of Fluid Mechanics*. 19: 481-490.

[55] Turner, J. S. 1973. *Buoyancy Effects in Fluids*. Cambridge University Press, 367 pp.

[56] Wang, C. P. 1971. Motion of an isolated buoyant thermal. *The Physics of Fluids*. 14(8): 1643-1647.

[57] Woodward, B. 1959. The motion in and around isolated thermals. *Quarterly Journal of the Royal Meteorological Society*. 85(364): 144-151.

[58] Wong, P. P. 2005. Reclamation. In M. L. Schwartz (Ed.), *Encyclopedia of Coastal Science*. The Netherlands: 791-794.

[59] Yamada, H. and Matsui, T. 1978. Preliminary study of mutual slip-thorough of a pair of vortices. *Physics of Fluids*. 21: 292-294.